CODED MODULATION TECHNIQUES WITH BIT INTERLEAVING AND ITERATIVE PROCESSING FOR IMPULSIVE NOISE CHANNELS

A Thesis Submitted
to the College of Graduate Studies and Research
in Partial Fulfillment of the Requirements
for the Degree of Master of Science
in the Department of Electrical and Computer Engineering
University of Saskatchewan

by

Trung Q. Bui

Saskatoon, Saskatchewan, Canada

PERMISSION TO USE

In presenting this thesis in partial fulfillment of the requirements for a Postgraduate degree from the University of Saskatchewan, it is agreed that the Libraries of this University may make it freely available for inspection. Permission for copying of this thesis in any manner, in whole or in part, for scholarly purposes may be granted by the professors who supervised this thesis work or, in their absence, by the Head of the Department of Electrical and Computer Engineering or the Dean of the College of Graduate Studies and Research at the University of Saskatchewan. Any copying, publication, or use of this thesis, or parts thereof, for financial gain without the written permission of the author is strictly prohibited. Proper recognition shall be given to the author and to the University of Saskatchewan in any scholarly use which may be made of any material in this thesis.

Request for permission to copy or to make any other use of material in this thesis in whole or in part should be addressed to:

Head of the Department of Electrical and Computer Engineering
57 Campus Drive
University of Saskatchewan
Saskatoon, Saskatchewan, Canada
S7N 5A9

ACKNOWLEDGMENTS

I would like to express my deepest appreciation and gratitude to my supervisor, Professor Ha Nguyen for his support and guidance during my studies. He has been a great source of knowledge and has inspired me with many ideas which are very useful for my research. His patience, encouragement and availability made this thesis possible.

The financial support in the form of a Graduate Scholarship from the Government of Vietnam is gratefully acknowledged. This financial source is important to help me working on my research and finish this thesis.

I would like to say thank you to my labmates as well as all of my friends for their support and encouragement. Without them, life here would have been more difficult.

Finally, my deepest love and gratitude is devoted to my parents, my sisters and my girlfriend. They always extend their love, supporting and encouragement. To them, I dedicate this thesis.

UNIVERSITY OF SASKATCHEWAN

Electrical and Computer Engineering Abstract

CODED MODULATION TECHNIQUES WITH BIT INTERLEAVING AND ITERATIVE PROCESSING FOR IMPULSIVE NOISE CHANNELS

Student: Trung Q. Bui

Supervisor: Prof. Ha H. Nguyen

M.Sc. Thesis Submitted to the

College of Graduate Studies and Research

August, 2006

ABSTRACT

Power line communications (PLC) suffers performance degradation due mainly to impulsive noise interference generated by electrical appliances. This thesis studies coded modulation techniques to improve the spectral efficiency and error performance of PLC. Considered in the first part is the application of bit-interleaved coded modulation with iterative decoding (BICM-ID) in class-A impulsive noise environment. In particular, the optimal soft-output demodulator and its suboptimal version are presented for an additive class-A noise (AWAN) channel so that iterative demodulation and decoding can be performed at the receiver. The effect of signal mapping on the error performance of BICM-ID systems in impulsive noise is then investigated, with both computer simulations and a tight error bound on the asymptotic performance. Extrinsic information transfer (EXIT) chart analysis is performed to illustrate the convergence properties of different mappings. The superior performance of BICM-ID compared to orthogonal frequency-division multiplexing (OFDM) is also clearly demonstrated.

Motivated by the successes of both BICM-ID and OFDM in improving the error performance of communications systems in impulsive noise environment, the second part of this thesis introduces a novel scheme of bit-interleaved coded OFDM with iterative decoding (BI-COFDM-ID) over the class-A impulsive noise channel. Here, an iterative receiver composed of outer and inner iteration loops is first described in detail. Error performance improvements of the proposed iterative receiver with different iteration strategies are presented and discussed. Performance comparisons of BI-COFDM-ID, BICM-ID and iteratively decoded OFDM are made to illustrate the superiority of BI-COFDM-ID. The effect of signal mapping on the error performance of BI-COFDM-ID is also studied.

Table of Contents

List of Tables

List of Figures

ABBREVIATIONS

APP	A Posteriori Probability
ASK	Amplitude Shift Keying
AWGN	Additive White Gaussian Noise
AWAN	Additive White class-A Noise
BER	Bit Error Rate
BICM	Bit-Interleaved Coded Modulation
BICM-ID	Bit-Interleaved Coded Modulation with Iterative Decoding
BI-COFDM-ID	Bit-Interleaved Coded OFDM with Iterative Decoding
BPSK	Binary Phase Shift Keying
CDMA	Code-Division Multiple Access
CN	Complex Number
DSL	Digital Subscriber Lines
dB	Decibel
EXIT	Extrinsic Information Transfer
FSK	Frequency Shift Keying
IDFT	Inverse Discrete Fourier Transform
IFFT	Inverse Fast Fourier Transform
LLR	Log Likelihood Ratio
MAP	Maximum A Posteriori Probability
MCM	Multilevel Coded Modulation
ML	Maximum Likelihood
MLL	Maximum Log Likelihood
MMSE	Minimum Mean Square Error
OFDM	Orthogonal Frequency-Division Multiplexing
PEP	Pairwise Error Probability
PLC	Power Line Communications

pmf	Probability Mass Function
pdf	Probability Density Function
PSK	Phase Shift Keying
QAM	Quadrature Amplitude Modulation
QPSK	Quadrature Phase Shift Keying
RSC	Recursive Systematic Convolutional
SISO	Soft-Input Soft-Output
SNR	Signal-to-Noise Ratio
SP	Set Partitioning
SSP	Semi Set Partitioning
TCM	Trellis-Coded Modulation

1. Introduction

After many years of industrialization, electrical distribution grids have constituted a universal wiring system that hooks up homes and offices together. Power grids were originally designed to transmit electric power from a small number of sources (the generators) to a large number of sinks (the consumers) in the frequency range of 50-60 Hz. Initially, the first data transmissions over power lines were primarily done only to protect sections of the power distribution system in case of faults. However, nowadays, the use of existing power lines for transferring voice or data signals has received considerable interest, both in research community and in the industry. The market for power line communications (PLC) is two-fold: to the home, or "last mile" access; and in the home, or "last inch" access. The basic concepts of the "last mile" and "last inch" accesses are briefly illustrated in Figures 1.1 and 1.2, respectively [1].

For the "last mile" access, PLC is one of several possible techniques that include cable modem, different types of digital subscriber lines (xDSL) and broad-band wireless connections. PLC is not widely thought to be superior to other technologies, nor are the other technologies without problems or clearly superior to PLC in all respects [1]. According to many studies, power line communications could be better than the other "last inch" access technologies such as cable, wireless links and HomePNA (the phone-line networking based on the specifications developed by Home Phone Networking Alliance). In the home, the ubiquitous-multiple sockets in each room provide considerable and dispersed capacity of PLC. The development of the "last inch" by home-networking companies in the form of wireless network adapters and power-line adapters is gradually leading to widespread home networking; i.e., a wide array of devices connected inside the home in a intra-home network. This "in-

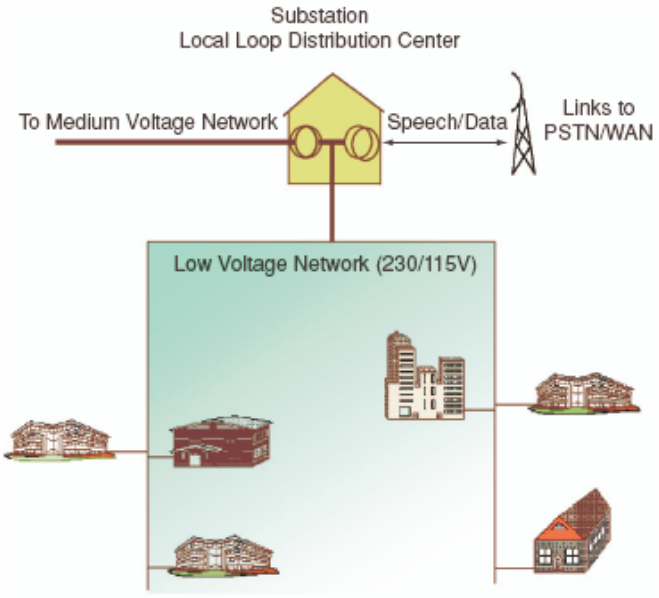

Figure 1.1: The "last mile" broadband access to homes from the local distribution center [1].

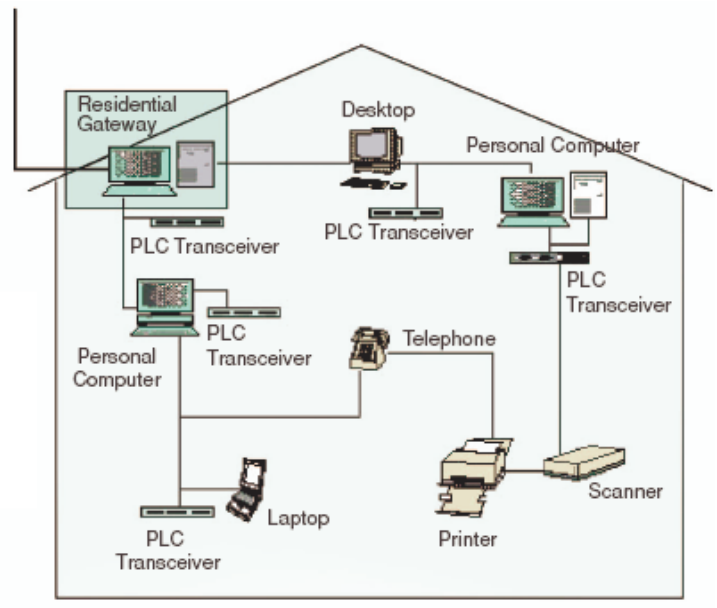

Figure 1.2: The "last inch" or in-home networking [1].

home networking" could transform all power outlets in the household into broadband connections for PCs, telephones and their accessories, and other "enabled" electric appliances as well. For example, within home automation and intelligent buildings, PLC can also provide a natural communications line for various devices such as alarm sensors, controllers, and even slow scan TV images for security purposes [2]. Furthermore, the birth and growth of the Internet have accelerated the demand for digital telecommunications services to every home [3]. If the electricity distribution network can carry such services, every premises, factory, office, and organization will be interconnected and form a truly global information superhighway network.

However, the power carrier was not specifically designed for data or voice transmission and presents a harsh environment for it. Varying levels of impedance and attenuation due to electrical hardware configurations are frequent. Such variations and other interferences from various sources lead to a very poor performance of PLC systems. Those interferences, referred to as man-made noise, have statistical characteristics much different from that of classical Gaussian interference. More specifically, man-made noise is typically impulsive.

In order to determine the optimum receiving system for a given class of signals and analyze its performance over the impulsive noise environment, a mathematical model of impulsive noise is required. For almost all cases of interest, this impulsive noise can be characterized by an envelope and a phase (or quadrature and imaginary components). However, the main problem for any digital communications system is to develop a model for this interference that fits all the available measurement; is physically meaningful when the nature of noise sources, their distributions in time and space, propagation, etc., are considered; is directly relatable to the physical mechanism giving rise to the interference; and is still simple enough so that the required statistics can be obtained for solving signal detection problems [4].

Various models have been proposed to meet these requirements. The simplest model of impulsive noise, namely the two-term Gaussian mixture impulsive noise, is to separate this interference into two terms of Gaussian noise. The relationship of the

appearance probability for each term and the connection between the two terms via their variances define the characteristics of the impulsive noise. Due to its simplicity, the two-term Gaussian mixture impulsive noise is used in [5–8]. Another model available to date which is more accurate and also meets the above requirements is a relatively simple model that incorporates background noise and impulsive noise. This model is first suggested in [9] and known as Middleton's class-A noise. This noise model corresponds to an independent and identically distributed (i.i.d.) discrete-time random process whose probability density function is an infinite weighted sum of Gaussian densities, with decreasing weights and increasing variance for the Gaussian densities [10]. Middleton's class-A noise model has been used widely in the performance analysis of communications systems disturbed by impulsive noise [11–16]. This thesis, therefore, shall also concentrate on the design of digital communication systems over class-A impulsive noise environment.

Generally, to transmit digital signals over impulsive noise environment, one can use many of the same techniques widely implemented in wireline and wireless communications. Basic modulation techniques such as binary phase shift keying (PSK), binary frequency shift keying (FSK) and binary amplitude shift keying (ASK) can be used for low data rate communication. For a higher data rate up to 1Mb/s, code-division multiple access (CDMA) offers a more effective solution. Other more advanced techniques such as M-ary PSK, M-ary quadrature amplitude modulation (QAM), M-ary FSK, as well as orthogonal frequency-division multiplexing (OFDM) can be used when higher data rates up to 10Mb/s are desired [17]. A thorough study of signal modulation over power lines is given in [18].

Modulation techniques can only be used for low data rates and/or high error probability communications. Hence, they are only suitable for applications of protection purposes and telemetering in which the high precision is not required. For CDMA, the signal of each user is spread using a spreading code at the transmitter. It is recovered at the receiver by de-spreading using the same code. CDMA provides robustness against impulsive noise and other forms of interference. It seems, therefore, to be a

potential candidate for PLC. However, in CDMA systems, the processing gain needs to be high to effectively counter impulsive noise and interference from other users. With low processing gain, the robustness against interference and noise is lost and the signal quality may deteriorate to unacceptable levels for all users. While the main advantage of CDMA technique can not be fully exploited for impulsive noise environment, OFDM has been proposed as an attractive candidate for PLC due to its merits in having simple channel estimation, high bandwidth efficiency as well as flexibility in providing high data rates. Nevertheless, it has been demonstrated in [19–21] that the classical OFDM receiver designed for the AWGN channel is highly suboptimal for the impulsive noise environment. This is because the rich structure of impulsive noise is not properly exploited in such a receiver.

Suitable error control strategies can also be applied in order to ensure reliable communication as well as to reduce the bit error rate (BER) in a hostile environment as in an impulsive channel. The use of some forward error correcting (FEC) codes such as trellis codes and turbo codes in the design of a digital communications system can eliminate the effects of impulsive noise. In general, FEC codes add redundant information in a controlled manner to the original message, thus enabling the receiver to retrieve the message even if it contains erroneous bits [22]. For the trellis coded design, the information to be transmitted is first encoded with a convolutional code. At the receiving end, Viterbi decoding is performed to recover the information. For the design with turbo codes, the interleaver is used to arrange the code data such that erroneous bits are randomly distributed over many codewords rather than a few codewords [23]. Moreover, the iterative decoding also helps to increase the reliability of the decision after each iterative step. Both of the above designs can help to combat impulsive noise. However since coding adds extra bits into the original message, it increases the required transmission bandwidth. To improve the efficiency of the system with respect to bandwidth, combining a higher-order modulation with error control coding is necessary.

The integration of modulation and channel coding results in a coded modulation

system and it was first studied by Massey [24]. Coded modulation that jointly optimizes coding and modulation is now a popular and powerful technique to improve the performance of the digital communication systems that operate with limited bandwidths [25].

Since the invention of turbo codes [26], interleaving and iterative processing have also been applied to coded modulation systems. It was shown in [27–32] that with iterative decoding, bit-interleaved coded modulation (BICM), a bandwidth-efficient approach primarily considered in the past for fading channels, can in fact be used to provide excellent error performance over both Gaussian and fading channels. It was first suggested in [10] that BICM could be a fruitful coding option for PLC systems due mainly to the fact that BICM links binary coding and M-ary modulation in a simple way. The structure of BICM is simpler than that of trellis coded modulation (TCM) or multilevel coded modulation (MCM) and it allows a large degree of flexibility (e.g., the choice of the channel code can be made independent of the modulation scheme). The suitability of BICM as a coding option in PLC systems becomes more evident with recent results obtained by applying iterative (turbo) decoding for BICM. In particular, it is shown in [29, 33–37] that using suitable mappings, the error performance of BICM with iterative decoding (BICM-ID) significantly improves over that of the conventional BICM with Gray mapping. This thesis is therefore primarily concerned with the application of BICM-ID in impulsive noise environment.

1.1 Thesis contributions

In the first part of this thesis, the application of BICM-ID systems over class-A impulsive noise is investigated. In general, an optimal or suboptimal receiver designed for an additive white Gaussian noise (AWGN) channel does not work well for the systems disturbed by impulsive noise. Hence, to improve the error performance of BICM-ID systems in the presence of impulsive noise, an optimum soft output demodulator as well as its sub-optimum version are designed so that the iterative demodulation and decoding can be performed at the receiver.

The effects of signal mapping on the error performance of BICM-ID disturbed by impulsive noise is also investigated with both computer simulations and a tight error bound on the asymptotic performance. For given signal constellation, interleaver and convolutional code, signal mapping plays an important role in determining the error performance of a BICM-ID system. Generally, there are two approaches to study the effect of signal mapping on the performance of BICM-ID. The first technique is based on the error bound [14, 27–29, 34], which is only related to the asymptotic performance of the systems. Another technique is based on the extrinsic information transfer (EXIT) chart [31, 32, 38]. Both of these techniques are applied in this thesis to study the effects of signal mapping designs in BICM-ID over the impulsive noise channel. Performance comparisons of BICM-ID with uncoded binary PSK (BPSK), coded BPSK and OFDM are also clearly demonstrated.

Motivated by recent investigations of OFDM technique to combat both impulsive noise and multipath effects [20, 21], this thesis also introduces a novel design of bit-interleaved coded OFDM with iterative decoding (BI-COFDM-ID) to further improve the error performance of PLC systems in the environment with less impulsive noise. In particular, two iteration loops at the receiver of BI-COFDM-ID are introduced. The design of each iteration loop is presented and the effects of iteration scheduling are investigated. Finally, performance comparison of BI-COFDM-ID with BICM-ID and iteratively-decoded OFDM are also carried out.

1.2 Thesis organization

The remaining of this thesis is organized as follows.

Chapter 2 gives an introduction to impulsive noise, where the Midlenton's class-A impulsive noise is the main topic. The probability density function (pdf) as well as the parameters defining the characteristics of class-A impulsive noise are clearly described.

Chapter 3 provides an overview of common techniques to combat impulsive noise.

First, QAM is reviewed as a very simple transmission technique for PLC. Then, the applications of OFDM and binary turbo codes in impulsive noise environment are considered. Described at the end of this chapter is the recently proposed technique, referred to as iteratively-decoded OFDM [20].

The main contribution of this thesis is contained in Chapter 4, where the application of BICM-ID over the class-A impulsive noise channel is thoroughly investigated and analyzed. First, the optimum and suboptimum receivers are designed for the impulsive noise channels. Then the effect of signal mapping on the error performance is studied by both computer simulation and a tight error bound on the asymptotic performance. The convergence properties of different mappings are investigated with the EXIT chart. The last part of this chapter compares the performance of BICM-ID with that of uncoded and coded BPSK as well as OFDM.

Chapter 5 presents another important contribution of this thesis. This chapter proposes the use of BI-COFDM-ID for the environment with less impulsive noise. The block diagram and the main principle of two iterative decoding loops at the receiver are introduced and discussed. The effects of signal mapping in BI-COFDM-ID is studied with three different mapping schemes of 8-PSK constellation. The advantage of BI-COFDM-ID is illustrated by comparing its error performance with that of OFDM and BICM-ID.

Finally, Chapter 6 draws the conclusions and gives suggestions for further studies.

2. Impulsive noise

2.1 Overview

Noise can be defined as an unwanted signal that interferes with the communications, measurement, perception or processing of an information-bearing signal. A noise itself is a signal that conveys information regarding the source of the noise. The sources of the noise are many, vary and include thermal noise intrinsic to electric conductors, shot noise inherent in electrical current flows, switching, and interferences due to varying levels of impedance and attenuation, etc. Noise is one of the main factors limiting the capacity of data transmission in communications. Therefore, the modeling and removal of the effects of noise have been at the core of theory and practice for digital communications systems in general and power line communications in particular [39].

Noise in PLC is a significant problem for data transmission. This is because it rarely has properties similar to the easily-analyzed Gaussian noise of the receiver's front-end. Noise in PLC comes from widely varying noise sources. The background noise is caused by noise sources with low power, ingress of broadcast stations in the medium and shortwave broadcast band, and switching power supplies. The channel between any two outlets in a home exhibits a transfer function of an extremely complex transmission line network with many stubs having terminating loads of various impedances. The amplitude and phase responses of such a system fluctuate extensively with frequency. Some frequencies may observe little attenuation in the transmitted signal, while at others the signal may be completely distorted by noise. Moreover, the PLC channel transfer function is time varying. This is due to the fact that a consumer may plug a new device into the power line at any time, or some appliances may have a time-varying load impedance, which can be the case with

switching power supplies or motors. Light dimmers and related products that use triacs create impulsive noise on every cycle or half cycle of the power. Inadequately designed switching power supplies induce impulsive noise into the power line consisting of high harmonic content related to the switching frequency of the supply. As a consequence of this noise diversity, the power line channel represents a non-Gaussian noise environment [22].

As reported in [40], the noise in PLC channels can be classified as background noise and impulsive noise. While background noise displays stationary characteristics, impulsive noise appears for short intervals, but presents a high power spectral density (PSD) of up to 40 dB above the background noise. For this reason impulse noise is considered the main source of errors in data transmission over power lines. PLC transceivers can easily tackle background noise; it is the impulse noise that is difficult to deal with. If the disturbance of impulse noise is shorter than the duration of a transmitted symbol, there is no influence of disturbance on information data, but in a situation contrary to this, impulse noise can distort data.

From the above discussions, a knowledge and mathematical model of impulsive noise in PLC is necessary to design a proper transmission scheme for PLC systems. This chapter begins with a study of the characteristics of impulsive noise, and then proceeds to consider several methods for statistical modeling of impulsive noise in PLC.

2.1.1 Impulsive noise

In this section, the mathematical concepts of analog and digital impulses are introduced. Consider the unit-area pulse, $p(t)$, shown in Fig. 2.1(a). As the pulse width, ε, tends to zero, the pulse tends to an impulse [39]. The impulse function shown in Fig. 2.1(b) is defined as a pulse with an infinitesimal time width as:

$$\delta(t) = \lim_{\varepsilon \to 0} p(t) = \begin{cases} 1/\varepsilon, & |t| \leq \varepsilon/2 \\ 0, & |t| > \varepsilon/2. \end{cases} \tag{2.1}$$

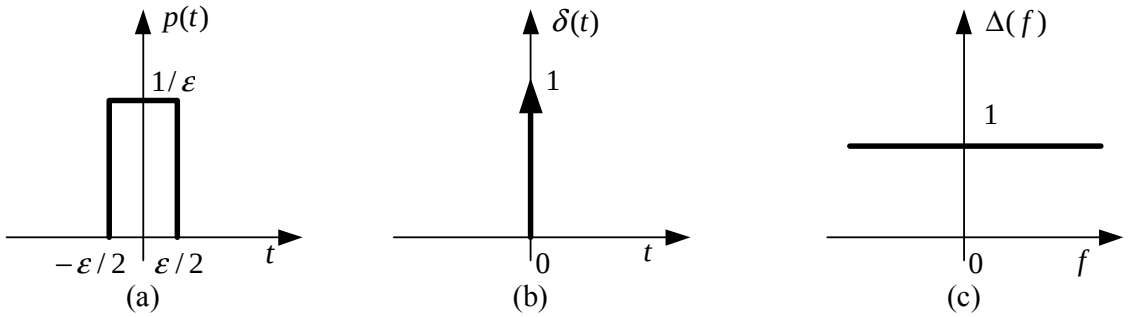

Figure 2.1: (a) An unit-area pulse; (b) the pulse becomes an impulse as $\varepsilon \to 0$; (c) the spectrum of the impulsive function.

The integral of the impulsive function is given by:

$$\int_{-\infty}^{\infty} \delta(t)dt = \varepsilon \times \frac{1}{\varepsilon} = 1 \tag{2.2}$$

The Fourier transform of the impulse function is obtained as:

$$\Delta(f) = \int_{-\infty}^{\infty} \delta(t)\mathrm{e}^{-j2\pi ft}dt = \mathrm{e}^{0} = 1, \ \ -\infty < f < \infty \tag{2.3}$$

where f is the frequency variable.

A digital impulse, $\delta(m)$, is defined as a signal with an "on" duration of one sample, and is expressed as:

$$\delta(m) = \begin{cases} 1, & m = 0 \\ 0, & m \neq 0. \end{cases} \tag{2.4}$$

where the variable m designates the discrete-time index. Using the Fourier transform relation, the frequency spectrum of digital impulse is given by:

$$\Delta(j\omega) = \sum_{m=-\infty}^{\infty} \delta(m)\mathrm{e}^{-j2\omega m} = 1, \ \ -\infty < \omega < \infty. \tag{2.5}$$

In communication systems, a real impulsive-type noise has a duration that is normally more than one sample long. An impulsive noise also originates at some point in time and space, and then propagates through the channel to the receiver.

Impulsive noise is a non-stationary, binary-state sequence of impulses with random amplitudes and random positions of occurrence. The non-stationary nature of

impulsive noise can be seen by considering the power spectrum of the noise process with a few impulses per second: when the noise is absent the process has zero power, and when an impulse is present the noise power is the power of the impulse. Therefore the power spectrum, and hence the autocorrelation of impulsive noise are binary state, time-varying processes.

2.1.2 Statistical models for impulsive noise

In this section, a number of statistical models for the characterization of an impulsive noise process are reviewed. An impulsive noise sequence, $n_i(m)$, consists of short duration pulses of random amplitudes, durations and times of occurrence, and may be modeled as the output of a P-tap filter as [39]:

$$n_i(m) = \sum_{k=0}^{P-1} h_k n(m-k) b(m-k), \tag{2.6}$$

where $b(m)$ is a binary-valued random sequence modeling the time of occurrence of impulsive noise, $n(m)$ is a continuous-valued random process that models the impulse amplitudes and h_k is the impulse response of a filter that models the duration and the shape of each impulse. The two most basic and popular statistical processes used for modeling impulsive noise as an amplitude-modulated binary sequence are the Bernoulli-Gaussian and Poisson-Gaussian processes, which are discussed next.

Bernoulli-Gaussian model of impulsive noise

In a Bernoulli-Gaussian model of impulsive noise, the random time of occurrence of the impulses is modeled by a binary Bernoulli process, $b(m)$, and the amplitude of the impulses is modeled by a Gaussian process. A Bernoulli process, $b(m)$, is a binary-valued process that takes a value of "1" with a probability of α and a value of "0" with a probability of $1-\alpha$. The probability mass function (pmf) of a Bernoulli process is thus given by

$$P_B[b(m)] = \begin{cases} \alpha, & \text{for } b(m) = 1 \\ 1-\alpha, & \text{for } b(m) = 0. \end{cases} \tag{2.7}$$

A zero-mean Gaussian probability density function (pdf) of the random amplitude of impulsive noise is given by

$$p_N[n(m)] = \frac{1}{\sqrt{2\pi}\sigma_n} \exp\left\{-\frac{n^2(m)}{2\sigma_n^2}\right\}, \tag{2.8}$$

where σ_n^2 is the variance of the noise amplitude. In a Bernoulli-Gaussian model the pdf of impulsive noise, $n_i(m)$, is given as

$$p_N^{BG}[n_i(m)] = (1-\alpha)\delta[n_i(m)] + \alpha p_N[n_i(m)], \tag{2.9}$$

where $\delta[n_i(m)]$ is Kronecker delta function. Note that the function $p_N^{BG}[n_i(m)]$ is a mixture of a discrete probability mass function $\delta[n_i(m)]$ and a continuous pdf $p_N[n_i(m)]$.

Poisson-Gaussian model of impulsive noise

In a Poisson-Gaussian model the probability of occurrence of an impulsive noise event is modeled by a Poisson process, and the distribution of the random amplitude of impulsive noise is modeled by a Gaussian process. The Poisson process, as described in [41], is a random event-counting process. In a Poisson model, the probability of occurrence of k impulsive noise events in a time interval T is given by

$$P(k,T) = \frac{(\lambda T)^k}{k!} \mathrm{e}^{-\lambda T}, \tag{2.10}$$

where λ is a rate function with the following properties:

- Pr(one impulse in a small time interval Δt) $= \lambda \Delta t$
- Pr(zero impulse in a small time interval Δt) $= 1 - \lambda \Delta t$

It is assumed that no more than one impulsive noise event can occur in a time interval Δt. In a Poisson-Gaussian model, the pdf of impulsive noise, $n_i(m)$, in a small time interval Δt is given by

$$p_N^{PG}[n(m)] = (1-\lambda\Delta t)\delta[n_i(m)] + \lambda \Delta t p_N[n_i(m)], \tag{2.11}$$

where, as before, $p_N[n_i(m)]$ is the Gaussian pdf.

2.2 Impulsive noise models in PLC

As mentioned before, noise in power line communications is classified as background noise and impulsive noise. Background noise is stationary and can be modeled by the classical Gaussian distribution. To model impulsive noise, one can use many different models. However, the most widely used models have been derived from the two basic models introduced in Section 2.1.2. These models are the two-term mixture Gaussian and Midlenton's class-A impulsive noise models.

2.2.1 Two-term mixture Gaussian model of noise in PLC

In PLC, to simplify the system analysis, a simple noise model, namely the two-term mixture Gaussian impulsive noise, is normally used. The two-term mixture Gaussian model is based on the Bernoulli-Gaussian model as discussed in Section 2.1.2. The probability of occurrence of impulsive noise is a Bernoulli random process and its amplitude is controlled by a Gaussian distribution. The background noise is also modeled by another Gaussian distribution. Hence, the pdf of two-term mixture Gaussian impulsive noise is given by:

$$p_N(n) = (1-\epsilon)\mathcal{N}(0,\sigma^2) + \epsilon\mathcal{N}(0,\kappa\sigma^2), \tag{2.12}$$

where ϵ is the probability of impulsive noise occurrence, $\mathcal{N}(0,\sigma^2)$ is Gaussian distribution of zero mean and variance σ^2 that represents background noise, $\mathcal{N}(0,\kappa\sigma^2)$ models the impulsive noise component that is also Gaussian distribution but its variance is κ times bigger than that of background noise.

Although the two-term mixture Gaussian model is simple and it is frequently used for analyzing PLC systems [5–8], it does not provide a very accurate model of the real impulsive noise. Another model, which is more accurate than the two-term mixture Gaussian model and also widely used, is discussed in the next section.

2.2.2 Midlenton's class-A model of impulsive noise in PLC

A relatively simple model which incorporates background noise and impulsive noise based on the Poisson-Gaussian model is known as Midlenton's class-A impulsive noise model and it was first suggested in [9]. Because Midlenton's class-A impulsive noise model is more accurate and also meets all the basic requirements in modeling the real impulsive noise, this model has been used widely in performance analysis of PLC systems [11, 12, 16]. This thesis also relies on Midlenton's class-A to model impulsive noise and design communications systems over power lines.

Midelenton's class-A model uses the Poisson-Gaussian model to represent the background noise and impulsive noise. The occurrence probability of impulsive noise is modeled by a Poisson random process with the probability of having m impulsive noise events in a time interval T given by

$$P = \frac{(\lambda T)^m \mathrm{e}^{-\lambda T}}{m!}. \tag{2.13}$$

The amplitudes of both background and impulsive noise are modeled by Gaussian random processes. Let $A = \lambda T$ and call it the impulsive index. Then the probability density function of Midlenton's class-A impulsive noise is written as

$$p_A(n) = \sum_{m=0}^{\infty} \mathrm{e}^{-A} \frac{A^m}{m!} \frac{1}{2\pi\sigma_m^2} \exp\left(-\frac{|n|^2}{2\sigma_m^2}\right), \tag{2.14}$$

where $\sigma_m^2 = \sigma^2 \frac{m/A+\Gamma}{1+\Gamma}$ is the mth impulsive power, σ^2 is total noise power (including the powers of impulsive noise and Gaussian background noise), and $\Gamma = \sigma_G^2/\sigma_I^2$ is Gaussian-to-impulsive noise power ratio (GIR) with σ_G^2 and σ_I^2 are the powers of Gaussian and impulsive noise, respectively. When A is increased, the impulsiveness reduces and the noise comes closer to Gaussian noise. Equation (2.14) also shows that sources of impulsive noise have a Poisson distribution, and each impulsive noise source generates a characteristic Gaussian noise with a different variance. Let $N_0 = 2\sigma^2$ be the one-sided power spectral density of the total white noise. The pdf of class-A impulsive noise can be written as a function of A, Γ and N_0 as follows:

$$p_A(n) = \sum_{m=0}^{\infty} \mathrm{e}^{-A} \frac{A^m}{m!\pi N_0} \frac{A(1+\Gamma)}{m+A\Gamma} \exp\left[-\frac{A(1+\Gamma)}{m+A\Gamma}\frac{|n|^2}{N_0}\right]. \tag{2.15}$$

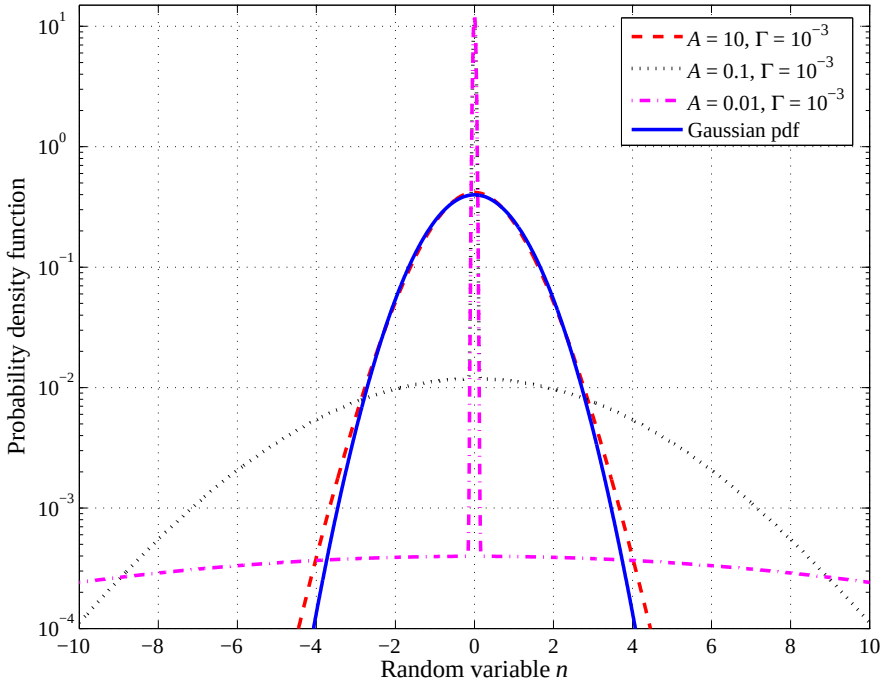

Figure 2.2: Pdf of the impulsive noise with different values of impulsive index A.

The effects of impulsive parameters A and Γ are illustrated in Figs. 2.2 and 2.3. As can be seen from in Fig. 2.2 when the GIR is kept constant to be $\Gamma = 10^{-3}$ and the impulsive index A is changed from a large to a small value, the characteristic distribution of impulsive noise changes from a Gaussian-like distribution to a really impulsive one. In particular, when $A = 10$, the distribution of impulsive noise comes very close to that of the corresponding Gaussian distribution. On the other hand, at $A = 0.01$, this distribution shows an impulsive characteristic. Similar observations can also be made when the impulsive index value A is kept constant while Γ is varying as shown in Fig. 2.3.

The characteristics of impulsive noise can also be clearly observed from the sample plots shown in Figs. 2.4 and 2.5. In particular, compared in Fig. 2.4 are the amplitude distributions of Gaussian noise and impulsive noise which have the same normalized variance of 1. The impulsive noise considered in this figure has parameters $\{A = 0.01,\ \Gamma = 10^{-3}\}$. Observe that the amplitudes of Gaussian noise samples take on many different values in a small range of $[-3, +3]$. On the other hand, almost all

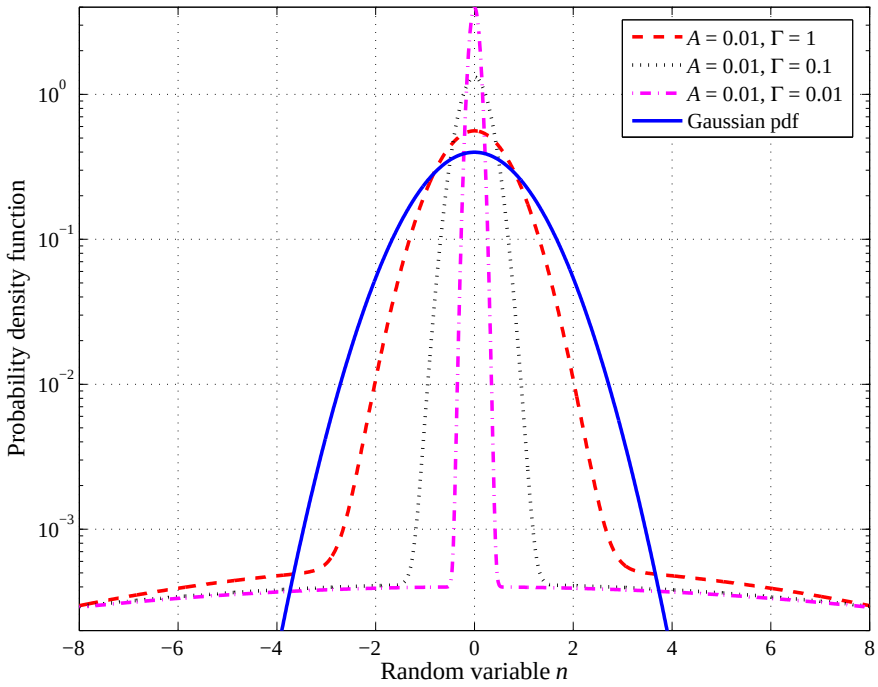

Figure 2.3: Pdf of the impulsive noise with different values of GIR Γ.

impulsive noise amplitudes distribute in a much narrower range, except some peaked samples with very high amplitudes reflecting the impulsiveness nature of the noise. Of course, the above observation about the amplitude distribution of the impulsive noise matches the pdf shown in Fig. 2.2. In other words, in the impulsive noise environment, background noise part with low amplitudes happens with a very high probability, whereas, impulsive noise part appears in much higher amplitudes with a very low probability.

Figures 2.4 and 2.5 also illustrate the effects of the impulsive noise parameters A and Γ to the amplitude distribution of class-A impulsive noise. Again, it can be seen that if A or Γ increases, the amplitude distribution of impulsive noise comes closer to that of Gaussian noise.

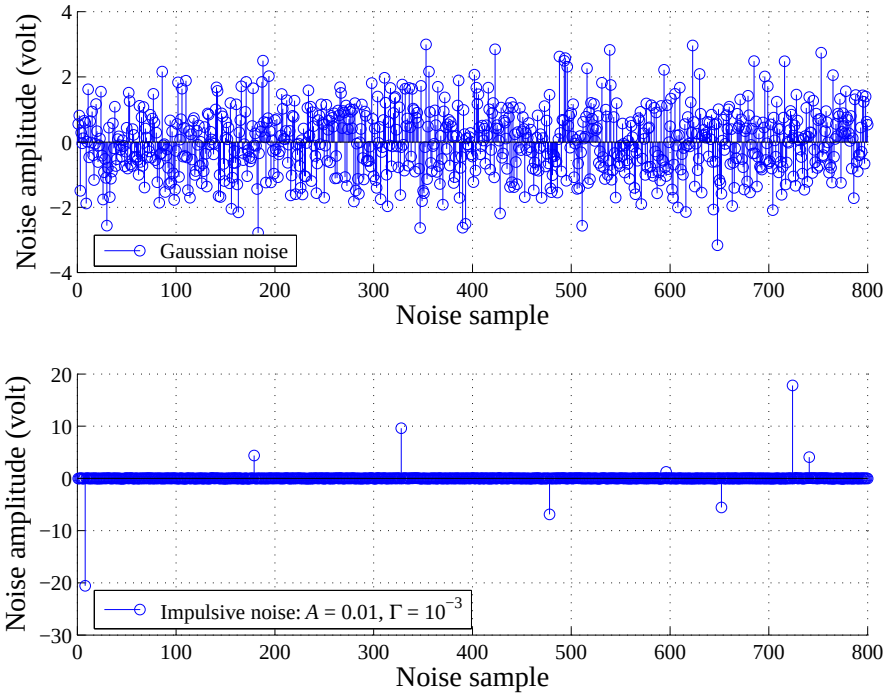

Figure 2.4: Examples of Gaussian noise and impulsive noise with $A = 0.01$, $\Gamma = 10^{-3}$.

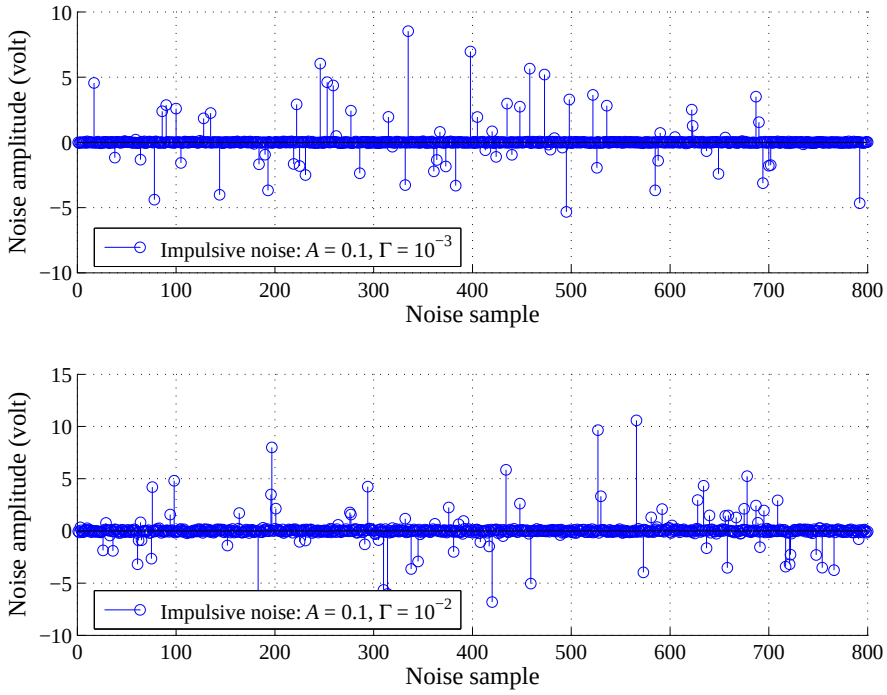

Figure 2.5: Examples of impulsive noise with $A = 0.1$ and two different values of Γ.

3. Techniques to combat impulsive noise

To combat impulsive noise, one can use many of the same techniques widely implemented for communication systems over Gaussian noise environment. However, as mentioned in previous chapters, the characteristic of impulsive noise is much different from that of classical Gaussian noise. In general, an optimal or suboptimal receiver designed for an additive white Gaussian noise (AWGN) channel normally does not work well for the systems disturbed by impulsive noise. Therefore, it is necessary to design new optimal or sup-optimal receivers for communications systems operating in impulsive noise environment.

This chapter reviews some of the most relevant techniques to combat impulsive noise. It also serves as the background in order to present and describe our contributions in Chapters 4 and 5.

3.1 Single-carrier quadrature amplitude modulation (QAM)

In digital communications, QAM is a modulation scheme that provides a high spectrum efficiency [42]. The performance analysis of QAM under class-A impulsive noise was first reported in [43]. However, this work only considers the effects of impulsive noise to the error performance of the QAM system employing a conventional receiver, i.e., the receiver designed for Gaussian noise. The results in [43] clearly demonstrates that performance of the QAM system with a conventional receiver is severely degraded when noise contains strong impulsiveness, i.e., when A or Γ is small.

In [11], the application of QAM for an impulsive noise channel was further studied. By explicitly considering class-A impulsive noise statistical characteristic, the authors in [11] propose an optimum receiver to combat impulsive noise more effectively. The main contributions of the work in [11] are reviewed in the following.

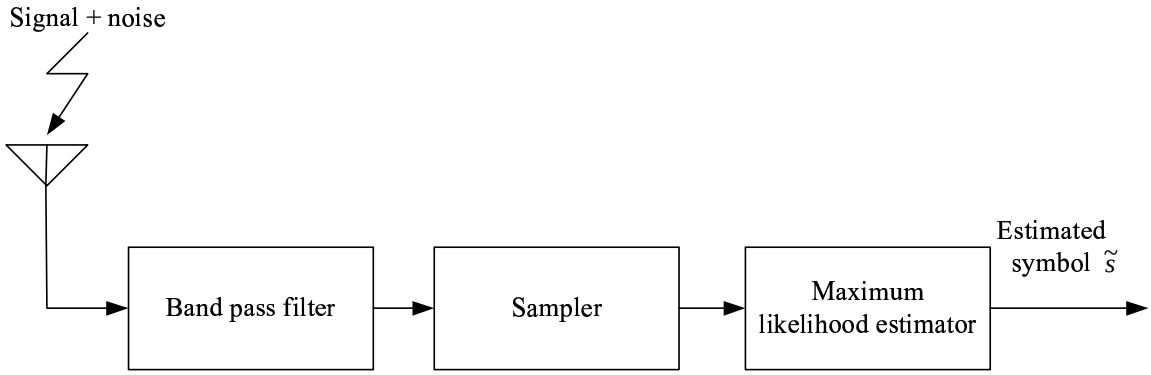

Figure 3.1: The receiver model of QAM.

The block diagram of a QAM receiver model of QAM over impulsive noise is illustrated in Fig. 3.1. If K samples are taken during one symbol duration, the received symbol $\mathbf{r}$ can be represented as:

$$\mathbf{r} \quad = \quad \{r_1, r_2, \ldots, r_K\}, \tag{3.1}$$

where r_k is the kth sample of the received symbol. In the following analysis, the K samples, $r_1, r_2, \ldots, r_K$, are assumed to be statistically independent.

Similarly, the transmitted symbol and additive class-A impulsive noise are described by $\mathbf{s} = \{s_1, s_2, \ldots, s_K\}$ and $\mathbf{n} = \{n_1, n_2, \ldots, n_K\}$, respectively.

The probability density function of $\mathbf{r} = \mathbf{s} + \mathbf{n}$, given that $\mathbf{s}$ was sent, is expressed as

$$p(\mathbf{r}|\mathbf{s}) = p(\mathbf{n} = \mathbf{r} - \mathbf{s}) = \prod_{k=1}^{K} p_A(r_k - s_k) \tag{3.2}$$

In general, the probability density given in (3.2) is called the "likelihood". A receiver based on the maximum likelihood detection selects the symbol that maximizes this equation for a given $\mathbf{r}$. The receiver with this strategy minimizes the symbol error probability, and in this sense, a receiver which performs maximum likelihood detection is called an optimum receiver. Substituting the pdf of the complex class-A impulsive noise in (2.14) into (3.2), one obtains the likelihood for class-A impulsive noise as

$$p(\mathbf{r}|\mathbf{s}) = \prod_{k=1}^{K} \sum_{m=0}^{\infty} \mathrm{e}^{-A} \frac{A^m}{m!} \frac{1}{2\pi\sigma_m^2} \exp\left(-\frac{|r_k - s_k|^2}{2\sigma_m^2}\right) \tag{3.3}$$

The receiver that performs maximum likelihood detection under class-A impulsive noise environment selects the symbol $\mathbf{s}$ that maximizes (3.3) as the transmitted one. Designing the receiver based on this complicated equation has a great difficulty. Under the condition that the impulsive index A is sufficiently small, the infinite sum in (3.3) can be approximated by the maximum value of its first three terms [11].

By using the above optimal or sub-optimal receiver, performance of the QAM systems designed for impulsive noise is much better than that using the conventional receiver and great performance improvement can be achieved. In particular, the authors in [11] report that in the case of $A = 0.1$ and $\Gamma = 10^{-3}$, the performance improvement is about 40 dB at the symbol error probability of 10^{-2}.

3.2 Orthogonal frequency division multiplexing (OFDM)

Another common method to improve the performance of PLC systems in the presence of impulsive noise is to use orthogonal frequency-division multiplexing (OFDM) technique. The basic principle behind OFDM is to use a properly chosen linear transform at the transmitter and its inverse transform at the receiver. The transmitted signal passes both transforms and is therefore unaffected, whereas the impulsive noise passes the receiver's transform only. The energy of individual impulses is therefore dispersed (or smeared) over the increased symbol duration [44, 45]. In this way, the error floor that is typical for uncoded transmission over impulsive noise channels [4] is partially eliminated.

Fig. 3.2 shows the simplified block diagram of an OFDM system. Let N be the number of subcarriers. In OFDM, the symbol stream after the M-ary modulator is passed through a serial-to-parallel converter, whose output is a set of N M-ary symbols $\{S_0, S_1, \ldots, S_{N-1}\}$ corresponding to the symbols transmitted over each of the subcarriers. In order to generate the transmitted signal, an inverse discrete Fourier transform (DFT) is performed on these N symbols. Typically, N is chosen to be a power of 2 and the DFT can be efficiently implemented using the inverse fast Fourier transform (IFFT) algorithm. The IFFT yields the OFDM symbol consisting of the

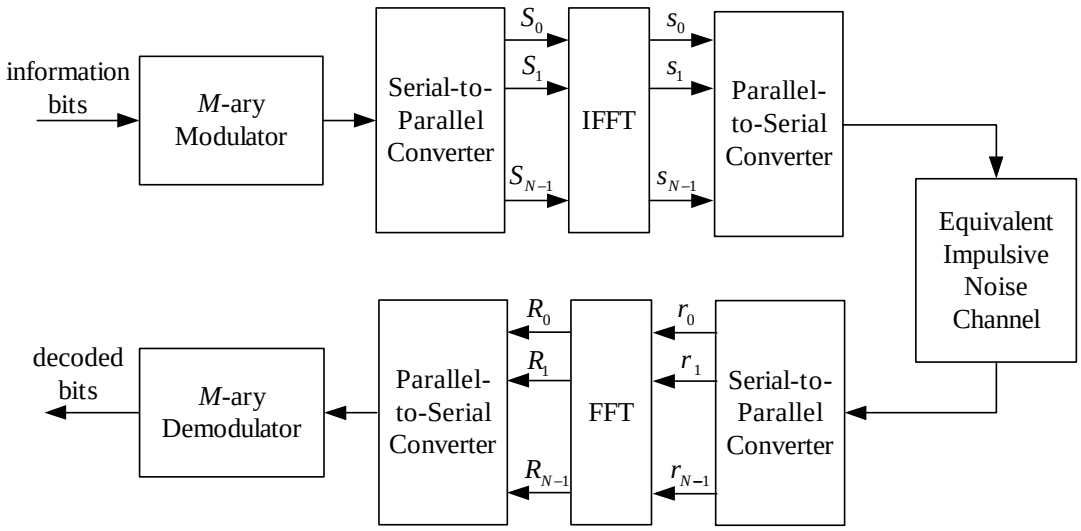

Figure 3.2: Block diagram of an OFDM system.

sequence $\{s_0, s_1, \ldots, s_{N-1}\}$ of length N, where

$$s_k = \frac{1}{\sqrt{N}} \sum_{i=0}^{N-1} S_i \mathrm{e}^{j2\pi ki/N}, \quad 0 \le k \le N-1. \tag{3.4}$$

Assuming perfect synchronization and timing, the received symbols after filtering and sampling can be expressed as,

$$r_k = s_k + n_k, \quad 0 \le k \le N-1, \tag{3.5}$$

where, as before, n_k is additive white complex class-A impulsive noise, whose pdf is given in (2.14).

Now at the receiver, the N-point FFT is first performed on the sequence $\{r_0, r_1, \ldots, r_{N-1}\}$ of N received symbols to yield:

$$\begin{aligned} R_k &= \frac{1}{\sqrt{N}} \sum_{i=0}^{N-1} r_i \mathrm{e}^{-j2\pi ki/N} \\ &= S_k + \tilde{n}_k, \quad 0 \le k \le N-1, \end{aligned} \tag{3.6}$$

where the noise samples $\{\tilde{n}_0, \tilde{n}_1, \ldots, \tilde{n}_{N-1}\}$ are simply the N-point FFT of the original impulsive noise samples $\{n_0, n_1, \ldots, n_{N-1}\}$. They are given by,

$$\tilde{n}_k = \frac{1}{\sqrt{N}} \sum_{i=0}^{N-1} n_i \mathrm{e}^{-j2\pi ki/N}, \quad 0 \le k \le N-1. \tag{3.7}$$

The outputs of FFT are then passed to the parallel-to-serial converter. Finally, the conventional M-ary demodulator is applied to demodulate each of the sample r_k, $0 \leq k \leq N-1$. Here the term "conventional M-ary demodulator" refers to the demodulator optimally designed for AWGN, i.e., by assuming that the noise $\tilde{n}_k$ in (3.6) and (3.7) is Gaussian.

The major difference between OFDM and the conventional single-carrier system is the characteristic of the additive noise. With FFT operation, the original impulsive noise is spread over N data symbols as in (3.6). As will be seen later, this is the main reason that OFDM can improve the error performance over the uncoded single-carrier system in impulsive noise.

3.3 Binary turbo coded modulation

With an excellent error performance due to iterative decoding, turbo code has been proved as one of the most potential candidate for single-carrier digital communication systems. The principles of turbo codes were first presented in [26] and clearly discussed in [23] for the classical Gaussian noise environment. Application of turbo codes to improve the error performance of communications systems corrupted by impulsive noise was recently investigated in [6, 12]. This section provides a brief discussion of the turbo coded system proposed in [12] to combat impulsive noise.

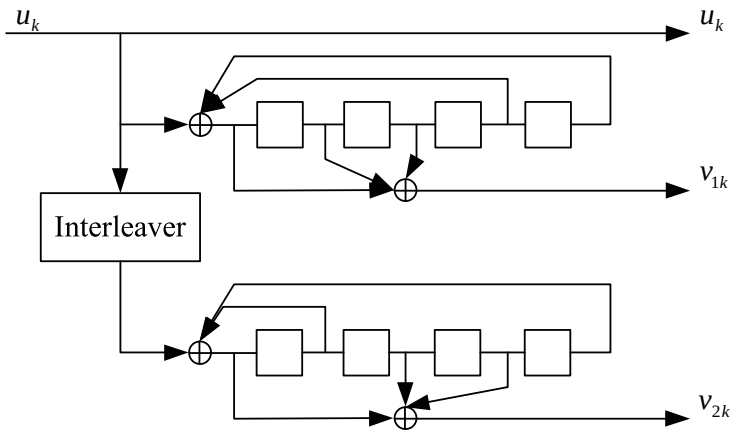

Figure 3.3: An example of turbo encoder with two identical RSC encoders.

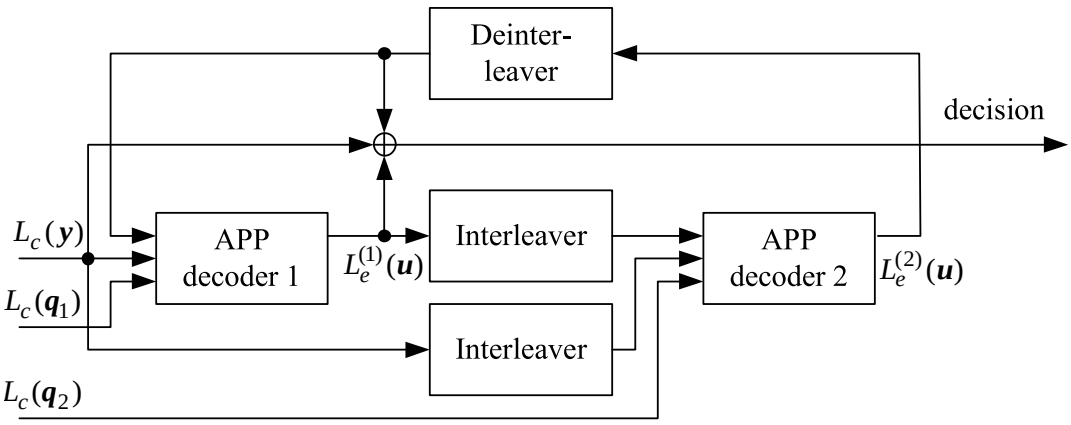

Figure 3.4: Turbo decoder.

Consider an example of turbo coded system where the encoder and the decoder are shown in Fig. 3.3 and Fig. 3.4, respectively. The turbo encoder employs two identical recursive systematic convolutional (RSC) codes. The output of the encoder includes $\mathbf{u} = \{u_1, \ldots, u_N\}$, $\mathbf{v}_1 = \{v_{11}, \ldots, v_{1N}\}$ and $\mathbf{v}_2 = \{v_{21}, \ldots, v_{2N}\}$. The interleaver in Fig. 3.3 is a random block interleaver of size N.

Denote the sequences of the match filter's outputs as $\mathbf{y} = \{y_1, \ldots, y_N\}$, $\mathbf{q}_1 = \{q_{11}, \ldots, q_{1N}\}$ and $\mathbf{q}_2 = \{q_{21}, \ldots, q_{2N}\}$ which correspond to $\mathbf{u}$, $\mathbf{v}_1$, $\mathbf{v}_2$, respectively. The decoder has two *a posteriori probability* (APP) decoders which correspond to the two RSC codes in the encoder. Each APP is either an optimal or suboptimal *maximum a posteriori* (MAP) decoder. More details about the MAP decoder and the calculation of the log likelihood ration (LLR) of the *a posteriori probability* can be found in [12, 26, 46–48].

In [12], the authors show that a decoder of a turbo coded system under the impulsive noise environment differs from that of the conventional one in computing the channel value L_c. In particular, the L_c for a turbo coded system disturbed by impulsive noise needs to take into account the distribution characteristic of class-A impulsive noise. Therefore the channel value L_c is computed as

$$L_c(y_k) = \ln \frac{P\{y_k | u_k = +1\}}{P\{y_k | u_k = -1\}} = \ln \frac{p_A(y_k - 1)}{p_A(y_k + 1)} \tag{3.8}$$

where $p_A(\cdot)$ is the pdf of class-A impulsive noise and given in (2.14).

The results in [12] show that the optimal or sub-optimal decoder implemented for impulsive noise can greatly improve the error performance of a turbo coded system over impulsive noise environment. For example, with channel parameters $\{A = 0.1,\ \Gamma = 0.1\}$, the performance improvement can reach 10dB coding gain at the bit error rate (BER) of 10^{-5}.

3.4 Iteratively-decoded OFDM

The technique discussed in this section is a linear transform defined over complex numbers as an encoding operation. The resulting codes are called *complex number* (CN) codes. CN codes might be used "stand alone". They can also be used as inner codes in a product encoding scheme where the outer code is optimized to increase the Euclidean distance between the codewords. This might be a good approach to design codes, providing both a good distance profile and a large Euclidean distance between the codewords. The simplified block diagram of a system using the CN codes is illustrated in Fig. 3.5.

In the literature, the principle of CN codes was first conceived in 1963 for the transmission over impulsive noise channels [44]. The principle of CN codes is also applied in a different area of communication theory. More importantly, orthogonal frequency-division multiplexing (OFDM) described in Section 3.2 can be interpreted as a special CN code where the generator matrix $\mathbf{G}$ is chosen to be the following inverse Fourier transform matrix:

$$\mathbf{G} = \frac{1}{\sqrt{N}} \begin{bmatrix} \mathrm{e}^{j\frac{2\pi}{N}\times 0\times 0} & \mathrm{e}^{j\frac{2\pi}{N}\times 0\times 1} & \dots & \mathrm{e}^{j\frac{2\pi}{N}\times 0\times (N-1)} \\ \mathrm{e}^{j\frac{2\pi}{N}\times 1\times 0} & \mathrm{e}^{j\frac{2\pi}{N}\times 1\times 1} & \dots & \mathrm{e}^{j\frac{2\pi}{N}\times 1\times (N-1)} \\ \dots & \dots & \dots & \dots \\ \mathrm{e}^{j\frac{2\pi}{N}\times (N-1)\times 0} & \mathrm{e}^{j\frac{2\pi}{N}\times (N-1)\times 1} & \dots & \mathrm{e}^{j\frac{2\pi}{N}\times (N-1)\times (N-1)} \end{bmatrix} \tag{3.9}$$

The classical OFDM receiver (see Section 3.2) is designed for the AWGN channel and, therefore, simply multiplies the received vector with $\mathbf{G}^{-1}$. Over impulsive noise

channels, this decoder disperses the energy of single impulses over several consecutive symbols, similar to smearing-filters approach. The typical argument is that this makes the transmission scheme robust against impulsive noise [45]. However, it is shown in [14, 19] that this "decoding" approach is highly suboptimal in terms of the achievable decoding error rates. This is because the rich structure of impulsive noise is not exploited in the decoding process.

The work in [20] proposes a decoder based on the turbo decoding principle and it is described in the following.

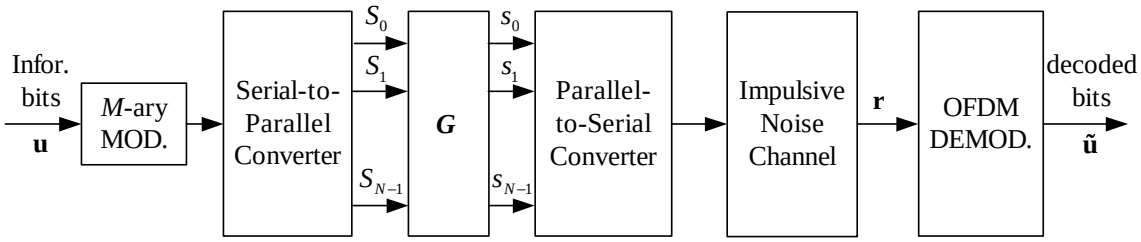

Figure 3.5: A simplified block diagram of the system using codes over *complex number*.

Let $\Psi \in \mathcal{C}$ denote the constellation, i.e., the discrete input alphabet with cardinality $|\Psi|$, where $\mathcal{C}$ denotes the complex numbers. Let $\mathbf{S} = \{S_0, \ldots, S_{N-1}\}$, $S_k \in \Psi$, denote the input to the CN encoder. We call the components S_k, $k = 0, \ldots, N-1$, the information symbols and assume that every $S_k \in \Psi$ is transmitted equally likely. Each vector $\mathbf{S}$ is encoded by a CN block code with codewords $\mathbf{s} = \{s_0, \ldots, s_{N-1}\}$ and code symbols $s_i \in \mathcal{C}$. Here and in the following we use capital letters to denote vectors or symbols in the domain of the information sequence (information domain) and lower case letters in the domain of the codewords (codeword domain). The encoding operation is defined by

$$\mathbf{s} = \mathbf{G} \times \mathbf{S} \tag{3.10}$$

The $N \times N$ generator matrix $\mathbf{G}$ is unitary and here is chosen as the inverse Fourier transform matrix. The sender transmits the code symbols over a memoryless additive impulsive noise channel. For ease of analysis, the channel impulsive noise was separated as back ground noise and impulsive noise. Hence the received symbols are

given by

$$r_k = s_k + i_k + g_k \tag{3.11}$$

where the g_k are independent and identically distributed (i.i.d.) zero mean complex Gaussian random variables with variance σ_g^2 and the following pdf:

$$p_{g_k}(x) = \frac{1}{2\pi\sigma_g^2} \exp\left(-\frac{|x|^2}{2\sigma_g^2}\right) \tag{3.12}$$

The impulsive noise i_k are also i.i.d. with variance σ_i^2. Its pdf is given by Middleton's class-A noise model.

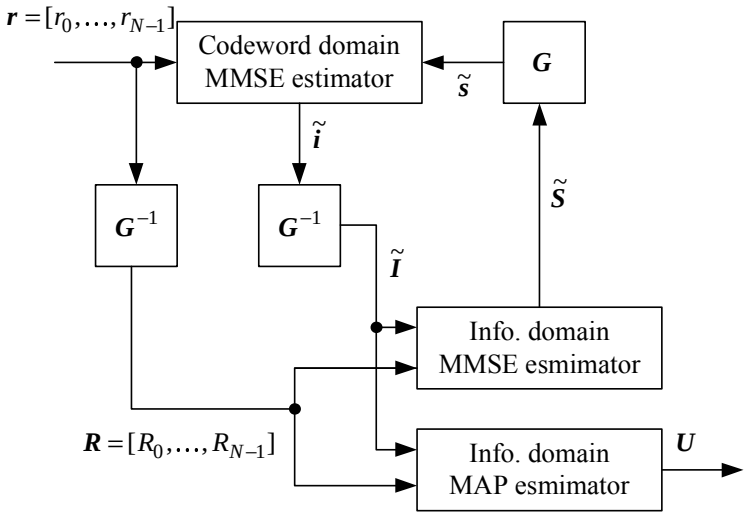

Figure 3.6: An iterative decoder of *codes over complex numbers*.

An iterative decoding algorithm is shown in Fig. 3.6. Unlike classical OFDM systems that treat impulsive noise at the receiver as Gaussian noise, the iterative decoder in [20] implements a sub-optimal decoding to estimate both impulsive noise and transmitted symbol. A detailed implementation of this iterative decoding is given in [20]. Here we only describe the most basic principles.

As depicted in Fig. 3.6, two information-exchanging estimators, one in the codeword and one in the information domain, are applied to obtain an estimate for the impulsive noise. Both estimators use only partial statistical information from their inputs which makes a low-complexity realization possible. The result from the iterative scheme is used to increase the reliability of the decision in the final decoding step. The decoded vector $\mathbf{U}$ is an estimate of the transmitted information vector $\mathbf{S}$.

To develop the estimators used in the algorithm shown in Fig. 3.6, knowledge about the statistical properties of their random input vectors is required. Since an exact description is too difficult, one can approximate the inputs by the simple linear model introduced in the following. First, consider the codeword domain. Using the independent random vectors $\mathbf{s}$, $\mathbf{i}$, and $\mathbf{g}$, any arbitrary random vector $\mathbf{y}$ of length N can be described by

$$\mathbf{y} = \tilde{\mathbf{y}} + \mathbf{e} = \alpha_s \mathbf{s} + \alpha_i \mathbf{i} + \alpha_g \mathbf{g} + \mathbf{e} \tag{3.13}$$

where $\mathbf{y} - \tilde{\mathbf{y}}$ is the error term of the linear model $\tilde{\mathbf{y}}$. The scalar coefficients $\alpha_s,\ \alpha_i,\ \alpha_g$ can be found by the least square regression estimation and $\mathbf{e}$ is the error vector. Similarly, for the information domain estimator, any arbitrary random vector $\mathbf{Y}$ of length N can be described by

$$\mathbf{Y} = \beta_s \mathbf{S} + \beta_i \mathbf{I} + \beta_g \mathbf{Z} + \mathbf{D} \tag{3.14}$$

Again, $\beta_s,\ \beta_i,\ \beta_g$ are scalar coefficients provided by the least square regression estimation, $\mathbf{Z}$ denotes the background Gaussian noise in the information domain and $\mathbf{D}$ is the error vector of the information domain estimator.

The detail information about the least square regression estimation is provided in Appendix A. With scalar coefficients and error estimation obtained from the least square regression estimation, the iterative decoding depicted in Fig. 3.6 is carried out to improve the performance of an OFDM system when the generator matrix $\mathbf{G}$ is chosen to be the inverse Fourier transform. As illustrated by simulation results in [20], the error performance is significantly improved by using this iterative decoding. Specifically, after 5 iterations the error performance can reach the Gaussian error bound, which means that impulsive noise can be completely eliminated.

Although all techniques to combat impulsive noise reviewed in this chapter are fairly common, they still have their own disadvantages. In particular, the uncoded techniques have a poorer error performance compared to the coded techniques. On the other hand, the coded techniques proposed so far do not give the best error performance nor good spectral efficiency. Hence, the next two chapters of this thesis

propose and analyze novel coded modulation techniques to combat impulsive noise more effectively. Superior performances of our proposed techniques compared to uncoded and coded techniques reviewed in this chapter will also be illustrated.

4. Bit-interleaved coded modulation with iterative decoding (BICM-ID)

According to the results from information theory, performance of a communications system with error control coding can be improved by increasing the codeword length. For a convolutional code or an equivalent block code formed from a convolutional code, the decoding performance is related to the constraint length of the code. Typically, one cannot benefit from using a long input data sequence, because the bits far apart on the trellis do not interact. Increasing the constraint length may bring significant improvement, but at the expense of exponentially increasing complexity in the maximum-likelihood (ML) decoding [29].

One clever way to circumvent the above dilemma is the recently proposed turbo coding scheme [26, 47], where two or more short-memory convolutional codes are concatenated in parallel or in serial through interleavers. Due to the pseudo-random interleaving, a global interaction is introduced among the bits over an entire block. As a result, error protection is achieved not only through the constraints on the local trellis transitions, but also through the influence of other trellis sections. Although a true ML decoder for such concatenated codes is hard to implement, iterative decoding methods which employ the maximum *a posteriori* probability (MAP) rule for each individual decoder have been shown to provide near-capacity performance [26, 46–48]. Compared with convolutional codes, turbo codes effectively take advantage of the potential of large block length but with the reasonable decoding complexity of the simple constituent codes.

A similar approach is to apply iterative decoding for the serial concatenation of encoding, bit-by-bit interleaving and high-order modulation. Unlike turbo codes, this scheme requires only one set of encoder/decoder; therefore, the receiver complexity

is significantly reduced. Moreover, by employing a high-order modulation a better bandwidth efficiency is achieved.

Motivated by the recent successes of BICM-ID in both AWGN and fading channels [25, 27, 30, 49, 50], one of the most important contributions of this thesis is to investigate the application of BICM-ID over an additive white class-A impulsive noise (AWAN) channel to improve the error performance as well as spectral efficiency of communications systems over impulsive noise environment in general, and PLC in particular.

4.1 System model

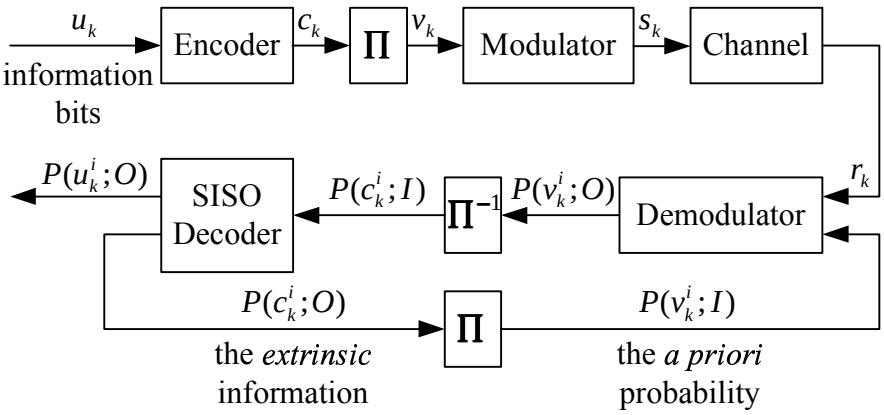

Figure 4.1: Block diagram of a BICM-ID system.

The transmitter of BICM-ID is a serial concatenation of a channel encoder, a bit interleaver Π and an M-ary memoryless modulator (where $M = 2^m$), as shown in Fig. 4.1. The information bits $\{u_k\}$ are first encoded by a convolutional code to produce a coded sequence $\{c_k\}$. The convolutional code should be chosen to be optimal in the sense that it gives the largest free Hamming distance d_H for a given code rate and constraint length. The coded sequence $\{c_k\}$ is then interleaved by the random interleaver Π. The pseudo-random interleaver permutes the encoded bits, as opposed to the channel symbols in the symbol-interleaved coded systems. The purpose of the interleaver is to break the effects of noise in one transmitted symbol and increase

the diversity order to the minimum Hamming distance d_H of the convolutional code. The interleaved sequence $\{v_k\}$ is mapped by the M-ary modulator into the symbol sequence $\{s_k\}$ for transmission. Each symbol s_k is chosen from a two-dimensional M-ary constellation Ψ according to some mapping rule $\mu(\cdot)$.

The baseband received signal over the kth symbol period can be written as:

$$r_k = s_k + n_k, \tag{4.1}$$

where n_k is impulsive noise. As discussed in Chapter 2, noise in PLC systems is impulsive in nature and Middleton's class-A model is commonly used to characterize the impulsive noise [4, 9, 11, 12]. The probability density function (pdf) of complex additive white class-A noise (AWAN) was discussed in Section 2.2.2. and can be written as a function of A, Γ and N_0 as follows:

$$p_A(n) = \sum_{m=0}^{\infty} \mathrm{e}^{-A} \frac{A^m}{m!\pi N_0} \frac{A(1+\Gamma)}{m+A\Gamma} \exp\left[-\frac{A(1+\Gamma)}{m+A\Gamma}\frac{|n|^2}{N_0}\right]. \tag{4.2}$$

At the receiver, the presence of bit-based interleaving makes the true maximum likelihood decoding of BICM too complicated to implement. Therefore the receiver in Fig. 4.1 uses a suboptimal, iterative method based on the soft input soft-output (SISO) demodulator and the SISO channel decoder. The SISO channel decoder uses the maximum *a posteriori* probability (MAP) algorithm in [47]. Similar to decoding of Turbo codes, here the demodulator and the channel decoder exchange the *extrinsic* information of the coded bits $P(v_k^i; O)$ and $P(c_k^i; O)$ through an iterative process.

In iterative processing, the feedback from the section which is less affected by the channel noise removes the ambiguity in the high-order demodulation and enhances the decoding of the weak data sections. With perfect knowledge of the other $m-1$ bits, an M-ary constellation, $M = 2^m$, is translated to binary modulation selected from $M/2 = 2^{m-1}$ possible sets of binary constellations. Therefore iterative decoding of BICM not only increases the intersubset Euclidean distance, but also reduces the number of nearest neighbors. This leads to a significant improvement over impulsive noise channels. Of course, if the feedback contains errors, wrong binary constellations

are chosen and this leads to the degradation of the system performance. This also explains why it is important to control well the feedback and the error propagation.

By using the soft-decision feedback in the iterative processing, it has been shown in [29] that the performance of BICM-ID can be further improved. It was also observed in [29] that the soft-decision feedback is the key to obtain coding gains in BICM while mitigating the error propagation. The detailed algorithm for the optimal soft-output demodulator, i.e., the MAP demodulator, is described in [29] for the case of an additive white Gaussian noise (AWGN) channel. For the channel disturbed by impulsive noise (i.e., AWAN channel), the optimal soft-output demodulator and its simplified version are devised in the next section.

4.2 Soft-output demodulators for AWAN channels

4.2.1 The optimal soft-output demodulator

Let $m = \log_2 M$ be the number of coded bits carried by one M-ary symbol. The *a posteriori* probabilities for coded bits can be computed as follows:

$$P(v_k^i = b|r_k) = \sum_{s_k \in \Psi_b^i} P(s_k|r_k) \sim \sum_{s_k \in \Psi_b^i} p(r_k|s_k)P(s_k), \tag{4.3}$$

where $i = \{1, 2, \cdots, m\}$, $b = \{0, 1\}$ and the signal subsets Ψ_b^i are defined as $\Psi_b^i = \{\mu([v_k^1, v_k^2, \cdots, v_k^m])|v_k^i = b\}$. The notation "$\sim$" indicates a replacement by an equivalent statistic. As in Fig. 4.1, denote $P(q; I)$ and $P(q; O)$ the *a priori* and *a posteriori* probabilities of random variable q, respectively. In the initial demodulation, assume that the symbols $\{s_i\}_{i=1}^M$ are equiprobable, i.e., $P(s_i) = \frac{1}{M}$, $i = 1, \ldots, M$. With this assumption, the demodulator computes the *extrinsic* probability $P(v_k^i; O)$ for each group of m coded bits per constellation symbol. After being deinterleaved, $P(v_k^i; O)$ becomes the *a priori* probability input $P(c_k^i; I)$ to the SISO decoder. The SISO decoder, in turn, calculates the *extrinsic* information $P(c_k^i; O)$ and $P(u_k^i; O)$. The hard decision is made from the knowledge of $P(u_k^i; O)$. Then $P(c_k^i; O)$ is re-interleaved and fed back as the *a priori* probability $P(v_k^i; I)$ for the next iteration.

Because an ideal interleaver makes m bits in one symbol independent, the *a priori* information $P(v_k^1; I), \cdots, P(v_k^m; I)$ can be assumed to be independent. Therefore, for each constellation symbol, the *a priori* probability is computed as:

$$\begin{aligned} P(s_k) &= P\left(\mu\left([v^1(s_k)\cdots v^m(s_k)]\right)\right) \\ &= \prod_{j=1}^{m} P(v_k^j = v^j(s_k); I), \end{aligned} \tag{4.4}$$

where $v^j(s_k)$ is the value of the jth bit in the label of symbol s_k. From the second iteration, the *extrinsic* information can be determined as follows:

$$\begin{aligned} P(v_k^i = b; O) &= \frac{P(v_k^i = b|r_k)}{P(v_k^i = b; I)} = \frac{\sum_{s_k \in \Psi_b^i} p(r_k|s_k) P(s_k)}{P(v_k^i = b; I)} \\ &= \sum_{s_k \in \Psi_b^i} p(r_k|s_k) \prod_{j \neq i} P(v_k^j = v^j(s_k); I) \end{aligned} \tag{4.5}$$

Equation (4.5) tells that one can calculate the *extrinsic* information for one bit by using the *a priori* probabilities of the other bits in the same channel symbol. Also, such calculation depends on the conditional probability density function $p(r_k|s_k)$. Concentrating on the case of two-dimensional constellation Ψ, the received signals and the constellation symbols are separated into imaginary and quadrature components.

Let $\{r_{k1}, r_{k2}\}$ and $\{s_{k1}, s_{k2}\}$ denote the two components of the received signal and constellation symbol at time k, respectively. Then $p(r_k|s_k)$ is given by:

$$\begin{aligned} p(r_k|s_k) &= p_A(r_k - s_k) = \sum_{m=0}^{\infty} \mathrm{e}^{-A} \frac{A^m}{m!} \frac{1}{\pi N_0} \frac{A(1+\Gamma)}{m + A\Gamma} \\ &\quad \times \exp\left[-\frac{A(1+\Gamma)}{m + A\Gamma} \frac{|r_k - s_k|^2}{N_0}\right], \end{aligned} \tag{4.6}$$

where $|r_k - s_k|^2 = (r_{k1} - s_{k1})^2 + (r_{k2} - s_{k2})^2$. Note that computing (4.6) involves infinite series of exponential functions and can be complicated. Similar to [12], for easy implementation the computation of $P(v_k^i = b; O)$ in (4.5) can be simplified as described in the following, which leads to a suboptimal soft-output demodulator.

4.2.2 The suboptimal soft-output demodulator

The *extrinsic* information can be computed in the log-domain as:

$$\lambda(v_k^i = b) = \ln\left\{P(v_k^i = b; O)\right\} = \ln\left\{ \sum_{s_k \in \Psi_b^i} \sum_{m=0}^{\infty} \mathrm{e}^{-A} \frac{A^m}{m!} \frac{1}{\pi N_0} \frac{A(1+\Gamma)}{m + A\Gamma} \times \right.$$
$$\left. \exp\left[-\frac{A(1+\Gamma)}{m+A\Gamma} \frac{|r_k - s_k|^2}{N_0}\right] \prod_{j \neq i} P(v_k^j = v^j(s_k); I) \right\} \tag{4.7}$$

Define

$$\delta_m(|r_k - s_k|) = \left[-\frac{A(1+\Gamma)}{m+A\Gamma} \frac{|r_k - s_k|^2}{N_0}\right]$$
$$+ \ln\left[\mathrm{e}^{-A} \frac{A^m}{m!} \frac{1}{\pi N_0} \frac{A(1+\Gamma)}{m+A\Gamma} \prod_{j \neq i} P(v_k^j = v^j(s_k); I)\right]. \tag{4.8}$$

Then (4.7) can be rewritten as:

$$\lambda(v_k^i = b) \;=\; \ln\left[\sum_{s_k \in \Psi_b^i} \sum_{m=0}^{\infty} \mathrm{e}^{\delta_m(|r_k - s_k|)} \right]. \tag{4.9}$$

Equation (4.9) can then be approximated in a much simpler manner by using the following Jacobian algorithm [12, 46]:

$$\begin{aligned} \ln(\mathrm{e}^a + \mathrm{e}^b) &= \max(a,b) + \ln(1 + \mathrm{e}^{-|a-b|}) \\ &= \max(a,b) + f_c(|a-b|), \end{aligned} \tag{4.10}$$

where $f_c(x) = \ln(1 + \mathrm{e}^{-x})$ is the correction function. This correction function can be approximated, precomputed and stored in a look-up table. In this thesis, the look-up table is determined by 10 integer values of x between 0 and 9.

4.3 Lower bound on the BER performance

Owing to the large coding gain produced by the iterative process, one is most interested in the asymptotic performance to which the iterative processing converges. This asymptotic performance can be analyzed with the error-free-feedback bound when the optimal soft-output demodulator is employed. The error-free-feedback bounds for

BICM-ID systems under Gaussian noise and Rayleigh fading channels were obtained in [29, 36]. Here, the error bound is derived for BICM-ID systems under AWAN. The derived bound is then used to evaluate different mappings of a given M-ary modulation.

In general, the union bound on the bit error rate (BER) of a BICM-ID with a convolutional code of rate k_c/n_c, a constellation Ψ, and labelling μ is given by:

$$P_b \leq \frac{1}{k_c} \sum_{d=d_H}^{\infty} \beta_d f(d, \Psi, \mu), \tag{4.11}$$

where β_d is the total information weight of all the error events at Hamming distance d and d_H is the minimum free Hamming distance of the code. The function $f(d, \Psi, \mu)$ is the average pairwise error probability, which depends on the mapping μ, the constellation Ψ and the Hamming distance d.

Let $\mathbf{c}$ and $\breve{\mathbf{c}}$ denote the input and estimated sequences with Hamming distance d between them. Let $\mathbf{x}$ and $\breve{\mathbf{x}}$ represent the signal sequences corresponding to $\mathbf{c}$ and $\breve{\mathbf{c}}$ respectively. Also without loss of generality, assume that $\mathbf{c}$ differs from $\breve{\mathbf{c}}$ in the first d consecutive bits. Thus $\mathbf{x}$ and $\breve{\mathbf{x}}$ can be considered to have a length of d M-ary symbols. That is $\mathbf{x} = [x_1, x_2 \cdots x_d]$ and $\breve{\mathbf{x}} = [\breve{x}_1, \breve{x}_2 \cdots \breve{x}_d]$. To obtain the function $f(d, \Psi, \mu)$, one needs to compute the pairwise error probability (PEP), $P(\mathbf{x} \to \breve{\mathbf{x}})$, which is the probability that the receiver makes a decision on $\breve{\mathbf{x}}$ given that $\mathbf{x}$ was transmitted. Following the same notations in [14], define $\Omega := w(\breve{\mathbf{x}}, \mathbf{r}) - w(\mathbf{x}, \mathbf{r})$, where $w(\mathbf{x}, \mathbf{r})$ is defined as the following additive decoding metric for a codeword of length d:

$$w(\breve{\mathbf{x}}, \mathbf{r}) = \sum_{l=1}^{d} \ln \left[\sum_{m=0}^{\infty} \frac{\alpha_m}{2\pi\sigma_m^2} \exp\left(-\frac{|r_l - x_l|^2}{2\sigma_m^2} \right) \right], \tag{4.12}$$

with $\alpha_m = \mathrm{e}^{-A} \frac{A^m}{m!}$ and, as before, $\sigma_m^2 = \frac{N_0}{2} \frac{m + A\Gamma}{A(1+\Gamma)}$. The PEP can then be calculated as:

$$P(\mathbf{x} \to \breve{\mathbf{x}}) = P(\Omega > 0 | \mathbf{x}) = \int_0^{\infty} p(\Omega = \zeta | \mathbf{x}) d\zeta. \tag{4.13}$$

Using the Chernoff bounding technique, this PEP can be upper-bounded by:

$$P(\mathbf{x} \to \breve{\mathbf{x}}) \;\; \leq \;\; \min_{\lambda} \prod_{l=1}^{d} C(x_l, \breve{x}_l, \lambda), \tag{4.14}$$

where $C(x_l, \breve{x}_l, \lambda)$ is the Chernoff factor, given as:

$$C(x_l, \breve{x}_l, \lambda) = \int_{-\infty}^{\infty} \mathrm{e}^{\lambda[\tilde{\omega}(\breve{x}_l, r_l) - \tilde{\omega}(x_l, r_l)]} p(r_l|x_l) dr_l, \tag{4.15}$$

with $\tilde{\omega}(x_l, r_l) = \ln p_A(r_l - x_l)$ and $\tilde{\omega}(\breve{x}_l, r_l) = \ln p_A(r_l - \breve{x}_l)$. Since the optimal demodulator is assumed, the Chernoff factor can be minimized with $\lambda = 1/2$, and as in [14], it is given by:

$$\begin{aligned} C(d_l) \;\; := \;\; C(x_l, \breve{x}_l, 1/2) = \frac{1}{2\pi} \times \int_{-\infty}^{\infty} \int_{-\infty}^{\infty} \sqrt{\sum_{m=0}^{\infty} \frac{\alpha_m}{\sigma_m^2} \exp\left[-\frac{(x - d_l/2)^2 + y^2}{2\sigma_m^2} \right]} \\ \times \sqrt{\sum_{m=0}^{\infty} \frac{\alpha_m}{\sigma_m^2} \exp\left[-\frac{(x + d_l/2)^2 + y^2}{2\sigma_m^2} \right]} dxdy, \end{aligned} \tag{4.16}$$

where $d_l := |x_l - \breve{x}_l|$ denotes the Euclidean distance between the two M-ary symbols x_l and $\breve{x}_l$.

Now the function $f(d, \Psi, \mu)$ can be obtained by averaging the PEP over all possible sequences $\mathbf{x}$ and $\breve{\mathbf{x}}$. Due to the success of iterative processing, one needs to consider only the pairs of signal symbols x_l and $\breve{x}_l$ whose labels differ in only 1 bit [29, 36]. Under the assumption that d_l is an i.i.d discrete random variable, $f(d, \Psi, \mu)$ can be bounded as follows:

$$f(d, \Psi, \mu) = E\{P(\mathbf{x} \to \breve{\mathbf{x}})\} \leq \prod_{l=1}^{d} E\{C(d_l)\} = [E\{C(d_l)\}]^d. \tag{4.17}$$

For each signal symbol $s_i \in \Psi$, let $s_{j(i,k)}$, where $k = 1, \ldots, m$, denotes the signal symbol whose label differs at position k compared to that of s_i. Then a direct and brute-force way to evaluate $E\{C(d_l)\}$ for any signal constellation and mapping is as follows:

$$\begin{aligned} E\{C(d_l)\} \;\; = \;\; \frac{1}{m2^m} \sum_{i=1}^{2^m} \sum_{k=1}^{m} \int_{-\infty}^{\infty} \int_{-\infty}^{\infty} \sqrt{\sum_{m=0}^{\infty} \frac{\alpha_m}{2\pi\sigma_m^2} \exp\left[-\frac{\left(x - |s_i - s_{j(i,k)}|/2\right)^2 + y^2}{2\sigma_m^2} \right]} \\ \times \sqrt{\sum_{m=0}^{\infty} \frac{\alpha_m}{2\pi\sigma_m^2} \exp\left[-\frac{\left(x + |s_i - s_{j(i,k)}|/2\right)^2 + y^2}{2\sigma_m^2} \right]} dxdy. \end{aligned} \tag{4.18}$$

However, for given signal constellation and mapping scheme, the probability mass function (pmf), $P(d_l)$, of the discrete random variable d_l can be easily obtained and $E\{C(d_l)\}$ is simply obtained by averaging $C(d_l)$ over such a pmf. For example, Table 4.1 tabulates the pmfs of d_l for different mapping schemes, namely Gray, set partitioning (SP) and semi set partitioning (SSP) mappings, of 8PSK (phase-shift keying) constellation as shown in Fig. 4.2. Such constellation and mappings will also be used in Section 4.6 to illustrate the error performance of BICM-ID.

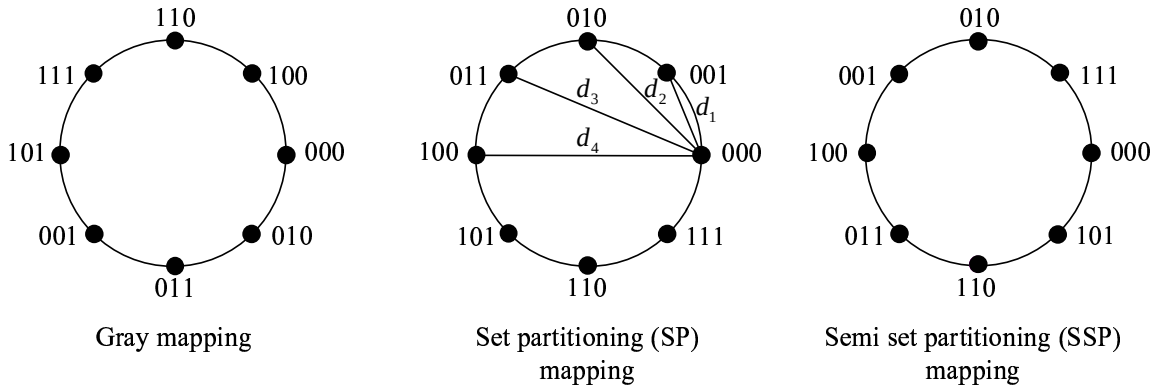

Figure 4.2: 8PSK with different mapping schemes.

Table 4.1: Pmfs of d_l for 8PSK and different mappings.

d_l	Gray mapping	SP mapping	SSP mapping
d_1	2/3	1/3	0
d_2	0	1/3	1/3
d_3	1/3	0	1/3
d_4	0	1/3	1/3

4.4 Convergence analysis with EXIT chart

It should be pointed out that the asymptotic error performance derived in the previous section only provides the asymptotic performance of BICM-ID. It, however, does not tell us how the iteration performance converges to this asymptotic performance. Nevertheless, as observed in [32, 38, 51], the convergence behavior of

iterative decoding in BICM-ID systems can be efficiently predicted by using the extrinsic information transfer (EXIT) chart. Hereafter, the EXIT chart obtained with the histogram method is investigated for BICM-ID over AWAN channels.

Following the same notations in [32,38,51], let A_1 and A_2 denote the log-likelihood values of the *a priori* information of the coded bits at the inputs of the demodulator and the SISO decoder, respectively. Similarly, let E_1 and E_2 denote the log-likelihood values of the *extrinsic* information at the outputs of the demodulator and the SISO decoder, respectively. Also let I_{A_1}, I_{A_2}, I_{E_1} and I_{E_2} represent the mutual information of the random variables A_1, A_2, E_1 and E_2, respectively. To compute this mutual information, one needs to know the distribution of each corresponding random variable. For a BICM-ID system disturbed by a real impulsive noise n, given the observation z and a coded bit X_1, the A_1-value can be computed as follows:

$$\begin{aligned} A_1 &= \ln\left\{\frac{p_A(z|v_k=1)}{p_A(z|v_k=0)}\right\} \\ &= \ln\left\{\frac{\sum_{m=0}^{\infty}\mathrm{e}^{-A}\frac{A^m}{m!}\sqrt{\frac{1}{\pi N_0}\frac{A(1+\Gamma)}{m+A\Gamma}}\exp\left(-\frac{A(1+\Gamma)}{m+A\Gamma}\frac{(z-1)^2}{N_0}\right)}{\sum_{m=0}^{\infty}\mathrm{e}^{-A}\frac{A^m}{m!}\sqrt{\frac{1}{\pi N_0}\frac{A(1+\Gamma)}{m+A\Gamma}}\exp\left(-\frac{A(1+\Gamma)}{m+A\Gamma}\frac{z^2}{N_0}\right)}\right\} \\ &= \ln\left\{\sum_{m=0}^{\infty}\frac{A^m}{m!}\sqrt{\frac{A(1+\Gamma)}{m+A\Gamma}}\exp\left(-\frac{A(1+\Gamma)}{m+A\Gamma}\frac{(z-1)^2}{N_0}\right)\right\} \\ &\quad -\ln\left\{\sum_{m=0}^{\infty}\frac{A^m}{m!}\sqrt{\frac{A(1+\Gamma)}{m+A\Gamma}}\exp\left(-\frac{A(1+\Gamma)}{m+A\Gamma}\frac{z^2}{N_0}\right)\right\}, \end{aligned} \tag{4.19}$$

where $z = X_1 + n$. Moreover, (4.19) can also be approximated by the Jacobian algorithm as follows. First, define

$$\kappa_m(x) = \left[-\frac{A(1+\Gamma)}{m+A\Gamma}\frac{x^2}{N_0}\right] + \ln\left[\frac{A^m}{m!}\sqrt{\frac{A(1+\Gamma)}{m+A\Gamma}}\right]. \tag{4.20}$$

Then (4.19) becomes:

$$\begin{aligned} A_1 &= \ln\left(\sum_{m=0}^{\infty}\mathrm{e}^{\kappa_m(z-1)}\right) - \ln\left(\sum_{m=0}^{\infty}\mathrm{e}^{\kappa_m(z)}\right) \\ &= \max_{m=0,\cdots,\infty}\{\kappa_m(z-1)\} - \max_{m=0,\cdots,\infty}\{\kappa_m(z)\} \\ &\quad + f_c(z-1) - f_c(z), \end{aligned} \tag{4.21}$$

where $f_c(\cdot)$ is the correction function defined in Section 4.2.

With the A_1-value computed from (4.21) or (4.19), the pdf of the random variable A_1 can be conveniently determined by means of Monte Carlo simulation. With this distribution of A_1, the mutual information $I_{A_1} = I(X_1; A_1)$ between the coded bit X_1 and the A_1-value is:

$$I_{A_1} = \frac{1}{2} \sum_{b=0}^{1} \int_{-\infty}^{\infty} p_{A_1}(\xi | X_1 = b) \log_2 \left[\frac{2 \times p_{A_1}(\xi | X_1 = b)}{p_{A_1}(\xi | X_1 = 0) + p_{A_1}(\xi | X_1 = 1)} \right] d\xi. \quad (4.22)$$

Similarly, the mutual information $I_{E_1} = I(X_1; E_1)$ that quantifies the extrinsic information E_1 at the output of the demodulator can be calculated with the pdf of the random variable E_1, which is also determined by the histogram method. Viewing I_{E_1} as a function of I_{A_1} and E_b/N_0, the extrinsic transfer characteristic of the demodulator is defined as:

$$I_{E_1} = T_1(I_{A_1}, E_b/N_0). \quad (4.23)$$

Equation (4.23) shows that the demodulator transfer characteristic not only depends on the E_b/N_0-value, but also the mapping scheme via I_{A_1}. Specifically, different mapping schemes result in different slopes of the transfer characteristics.

On the other hand, the transfer characteristic of the SISO decoder is defined as:

$$I_{E_2} = T_2(I_{A_2}). \quad (4.24)$$

Thus, the function T_2 represents the mutual information between the *a priori* knowledge A_2 and the *extrinsic* information E_2 of the SISO decoder. This relationship depends only on the convolutional code used in the system, not on the mapping scheme nor the value of E_b/N_0. To compute A_2 and its mutual information I_{A_2}, as well as E_2 and its mutual information I_{E_2}, one can follow a similar process as demonstrated above for the demodulator's transfer characteristic. Also note that, the pdfs of the random variables A_2 and E_2 can also be obtained by Monte Carlo simulation.

To visualize the exchange of the extrinsic information, the demodulator and decoder characteristics are depicted in a single diagram, which is commonly referred

to as the extrinsic information transfer (EXIT) chart [32]. Note that, after being deinterleaved, the *extrinsic* information of the demodulator becomes the *a priori* knowledge to the SISO decoder, i.e., $I_{A_2} = I_{E_1}$. Similarly, the *extrinsic* information of the SISO decoder, I_{E_2}, is interleaved to become the *a priori* knowledge, I_{A_1}, for the demodulator in the next iteration. The transfer characteristics of the individual demodulator and decoder blocks should approximately describe the true behavior of the iteration process in the demodulation/decoding of BICM-ID over an AWAN channel. In particular, the convergence behavior of the iterative receiver can be predicted by following the demodulation/decoding trajectory in the EXIT chart. Applying EXIT chart analysis for some specific BICM-ID systems under AWAN will be presented in Section 4.6.

4.5 Gaussian bound on the error performance over an AWAN channel

The "Gaussian bound" is derived by assuming that only the Gaussian noise is present on the channel, i.e., the impulsive noise part is set to zero or completely removed. The "Gaussian bound" is useful since it serves as a lower bound for any scheme. It also indicates how well a particular scheme, such as BICM-ID, combats impulsive noise. Under the assumption of zero impulsive noise, the received symbols can be written as

$$r_k = s_k + g_k, \tag{4.25}$$

where g_k are i.i.d. zero mean complex Gaussian random variables with variance σ_g^2 given by

$$\sigma_g^2 = \frac{\sigma^2}{1 + 1/\Gamma} = \frac{\sigma^2 \Gamma}{1 + \Gamma}, \tag{4.26}$$

Again, here σ^2 is the total power of the noise and Γ is the Gaussian to impulsive noise power ratio. The pdf of g_k is given

$$p_g(x) = \frac{1}{2\pi\sigma_g^2} \exp\left(-\frac{|g|^2}{2\sigma_g^2}\right) \tag{4.27}$$

For the uncoded communications system, the uncoded "Gaussian bound" is simply

the performance of uncoded BPSK modulation over a classical AWGN channel with noise variance as in (4.26). Hence, this bound is given by

$$P_{uncoded-bound} = Q\left(\frac{\sqrt{E_b}}{\sigma_g}\right), \tag{4.28}$$

where the Q function is defined as

$$Q(x) = \frac{1}{\sqrt{2\pi}} \int_x^\infty \mathrm{e}^{-t^2/2} dt \tag{4.29}$$

For BICM-ID, the Gaussian bound is derived similarly by assuming that the system is only corrupted by the background Gaussian noise with pdf and variance given in Equations (4.27) and (4.26), respectively. At the receiver, the conditional probability density function $p(r_k|s_k)$ used in the SISO demodulator is

$$p(r_k|s_k) \;\; = \;\; p_G(r_k - s_k) = \frac{1}{2\pi\sigma_g^2} \exp\left(-\frac{|r_k - s_k|^2}{2\sigma_g^2}\right), \tag{4.30}$$

With this conditional pdf, the iterative decoding can be carried out at the receiver to obtain the BICM-ID Gaussian bounds, which will be presented and discussed in Section 4.7.

4.6 Simulation and numerical results

Although any channel coding and constellation/mapping schemes can be used in the BICM-ID systems proposed in this chapter, this section concentrates on studying the error performance of a BICM-ID system employing 8PSK modulation and a 4-state rate-2/3 convolutional code, whose generator polynomials are $\mathbf{G} = [1001; 0001; 1100]$. This combination of channel code and modulation scheme yields a spectral efficiency of 2 bits/sec/Hz. Each information block has a length of 3999 bits. Three different mapping schemes shown in Fig. 4.2 are considered. Unless stated otherwise, in all simulation results reported in this thesis, at least 100 erroneous bits are counted to determine each BER point.

First, Fig. 4.3 compares the bit error rate (BER) performance of BICM-ID system employing 8PSK/SSP mapping for two different demodulators. The first demodulator, referred to as the "standard" demodulator, is the optimal demodulator for an

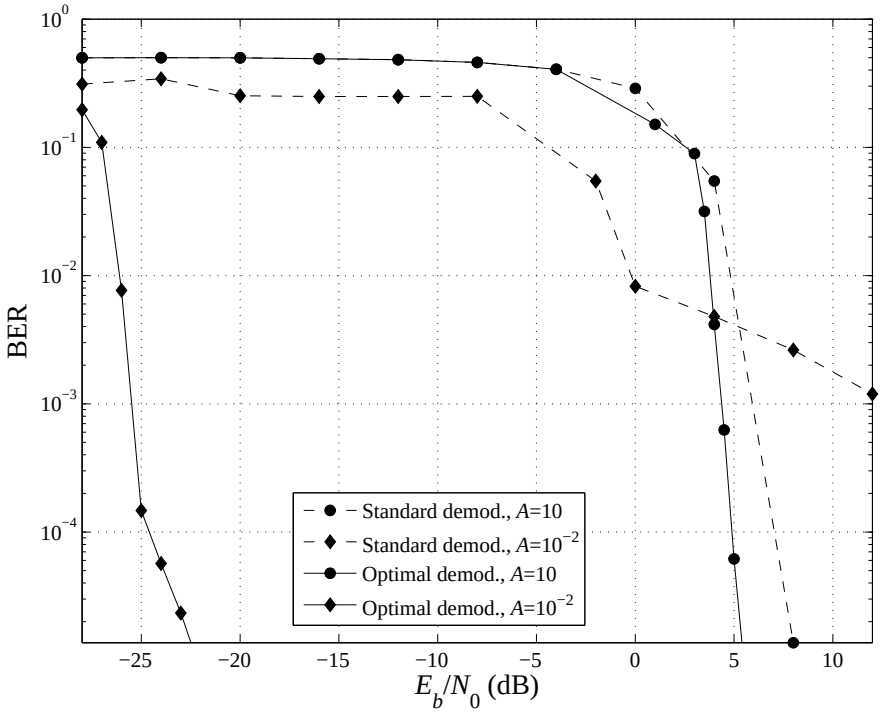

Figure 4.3: BER performance with 9 iterations of 8PSK/SSP mapping for BICM-ID over an AWAN channel: Comparison of different demodulators with different impulsive index parameters, $\Gamma = 10^{-3}$.

AWGN channel. The other demodulator is the one optimally designed for AWAN channels as described in Section 4.2. The comparison is investigated for two impulsive parameters of $A = 10$ and $A = 10^{-2}$ whereas the GIR parameter is fixed at $\Gamma = 10^{-3}$.

At the BER level of 10^{-3} one can observe a huge SNR gain of approximately 38dB by using the optimal demodulator over the standard one for AWAN channel parameters $\{A = 10^{-2}, \Gamma = 10^{-3}\}$.[1] When AWAN channel parameters are $\{A = 10, \Gamma = 10^{-3}\}$ the SNR gains are 2dB and 3dB at BER of 10^{-3} and 10^{-5}, respectively. These substantial gains thus clearly illustrate the advantage of having the optimal demodulator for BICM-ID in an impulsive noise environment. One can also expect the reduction of SNR gain when the impulsive index A increases. This is because when A is large enough (i.e., $A \geq 1$), the impulsive noise statistic comes close to

[1]Here, the SNR is defined as E_b/N_0, where E_b is the energy per information bit.

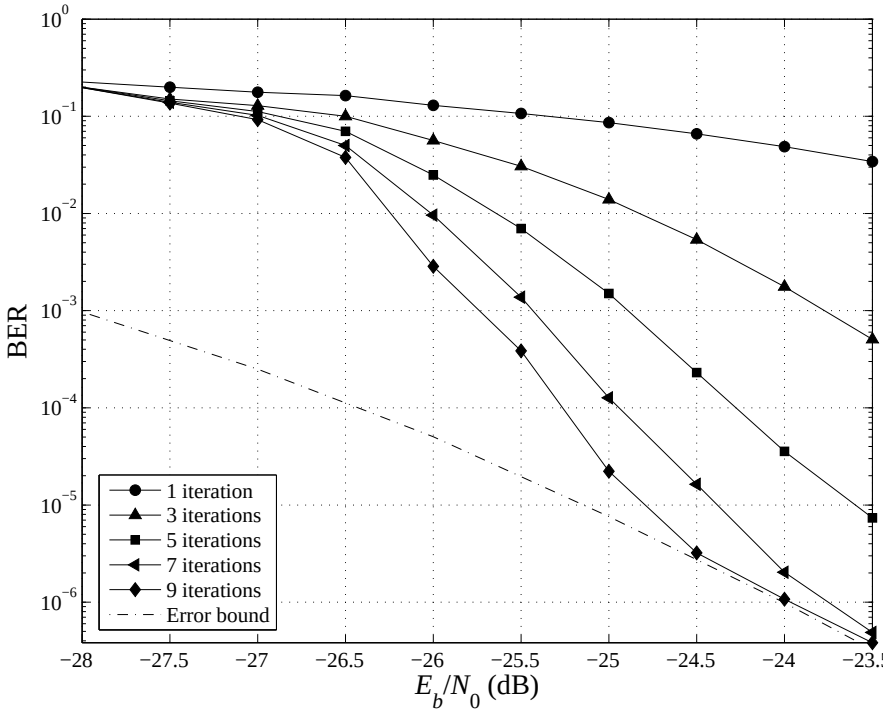

Figure 4.4: BER performance of BICM-ID over an AWAN channel with $A = 10^{-3}$ and $\Gamma = 10^{-3}$: 8PSK and SSP mapping.

that of Gaussian noise and there is not much difference in performance by using the optimal and standard demodulators.

Next, Fig. 4.4 shows the BER performance of 8PSK/SSP mapping when the parameters of impulsive noise channel are $\{A = 10^{-3}, \Gamma = 10^{-3}\}$, which means that the channel noise is highly impulsive. Also shown in the figure is the asymptotic performance bound, calculated as described in Section 4.3 by using the first 20 Hamming distances of the convolutional code. As can be seen from the figure, performance improvement due to iterations is very significant with SSP mapping. In particular, Fig. 4.4 shows that with 9 iterations the BER performance of 8PSK/SSP mapping can reach the error bound at SNR of -24.5dB, and starting at SNR of -23.5dB the error performance of 7, 8 and 9 iterations are practically the same and also reach the asymptotic performance bound.

Similarly, Fig. 4.5 shows the BER performance of 8PSK employing SP mapping.

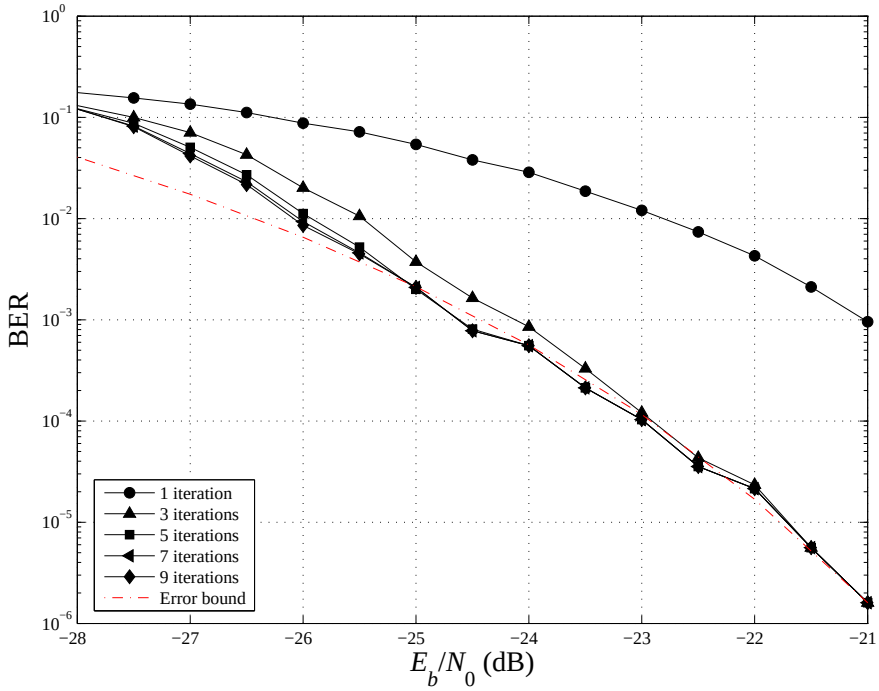

Figure 4.5: BER performance of BICM-ID over an AWAN channel with $A = 10^{-3}$ and $\Gamma = 10^{-3}$: 8PSK and SP mapping.

The parameters of impulsive noise channel are $\{A = 10^{-3}, \Gamma = 10^{-3}\}$ for this case. As shown in this figure, with SP mapping, iteration can also help to improve the error performance of BICM-ID. For example, after 5 iterations, a gain of 3.5dB in SNR can be obtained at the BER level of 10^{-3}. However, the iteration process in 8PSK/SP mapping does not improve the error performance as much as compared to 8PSK/SSP mapping. The error performance of BICM-ID with 8PSK/SP mapping also converges faster than that of BICM-ID with 8PSK/SSP mapping. Fig. 4.5 illustrates that after 5 iterations the iterative decoding does not improve the error performance any more.

The error performance of BICM-ID with 8PSK/Gray mapping is also shown in Fig. 4.6, where the impulsive noise parameters are $\{A = 10^{-3}, \Gamma = 10^{-2}\}$. Similar to the cases of AWGN and fading channels, it was observed that iterations do not improve BER performance for Gray mapping of BICM-ID in impulsive noise.

Figs. 4.7, 4.8 and 4.9 explicitly compare the error performance of different map-

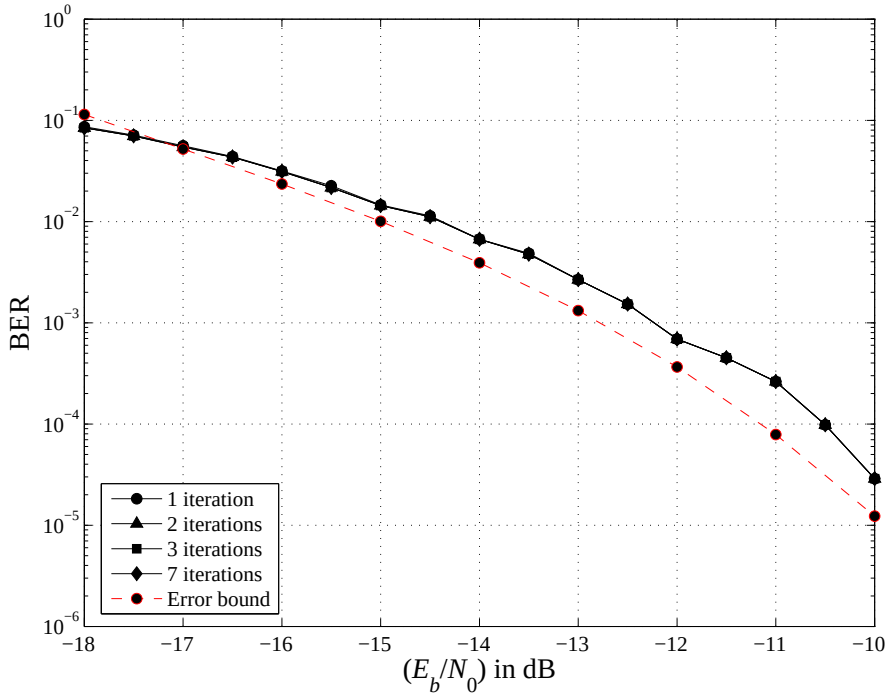

Figure 4.6: BER performance of BICM-ID over an AWAN channel with $A = 10^{-3}$ and $\Gamma = 10^{-2}$: 8PSK and Gray mapping.

ping schemes for 8PSK. Shown in each figure is the performance for a particular set of impulsive parameters, namely $\{A = 10, \Gamma = 10^{-3}\}$, $\{A = 10^{-3}, \Gamma = 10^{-3}\}$ and $\{A = 10^{-3}, \Gamma = 10^{-2}\}$. As can be observed from Fig. 4.7, when SNR is larger than 3.75dB (or -26.25dB in Fig. 4.8 and -16.25dB in Fig. 4.9) the SSP mapping always gives the best BER performance. For example, at the BER level of 10^{-5}, the SNR gains provided by the SSP mapping over the SP mapping are about 3dB, 3.5dB and 3.2dB corresponding to channel noise parameters of $\{A = 10, \Gamma = 10^{-3}\}$, $\{A = 10^{-3}, \Gamma = 10^{-3}\}$ and $\{A = 10^{-3}, \Gamma = 10^{-2}\}$, respectively. It can also be seen that Gray mapping performs very poor. In these three figures, besides the BER performance of each mapping scheme, the corresponding error bound on the asymptotic performance is also plotted. One can see the tightness of the error bounds in all cases, which suggests that the error bound derived in this thesis can be used as an effective tool for analyzing the asymptotic performance of different constellation/mapping schemes in BICM-ID systems under the impulsive noise.

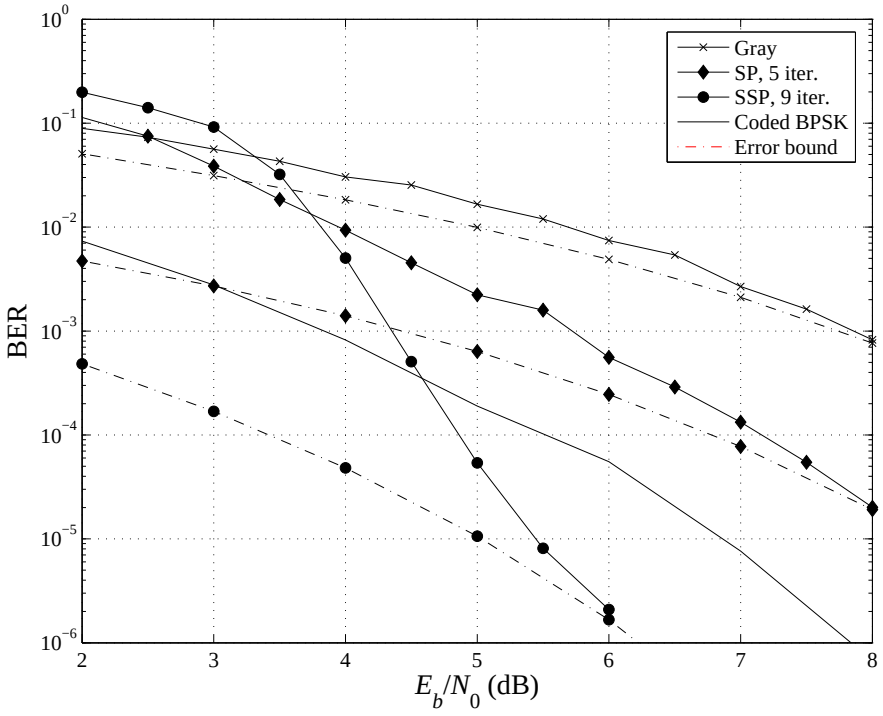

Figure 4.7: BER performance of 8PSK BICM-ID over an AWAN channel with $A = 10$ and $\Gamma = 10^{-3}$: Comparison of different mappings and coded BPSK.

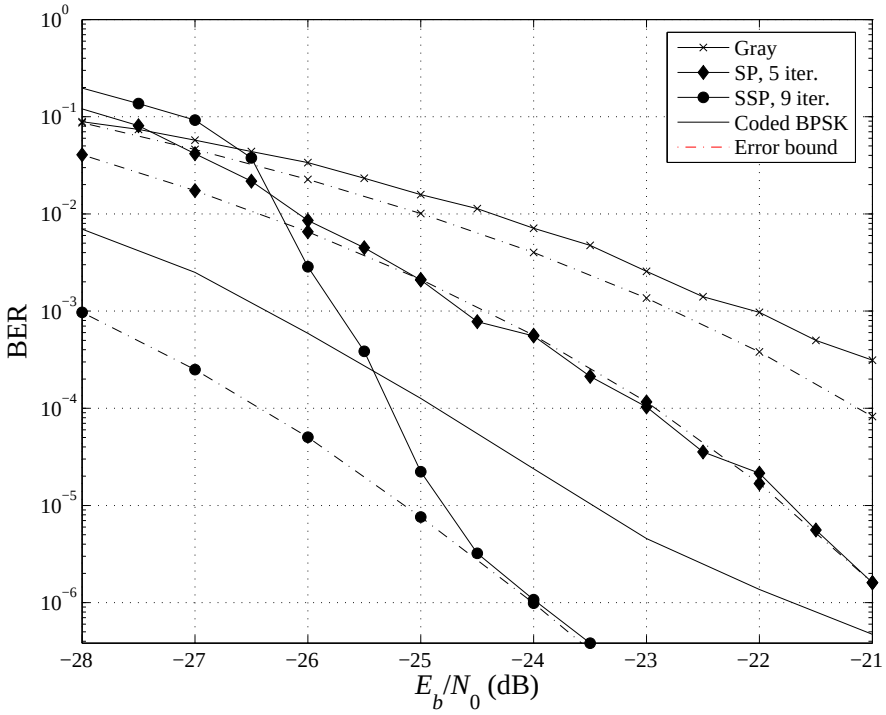

Figure 4.8: BER performance of BICM-ID over an AWAN channel with $A = 10^{-3}$ and $\Gamma = 10^{-3}$: Comparison of different mappings and coded BPSK.

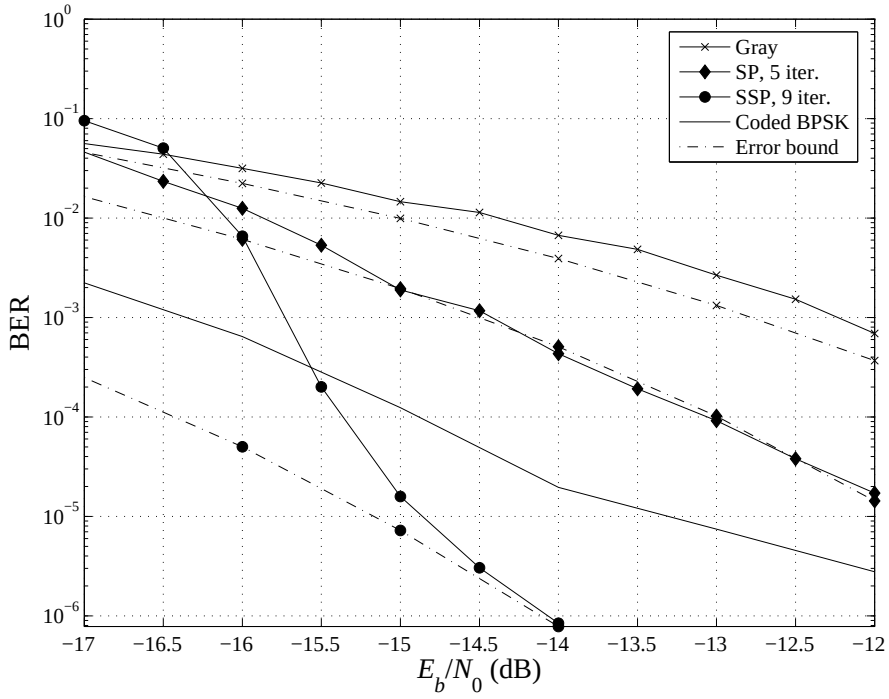

Figure 4.9: BER performance of BICM-ID over an AWAN channel with $A = 10^{-3}$ and $\Gamma = 10^{-2}$: Comparison of different mappings and coded BPSK.

The error performance of a coded system that employs the same convolutional code and BPSK modulation is also included in Figs. 4.7, 4.8 and 4.9. Note that the spectral efficiency of such a system is only 2/3 bits/sec/Hz, which is only one third of that of the systems employing 8PSK constellation. Observe that there is an error performance degradation suffered by the 8PSK system that employs Gray or SP mapping. Impressively, the 8PSK system with SSP mapping not only can provide three times higher spectral efficiency but can also achieve the error performance gain compared to the coded BPSK system. In particular, at the BER level of 10^{-6}, the SNR gains of 8PSK/SSP mapping over coded BPSK are about 1.6dB, 2.7dB and 2.5dB, as can be seen from Figs. 4.7, 4.8 and 4.9, respectively.

Fig. 4.10 then compares the BER performance of BICM-ID with 8PSK/SSP mapping after 9 iterations when the optimal and suboptimal demodulators are employed. It can be seen that for both sets of impulsive parameters, namely $\{A = 10^{-3}, \Gamma = 10^{-3}\}$ and $\{A = 10^{-3}, \Gamma = 10^{-2}\}$, the suboptimal demodulator only suffers about

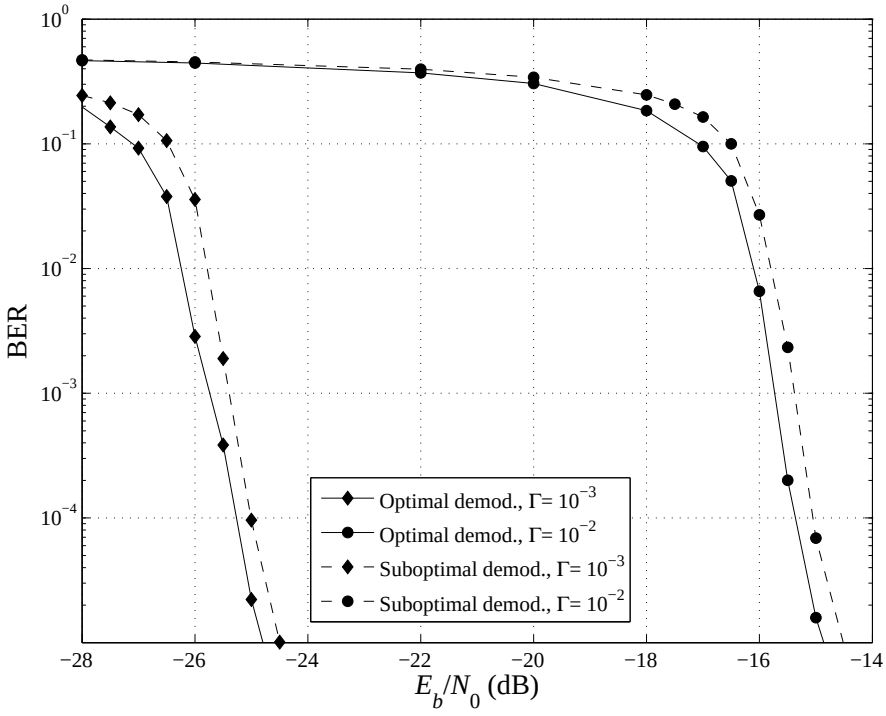

Figure 4.10: BER performance of BICM-ID with 8PSK/SSP mapping over an AWAN channel: Comparison of optimal and suboptimal demodulators after 9 iterations with different GIR parameters, $A = 10^{-3}$.

0.5dB degradation in SNR compared to the optimal demodulator. Such a small performance loss might be well justified by the lower computational complexity of the suboptimal demodulator.

It should be mentioned that Figs. 4.3, 4.7, 4.8, 4.9 and 4.10 also illustrate the dependence of BER performance on both the impulsive index A and the GIR Γ. Simple inspection of these figures shows that for all mapping schemes of 8PSK, performance of BICM-ID improves if the channel noise becomes more impulsive (i.e., corresponding to smaller value of A and/or Γ). This observation is similar to the ones made in [11, 12] for uncoded systems and coded systems with BPSK, respectively.

Next, Figs. 4.11 and 4.12 present the EXIT charts of iterative decoding for two different values of E_b/N_0, namely $E_b/N_0 = -26$dB and $E_b/N_0 = -23$dB, respectively. The impulsive parameters of the AWAN channel investigated in those figures

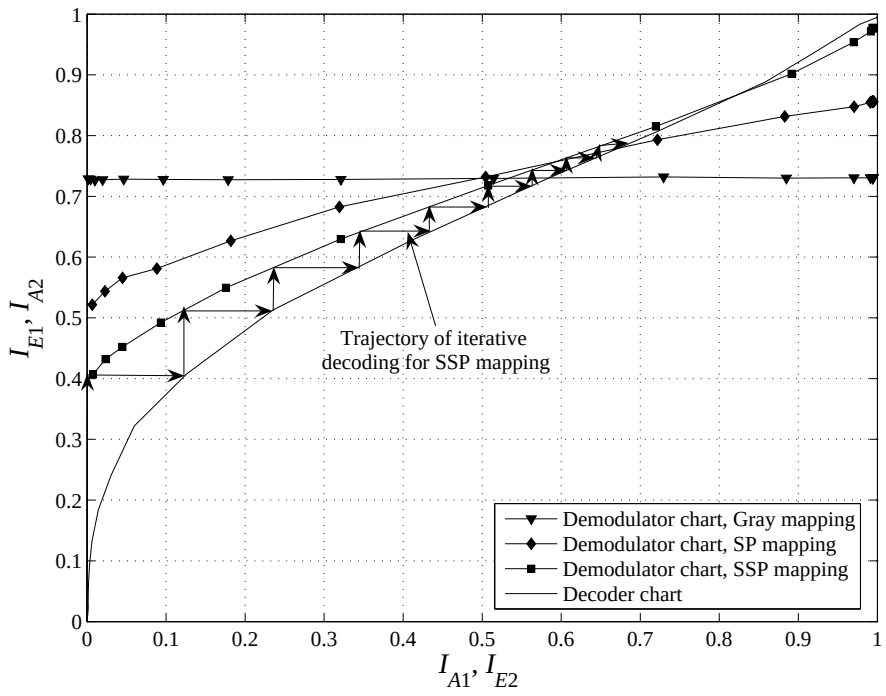

Figure 4.11: EXIT chart analysis of 8PSK BICM-ID with $A = 10^{-3}$ and $\Gamma = 10^{-3}$: Comparison of different mappings at $E_b/N_0 = -26$dB.

are $\{A = 10^{-3}, \Gamma = 10^{-3}\}$. It can be seen that the demodulator characteristics with Gray mapping appear to be constant regardless of the values of I_{A_1}. This implies that iterative decoding is useless with Gray mapping, a fact that is also confirmed by the BER performance results mentioned earlier. In contrast, the demodulator characteristics for both SP and SSP mappings increase as I_{A_1} increases, thus facilitating the effective operation of iterative decoding.

Comparing Figs. 4.11 and 4.12 shows that for all three mapping schemes of 8PSK under consideration, increasing E_b/N_0 raises the demodulator characteristics, i.e., opening the tunnel between the demodulator and the SISO characteristics. The wider opening of the tunnel is a crucial factor to provide a faster convergence of the iteration decoding. For example, following the decoding trajectories of SSP mapping shown in Figs. 4.11 and 4.12 it can be predicted that about 13 and 7 iterations are required for BER convergence at $E_b/N_0 = -26$dB and $E_b/N_0 = -23$dB, respectively. The fact that BER convergence happens after about 7 decoding iterations at $E_b/N_0 = -23$dB

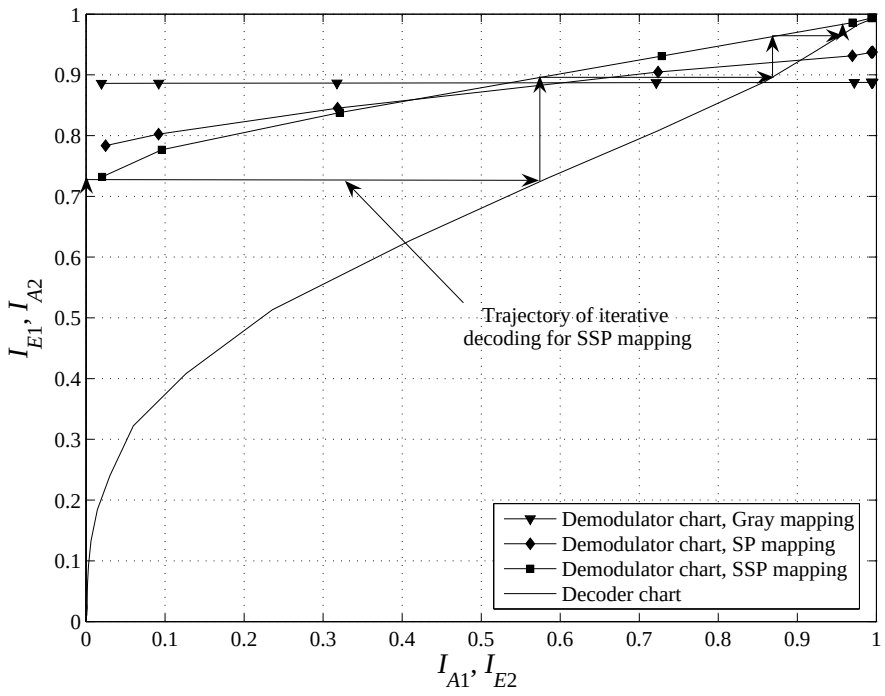

Figure 4.12: EXIT chart analysis of 8PSK BICM-ID with $A = 10^{-3}$ and $\Gamma = 10^{-3}$: Comparison of different mappings at $E_b/N_0 = -23$dB.

can be verified from Fig. 4.4. The difference in the number of decoding iterations required for BER convergence is simply due to the fact that increasing the E_b/N_0 value from -26dB to -23dB significantly opens the narrow tunnel to allow a faster convergence of the iterative decoding.

4.7 Comparisons of BICM-ID with uncoded OFDM

It has been demonstrated in the previous section that the use of M-ary modulations with appropriate mappings and properly designed iterative receiver can significantly improve both the error performance and spectral efficiency of BICM-ID over the conventional coded modulation systems that use BPSK modulation.

As discussed in Chapter 1, orthogonal frequency-division multiplexing (OFDM) is also a commonly used technique to combat impulsive noise [19, 45]. It is therefore of interest to compare the performance of BICM-ID and OFDM over the impulsive

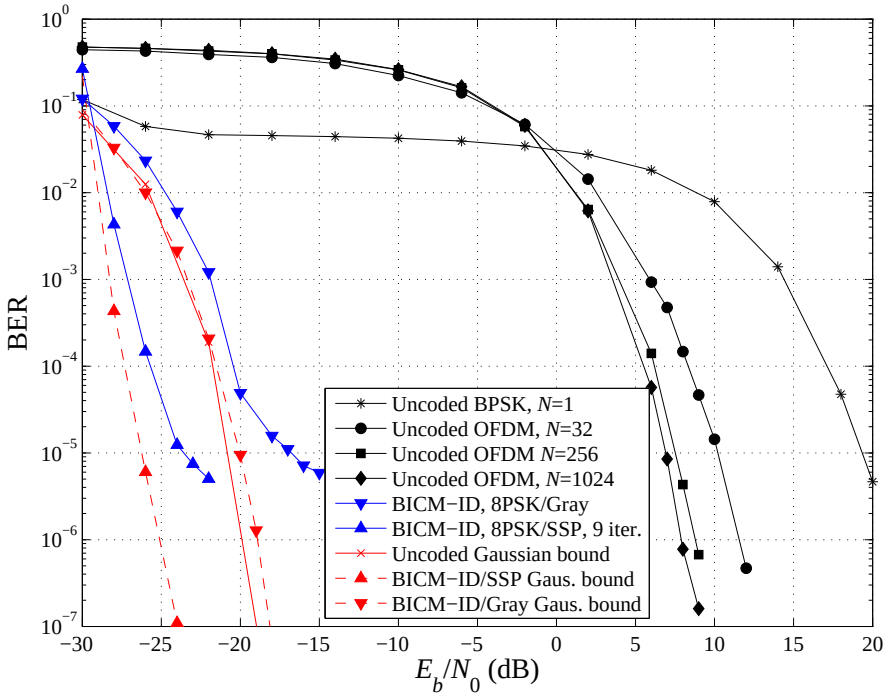

Figure 4.13: Performance comparison of BICM-ID and OFDM: $A = 0.1$, $\Gamma = 10^{-3}$ and at spectral efficiency of 1 bit/sec/Hz.

noise environment. The basic principle of OFDM is briefly reviewed in Section 3.2.

4.7.1 Comparisons with conventional OFDM

Consider an AWAN channel with impulsive parameters $\{A = 10^{-1}, \Gamma = 10^{-3}\}$ and $\{A = 10^{-3}, \Gamma = 10^{-3}\}$. Assume that BPSK modulation is used for each subcarrier of OFDM. This means that the spectral efficiency is 1 bit/sec/Hz. To have the same spectral efficiency of 1 bit/sec/Hz, a simple 4-state, rate-1/3 convolutional code with generator polynomials $\mathbf{G} = [01; 11; 11]$ is used for BICM-ID with 8PSK constellation.

Figs. 4.13 and 4.14 present the BER performance of OFDM systems with various number of subcarriers, namely $N = 1$, $N = 32$, $N = 256$ and $N = 1024$, together with the performance of BICM-ID. It can be clearly observed that, at high SNR values, OFDM significantly outperforms the uncoded BPSK system that uses a single carrier (i.e., it corresponds to OFDM with $N = 1$). For example, as shown in Fig. 4.13, at the BER level of 10^{-4}, an SNR gain of about 11dB is obtained by implementing an

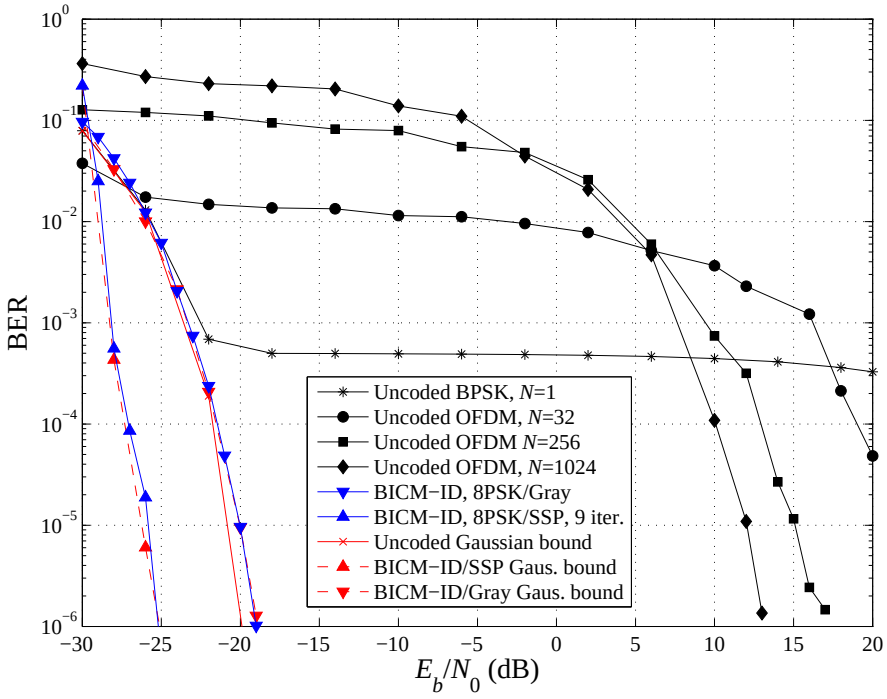

Figure 4.14: Performance comparison of BICM-ID and OFDM: $A = 0.001$, $\Gamma = 10^{-3}$ and at spectral efficiency of 1 bit/sec/Hz.

OFDM system with $N = 256$ subcarriers. In general, a higher SNR gain is achieved by using a larger number of subcarriers. But it also appears from either Fig. 4.13 or Fig. 4.14 that for the impulsive parameters under consideration, there is only a marginal improvement by increasing the number of subcarriers beyond $N = 256$. Note also that performance improvement achieved with OFDM at high SNR values comes at the expense of degraded performance at the low SNR region. This phenomenon is also observed in [19–21] and it is merely due to the suboptimality of the classical OFDM demodulator when applied to an impulsive noise environment [19–21].

From both Figs. 4.13 and 4.14, it is interesting to observe that BER performances of the proposed BICM-ID are much better than that of the conventional OFDM. For example, as shown in Figs. 4.13 and 4.14, at the BER level of 10^{-5}, even when using 8PSK/Gray mapping in the proposed BICM-ID, the SNR gains are 24dB and 32dB compared to the conventional OFDM with 1024 subcarriers, respectively. These gains certainly increase if SSP or SP mapping scheme is employed for BICM-ID.

Also plotted in Figs. 4.13 and 4.14 are the theoretical BER performance of ideal uncoded and coded receivers that can completely remove the impulsive noise, leaving only the Gaussian noise as the additive noise. These BER performances are thus the uncoded and BICM-ID Gaussian bounds mentioned in Section 4.5. They serve as the lower performance bounds for any practical uncoded and BICM-ID systems under impulsive noise. The Gaussian bounds in Figs. 4.13 and 4.14 clearly show that there are still huge performance gaps between the performance of OFDM systems and that of the ideal receiver. This implies that using OFDM with the classical M-ary demodulator still does not fully exploit the rich structure of the impulsive noise. The proposed BICM-ID, on the other hand, shows a great improvement.

Due to the fact that it can fully exploit the structure of the impulsive noise in its iteration decoding, the error performance of BICM-ID not only can reach the uncoded Gaussian bound but also surpass it. In particular, as shown in Figs. 4.13 and 4.14, the error performances of the proposed BICM-ID with 8PSK/SSP mapping can achieve about 4dB and 5.5dB SNR gains over the uncoded Gaussian bounds at the BER level of 10^{-5}, respectively. Moreover, the performance of the proposed BICM-ID can even reach the BICM-ID Gaussian bound when channel is highly impulsive. In other words, the ability of removing impulsive noise of the proposed BICM-ID increases significantly if the channel becomes more impulsive.

4.7.2 Comparisons with iteratively-decoded OFDM

As described in Section 3.4, a more advanced and complicated receiver was recently developed in [20] that can be applied to OFDM. In essence, the work in [20] views OFDM as a "code over complex numbers" and applies an iterative decoding for it. The iterative receiver proposed in [20] consists of two information-exchanging estimators, one in the "codeword" and one in the "information" domain. Such an iterative decoding of OFDM is shown to perform very close to the uncoded Gaussian bound [20]. The basic principle of this technique is described in Section 3.4.

It is relevant to point out, however, that the iterative decoding of OFDM proposed

in [20] is very different from the iterative receiver developed for BICM considered in this chapter. In particular, the iterations in the receiver of [20] are performed between the two estimators of the impusive noise. In contrast, the iterative processing at the receiver of BICM in this chapter is performed between the SISO channel decoder and the soft-output demodulator.

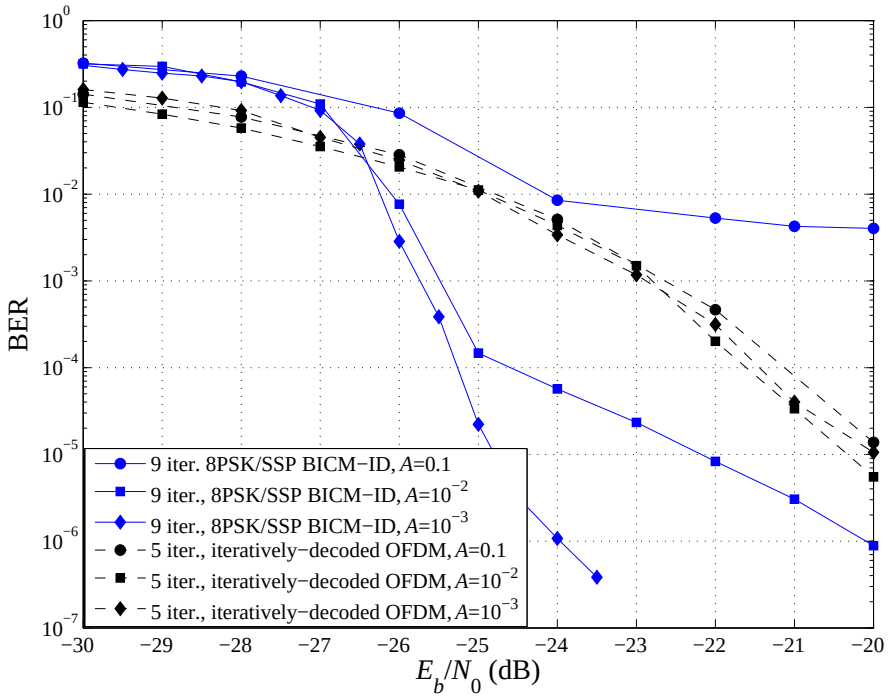

Figure 4.15: Performance comparison of BICM-ID and iteratively-decoded OFDM with $N = 1024$, at spectral efficiency of 2 bits/Sec/Hz.

Figure 4.15 shows performance comparison of the proposed BICM-ID with the iteratively-decoded OFDM in [20] with different impulsive parameters A, namely $A = \{0.1,\ 10^{-2},\ 10^{-3}\}$. To have a fair comparison, the spectral efficiency of both the proposed BICM-ID and the iteratively-decoded OFDM are kept the same at 2bits/Sec/Hz. As illustrated in Fig. 4.15, when the channel is very impulsive, i.e., $A < 0.1$, the error performance of the proposed BICM-ID is much superior to that of the iteratively-decoded OFDM. For example, when $A = 10^{-2}$ and $A = 10^{-3}$, at the BER level of 10^{-5} the SNR gains of the proposed BICM-ID over the iteratively-decoded OFDM are 2dB and 4.7dB respectively. However, if the channel is less

impulsive or comes closer to Gaussian noise, i.e., when $A \geq 0.1$, the performance of BICM-ID is poorer. This is because when the impulsive noise comes closer to Gaussian noise, the proposed BICM-ID looses its advantage of exploiting the structure of the impulsive noise in its iterative decoding. Hence, the proposed BICM-ID cannot provide a superior performance over the iteratively-decoded OFDM, which is specially designed for less impulsive channels. To overcome this disadvantage of the proposed BICM-ID, the next chapter proposes another novel technique to deal with channels having less impulsive noise.

5. Bit-interleaved coded OFDM with iterative decoding (BI-COFDM-ID)

As discussed before, the use of orthogonal frequency-division multiplexing (OFDM) technique to combat impulsive noise has recently received a strong interest [20, 21]. When the number of subcarriers in OFDM is sufficiently large, the transformation at the OFDM receiver essentially converts impulsive noise to Gaussian noise and a detector designed for an AWGN channel is generally applied to demodulate the transmitted symbols over each subcarrier.

Although the above implementation of OFDM is simple, it is by no means optimal. In fact it can perform poorer than the single-carrier system with a properly designed receiver. This is because converting impulsive noise to Gaussian noise removes the high structure of the impulsive noise and the detector does not make use of it.

Because of these disadvantages, a much more advanced and efficient receiver based on iterative processing is proposed in [20] for OFDM. In particular, the iterative receiver in [20] consists of two information-exchanging estimators, one in the "codeword" and one in the "information" domain. Such iterative decoding of OFDM is shown to perform very close to the performance of an equivalent system over an AWGN channel.

It is well-known (see also Chapter 4) that error performance of a communications system can be further improved by the use of error control coding. Applying powerful turbo codes [23, 26, 46] to combat impulsive noise is investigated in [12] where the authors also design an appropriate turbo receiver for an additive class-A noise (AWAN) channel.

As demonstrated in Chapter 4, BICM-ID is a spectral efficient coded modulation

technique for impulsive noise channel. The main advantage of BICM-ID is that it is simple in both design and implementation, as compared to other coded modulation techniques while it can still provide large coding gains. This is because BICM-ID requires only one soft-input soft-output (SISO) decoder instead of two as normally seen in turbo decoding [46]. In BICM-ID systems, the iterative processing is implemented between one SISO decoder and the soft-output demodulator. The complexity of the soft-output demodulator is relatively small compared to that of a SISO decoder [29] (which requires *forward* and *backward* recursions [47]), since the soft-output demodulator can be considered as a one-state (zero-memory) decoder. It was also clearly demonstrated in Chapter 4 that with a proper design of the soft-input soft-output (SISO) demodulator and appropriate mapping, the use of BICM-ID can improve the error performance as well as spectral efficiency of PLC systems.

Given the effectiveness of OFDM with iterative decoding for uncoded systems in [20] and BICM-ID for coded systems in Chapter 4, it is natural to combine both of these techniques in one system. This is precisely the main topic of this chapter and the system under consideration shall be referred to as bit-interleaved coded OFDM with iterative decoding (BI-COFDM-ID).

5.1 System model

The simplified block diagram of BI-COFDM-ID is shown in Fig. 5.1. The information bits $\{u_k\}$ are first encoded by a convolutional code to produce a coded sequence $\{c_k\}$. The coded sequence $\{c_k\}$ is then interleaved by the random interleaver Π. The interleaved sequence $\{v_k\}$ is mapped by the M-ary modulator into a symbol sequence. This symbol sequence is then passed through a serial-to-parallel converter, whose output is a set of N symbols $\{S_0, S_1, \ldots, S_{N-1}\}$, where S_k belongs to the M-ary constellation Ψ. Here N is number of subcarriers and the symbol S_k is transmitted over the kth subcarrier. In order to generate the transmitted signal, an inverse discrete Fourier transform (IDFT) is performed on these N symbols. Typically, N is chosen to be a power of 2 and the inverse DFT can be efficiently

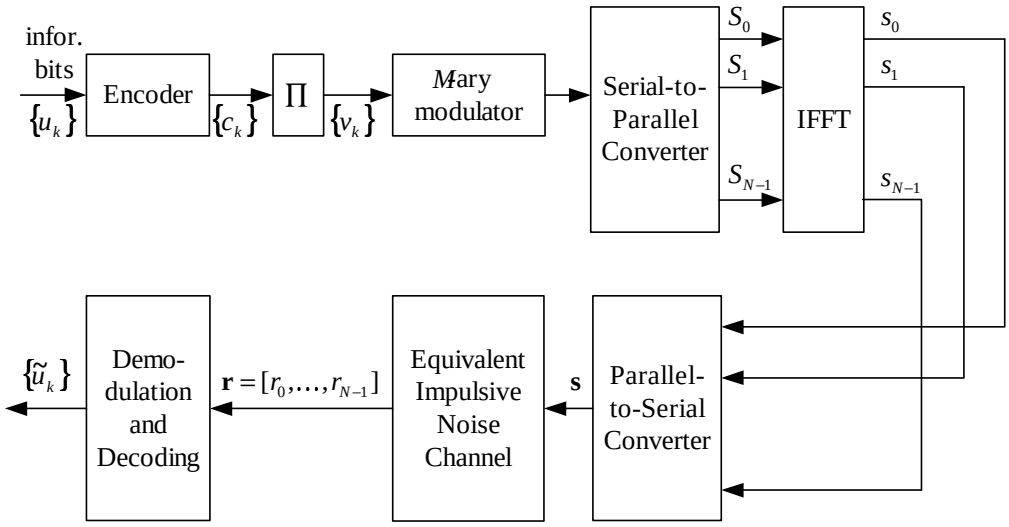

Figure 5.1: A simplified block diagram of a BI-COFDM-ID system.

implemented using the inverse fast Fourier transform (IFFT) algorithm. The IFFT yields the OFDM symbol consisting of sequence $\{s_0, s_1, \ldots, s_{N-1}\}$ of length N, where

$$s_k = \frac{1}{\sqrt{N}} \sum_{i=0}^{N-1} S_i \mathrm{e}^{j2\pi ki/N}, \quad 0 \le k \le N-1. \tag{5.1}$$

Assuming perfect synchronization and timing, the received symbols at the receiver are given by

$$r_k = s_k + i_k + g_k, \quad 0 \le k \le N-1, \tag{5.2}$$

Note that, the impulsive noise in (5.2) is separated into two components: i_k accounts for impulsive noise and g_k represents Gaussian noise. In particular, g_k's are independent and identically distributed (i.i.d.) complex Gaussian random variables with variance σ_g^2 and the following probability density function (pdf)

$$p_{g_k}(x) = \frac{1}{2\pi\sigma_g^2} \exp\left(-\frac{|x|^2}{2\sigma_g^2}\right) \tag{5.3}$$

The impulsive noise variables i_k are also i.i.d. with variance σ_i^2. Their pdf is given by Middleton's class-A noise model as [4, 9, 20]:

$$p_{i_k}(x) = \mathrm{e}^{-A}\delta(x) + \sum_{m=1}^{\infty} \mathrm{e}^{-A} \frac{A^m}{m!} \frac{1}{2\pi\sigma_m^2} \exp\left(-\frac{|x|^2}{2\sigma_m^2}\right) \tag{5.4}$$

with $\sigma_m^2 = \sigma_i^2 m/A$ and $\delta(\cdot)$ is Dirac delta function. For small impulsive index, A, e.g., $A = 0.1$, the noise is highly structured since only $1 - \mathrm{e}^{-A} \approx 9.5\%$ of the samples are hit by impulses.

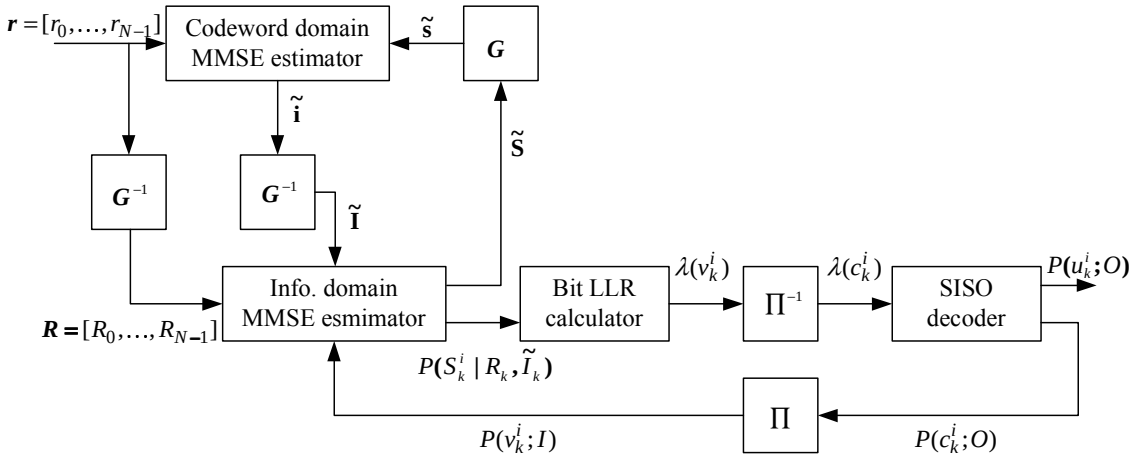

Figure 5.2: Block diagram of the proposed receiver for a BI-COFDM-ID system.

At the receiver, the problem of decoding the received vector $\mathbf{r} = [r_0, \ldots, r_{N-1}]$ arises. One can try to implement the maximum likelihood (ML) decoder to minimize the probability of a decoding error. However, this optimum receiver is very complicated due to the presence of the random interleaver. To overcome this problem, this section proposes a novel suboptimum iterative receiver as demonstrated in Fig. 5.2.

Similar to BICM-ID in [27, 29, 52–54], the iterative receiver implements the iterations between the SISO decoder and the SISO OFDM demodulator. Here, the OFDM demodulator is an iterative demodulator itself as proposed in [20]. Therefore there are two iteration loops, one within the OFDM demodulator (outer loop), and the other one is between the SISO decoder and the OFDM demodulator (inner loop). The key is how to transfer the information from the OFDM demodulator to the SISO decoder.

In particular, the outer loop exchanges the information between two estimators, one in the codeword domain and one in the information domain. The criterion for both estimators is the minimum mean-square error (MMSE). The MMSE estimator minimizes the error $\epsilon_{MSE} = E\{|y - \tilde{y}|^2\}$, where $\tilde{y}$ denotes the estimate obtained for

the actual value y. The input information for the outer loop includes the received symbol sequence $\mathbf{r}$ and the *a priori* information $P(v_k^i; I)$ fed back from the inner iteration loop. Let the capital letters denote vectors or symbols in the domain of the information sequence (information domain) and the lower case letters denote vectors or symbols in the domain of the codewords (codeword domain). To convert information between the two domains, a transform matrix $\mathbf{G}$ and its inverse $\mathbf{G}^{-1}$ are used. The transform matrix $\mathbf{G}$ here is chosen to be the inverse Fourier transform matrix corresponding to the IFFT at the transmitter, which is given in Equation (3.9).

The inputs of the codeword domain estimator are the received symbol sequence $\mathbf{r}$ and the estimated symbol sequence $\tilde{\mathbf{s}}$. With these inputs, the codeword domain MMSE estimator estimates a sequence of impulsive noise $\tilde{\mathbf{i}}$. To provide the inputs for the information domain MMSE estimator, the estimated impulsive noise sequence $\tilde{\mathbf{i}}$ together with the received sequence $\mathbf{r}$ are converted to $\tilde{\mathbf{I}}$ and $\mathbf{R}$ by multiplying with the inverse transform matrix $\mathbf{G}^{-1}$. The information domain MMSE estimator in the proposed BI-COFDM-ID differs from the one in [20]. Here, it not only uses $\tilde{\mathbf{I}}$ and $\mathbf{R}$ but also takes into account the *a priori* probability $P(v_k^i; I)$ to estimate the information sequence $\tilde{\mathbf{S}}$ and also compute the probability $P(S_k^i | R_k, \tilde{I}_k)$. After being converted to the codeword domain, the estimated information sequence $\tilde{\mathbf{s}}$ is then fed back as the input of the codeword domain MMSE estimator for the next iteration.

The inner loop, then, uses the information $P(S_k^i | R_k, \tilde{I}_k)$ as its input to calculate the bit log likelihood ratio (LLR), $\lambda(v_k^i)$. The LLR of the coded bits $\lambda(v_k^i)$ is then deinterleaved and passed to the SISO decoder. Similar to the SISO decoder used in BICM-ID [29, 37, 52], the SISO decoder in the receiver of the proposed BI-COFDM-ID also implements the maximum *a posteriori* probability (MAP) algorithm [47] to compute a hard decision as well as the *extrinsic* probability $P(c_k^i; O)$. For the information exchange between the SISO decoder and the OFDM demodulator, the *extrinsic* probability $P(c_k^i; O)$ is then interleaved to become the input of the outer loop.

Due to the iterations in both the the inner and outer loops, the proposed BI-COFDM-ID has the advantages of both BICM-ID and iteratively-decoded OFDM to combat impulsive noise. The key is how to implement the information exchanging so that the inner and outer loops can benefit from each other. The detailed algorithms for the outer and inner iteration loops over the impulsive noise channel are described in [20] and [52]. For the proposed BI-COFDM-ID, the strategies of implementing information exchange between the two iteration loops are investigated in the next section.

5.2 Iterative decoding of the proposed BI-COFDM-ID

5.2.1 Outer iterations

Similar to the iterative decoding algorithm in [20, 21], the outer iteration loop of the proposed BI-COFDM-ID exchanges information between two MMSE estimators. In the codeword domain, the MMSE estimator is the same as the one in [20]. However, the information domain MMSE estimator is modified to enable information exchanging between the inner and the outer loops. Therefore, this section first reviews the codeword domain estimator and then discusses the modified information domain MMSE estimator for the outer loop.

To obtain the estimations in the outer iteration loop, the approximations introduced in [20] are useful. In particular, if a vector of i.i.d complex random variables $\mathbf{x} = \{x_0, \ldots, x_{N-1}\}$ with $E\{x_k\} = 0$ and $E\{x_k x_k^*\} = 2\sigma_x^2$ is transformed by multiplying with the transform matrix $\mathbf{G}$, i.e., $\mathbf{y} = \mathbf{G}\mathbf{x}$, then the components of $\mathbf{y}$ are approximated as i.i.d complex random variables with $E\{y_k\} = 0$ and $E\{y_k y_k^*\} = 2\sigma_x^2$. Similarly, if the vector $\mathbf{x} = \{x_0, \ldots, x_{N-1}\}$ is transformed by the inverse matrix $\mathbf{G}^{-1}$, then $\mathbf{y} = \mathbf{G}^{-1}\mathbf{x}$ is also a vector of i.i.d complex random variables with $E\{y_k\} = 0$ and $E\{y_k y_k^*\} = 2\sigma_x^2$. In summary, by using these approximations, all the marginal pdfs used in the outer loop is given in Table 5.1. The implementation of each estimator is described as follows.

Table 5.1: Marginal pdfs for the vectors used in the first iteration loop.

	Codeword domain	Information domain
s_k	$\mathcal{N}(0, \sigma_s^2)$	$P(S_k)$
g_k	$\mathcal{N}(0, \sigma_g^2)$	$\mathcal{N}(0, \sigma_g^2)$
d_k	$\mathcal{N}(0, \sigma_{d^{(l)}}^2)$	pdf is unknown
e_k	pdf is unknown	$\mathcal{N}(0, \sigma_{e^{(l)}}^2)$

Codeword domain MMSE estimator

The inputs of the codeword domain MMSE estimator are:

$$\mathbf{r} \;=\; \mathbf{s} + \mathbf{i} + \mathbf{g} \tag{5.5}$$

$$\tilde{\mathbf{s}}^{(l-1)} \;=\; \beta_s^{(l-1)}\mathbf{s} + \beta_i^{(l-1)}\mathbf{i} + \beta_g^{(l-1)}\mathbf{g} + \mathbf{d}^{(l-1)} \tag{5.6}$$

where $\mathbf{r}$ is the received vector, $\tilde{\mathbf{s}}^{(l-1)}$ is an estimated vector provided by the information domain estimator in the preceding iteration, $\beta_s^{(l-1)},\ \beta_i^{(l-1)},\ \beta_g^{(l-1)}$ are the scalar coefficients provided by the least square regression estimation and $\mathbf{d}^{(l-1)}$ is the error term for information domain MMSE estimator. To simplify the notations the superscript $(l-1)$ will be omitted in following computations.

According to the approximations mentioned above, the highly structure of impulsive noise i_k is the only non-Gaussian signal component in the codeword domain and can, therefore, be well distinguished from $s_k,\ g_k$ and d_k. As a consequence, the codeword domain estimator is applied to estimate the impulsive noise vector $\mathbf{i}$. Also note that the inputs $\mathbf{r}$ and $\tilde{\mathbf{s}}$ of the codeword domain estimator are also approximated as vectors of i.i.d random variables. Hence, the MMSE estimation for each i_k is a function of only two complex numbers, i.e., r_k and $\tilde{s}_k$. Similar to [20], using Table 5.1 and Equations (5.5), (5.6) this estimation of i_k is given as follows:

$$\tilde{i}_k = \frac{\displaystyle\sum_{m=0}^{\infty} \frac{A^m}{m!} \frac{b_{\mathrm{Re}}(\mathbf{r},\tilde{\mathbf{s}}) + j b_{\mathrm{Im}}(\mathbf{r},\tilde{\mathbf{s}})}{2(\sigma_r^2\sigma_{\tilde{s}}^2 - \mathrm{cov}(\mathbf{r},\tilde{\mathbf{s}}))} \tilde{p}_{\mathrm{Re}}(\mathbf{r},\tilde{\mathbf{s}})\tilde{p}_{\mathrm{Im}}(\mathbf{r},\tilde{\mathbf{s}})}{\displaystyle\sum_{m=0}^{\infty} \tilde{p}_{\mathrm{Re}}(\mathbf{r},\tilde{\mathbf{s}})\tilde{p}_{\mathrm{Im}}(\mathbf{r},\tilde{\mathbf{s}})} \tag{5.7}$$

with [20]:

$$\begin{aligned}
\sigma_r^2 &= \sigma_s^2 + \sigma_m^2 + \sigma_g^2 \\
\sigma_{\tilde{s}^2} &= \beta_s^2\sigma_s^2 + \beta_i^2\sigma_m^2 + \beta_g^2\sigma_g^2 + \sigma_D^2 \\
\mathrm{cov}(\mathbf{r},\tilde{\mathbf{s}}) &= \beta_s\sigma_s^2 + \beta_i\sigma_m^2 + \beta_g\sigma_g^2
\end{aligned}$$

and the functions $b(\mathbf{r},\tilde{\mathbf{s}})$ and $\tilde{p}(\mathbf{r},\tilde{\mathbf{s}})$ are given as:

$$\begin{aligned}
b(\mathbf{r},\tilde{\mathbf{s}}) &= 2\sigma_m^2\left[\left(\sigma_{\tilde{s}^2} - \beta_i\mathrm{cov}(\mathbf{r},\tilde{\mathbf{s}})\right)\mathbf{r} + \left(\beta_i\sigma_r^2 - \mathrm{cov}(\mathbf{r},\tilde{\mathbf{s}})\right)\tilde{\mathbf{s}}\right] \\
\tilde{p}(\mathbf{r},\tilde{\mathbf{s}}) &= \frac{\exp\left(-\frac{1}{2}\frac{\sigma_{\tilde{s}}^2|\mathbf{r}|^2 - 2\mathrm{cov}(\mathbf{r},\tilde{\mathbf{s}})\mathbf{r}\tilde{\mathbf{s}} + \sigma_r^2|\tilde{\mathbf{s}}|^2}{\sigma_r^2\sigma_{\tilde{s}}^2 - \mathrm{cov}(\mathbf{r},\tilde{\mathbf{s}})^2}\right)}{\sqrt{\sigma_r^2\sigma_{\tilde{s}}^2 - \mathrm{cov}(\mathbf{r},\tilde{\mathbf{s}})^2}}
\end{aligned}$$

Furthermore, the abbreviations used in (5.7) are:

$$\begin{aligned}
\tilde{p}_{\mathrm{Re}}(\mathbf{r},\tilde{\mathbf{s}}) &= \tilde{p}\left(\mathrm{Re}\{\mathbf{r}\},\mathrm{Re}\{\tilde{\mathbf{s}}\}\right) \\
\tilde{p}_{\mathrm{Im}}(\mathbf{r},\tilde{\mathbf{s}}) &= \tilde{p}(\mathrm{Im}\{\mathbf{r}\},\mathrm{Im}\{\tilde{\mathbf{s}}\})
\end{aligned}$$

where the operators $\mathrm{Re}\{\cdot\}$ and $\mathrm{Im}\{\cdot\}$ evaluate the real and imaginary parts of a complex number, respectively. Similar abbreviations for $b_{\mathrm{Re}}(\mathbf{r},\tilde{\mathbf{s}})$ and $b_{\mathrm{Im}}(\mathbf{r},\tilde{\mathbf{s}})$ are also used in Equation (5.7). To estimate the whole vector $\tilde{\mathbf{i}}$, Equation (5.7) has to be calculated once for every component $\tilde{i}_k$. The complexity of this procedure grows linearly with the number of subcarriers N.

Information domain MMSE estimator

The information domain MMSE estimator used in the outer loop of the proposed BI-COFDM-ID differs from the one introduced in [20]. Here, the inputs of this estimator include $\mathbf{R}$, $\tilde{\mathbf{I}}$ and $P(S^i;I)$, where

$$\mathbf{R} = \mathbf{G}^{-1}\mathbf{r} = \mathbf{S} + \mathbf{I} + \mathbf{Z} \tag{5.8}$$

$$\tilde{\mathbf{I}}^{(l)} = \alpha_s^{(l)}\mathbf{S} + \alpha_i^{(l)}\mathbf{I} + \alpha_g^{(l)}\mathbf{Z} + \mathbf{E}^{(l)} \tag{5.9}$$

Basically, $\mathbf{R}$ is the received vector transformed into the information domain, $\tilde{\mathbf{I}}^{(l)}$ is the transformed output of the codeword domain estimator and $\mathbf{Z}$ denotes the background

Gaussian noise in the information domain. The *a priori* probability $P(S^i; I)$ is the information fed back from the inner loop to increase the reliability of the outputs of the codeword domain estimator.

In Equations (5.8) and (5.9), again $\alpha_s^{(l)},\ \alpha_i^{(l)},\ \alpha_g^{(l)}$ are the scalar coefficients also provided by the least square regression estimation and $\mathbf{E}^{(l)}$ is the error vector of the information domain estimator. To simplify notations, the superscript (l) will also be omitted in following calculations.

With these inputs and using the marginal pdfs approximated as in Table 5.1, the MMSE estimation of each S_k is

$$\begin{aligned} \tilde{S_k} &= E\{S_k|R_k, \tilde{I}_k\} \\ &= \frac{\sum_{S_k\in\Psi} S_k p(R_k, \tilde{I}_k|S)P(S_k)}{\sum_{S_k\in\Psi} p(R_k, \tilde{I}_k|S_k)P(S_k)} \end{aligned} \tag{5.10}$$

where $p(R_k, \tilde{I}_k|S_k)$ is given by [20, 21]:

$$p(R_k, \tilde{I}_k|S_k) = \frac{\exp\left(-\dfrac{\sigma^2_{R_k|S_k} aa^* - \mathrm{cov}(R_k, \tilde{I}_k|S_k)(ab^* + a^*b) + \sigma^2_{\tilde{I}_k|S_k} bb^*}{2\left[\sigma^2_{R_k|S_k}\sigma^2_{\tilde{I}_k|S_k} - \mathrm{cov}(R_k, \tilde{I}_k|S_k)^2\right]}\right)}{4\pi^2\left[\Sigma^2_{R_k|S_k}\sigma^2_{\tilde{I}_k|S_k} - \mathrm{cov}(R_k, \tilde{I}_k|S_k)^2\right]} \tag{5.11}$$

where $a = R_k - S_k,\ b = \tilde{I}_k - \alpha_s S_k$ and

$$\begin{aligned} \sigma^2_{R_k|S_k} &= \sigma^2_{\tilde{i}} + \sigma^2_g \\ \sigma^2_{\tilde{I}_k|S_k} &= \alpha_i^2\sigma^2_{\tilde{i}} + \alpha_g^2\sigma^2_g + \sigma^2_d \\ \mathrm{cov}(R_k, \tilde{I}_k|S_k) &= \alpha_i\sigma^2_{\tilde{i}} + \alpha_g\sigma^2_g \end{aligned}$$

Also note that in the first iteration, the probabilities $P(S_k)$ are assumed to be equiprobable and they are canceled in (5.10). However, from the second iteration, $P(S_k)$ are computed by using the *priori* probability information fed back from the second iteration loop.

Because an ideal interleaver makes m bits in one symbol independent, the *a priori* information $P(v_k^1; I), \cdots, P(v_k^m; I)$ can be assumed to be independent. Therefore, for

each constellation symbol, the probability $P(S_k)$ is calculated as

$$\begin{aligned} P(S_k) &= P\left(\mu\left([v^1(S_k)\cdots v^m(S_k)]\right)\right) \\ &= \prod_{j=1}^{m} P(v_k^j = v^j(S_k); I), \end{aligned} \tag{5.12}$$

where $v^j(S_k)$ is the value of the jth bit in the label of symbol S_k.

The other output of the information domain MMSE estimator is $P(S_k^i = b|R_k, \tilde{I}_k)$ which is delivered as the input information to the inner iteration loop. The computation of $P(S_k^i = b|R_k, \tilde{I}_k)$ is given as follows:

$$P(S_k^i = b|R_k, \tilde{I}_k) = \sum_{S_k \in \Psi_b^i} p(R_k|S_k, \tilde{I}_k) P(S_k|R_k, \tilde{I}_k) \tag{5.13}$$

where $i = \{1, \ldots, m\}$, $b = \{0, 1\}$ and Ψ_b^i are defined as $\Psi_b^i = \{\mu([S^1, S^2, \cdots, S^m])|S^i = b\}$. Similar to [21], the probability $P(S_k|R_k, \tilde{I}_k)$ is given by

$$P(S_k|R_k, \tilde{I}_k) = p(R_k, \tilde{I}_k|S_k) P(S_k) \tag{5.14}$$

with $p(R_k, \tilde{I}_k|S_k)$ is given in (5.11).

Under the assumption that the estimated impulsive noise components $\tilde{I}_k$ in the information domain are i.i.d and still have the class-A distribution, $p(R_k|S_k, \tilde{I}_k)$ can be determined as:

$$p(R_k|S_k, \tilde{I}_k) = \sum_{m=1}^{\infty} \mathrm{e}^{-A} \frac{A^m}{m!} \frac{1}{2\pi\sigma_m^2} \exp\left(-\frac{|R_k - S_k|^2}{2\sigma_m^2}\right) \tag{5.15}$$

where $\sigma_m^2 = \sigma_{\tilde{I}_k}^2 m/A$. Using Equations (5.11), (5.12), (5.13), (5.14) and (5.15) one can obtain the estimated values S_k as well as the probabilities $P(S_k^i = b|R_k, \tilde{I}_k)$.

5.2.2 Inner iterations

One of the outputs of the outer loop, namely the set of probabilities $P(S_k^i = b|R_k, \tilde{I}_k)$, is transferred to the inner loop as the input of the the bit LLR calculator. Using these probabilities, the bit LLR calculator computes the log likelihood ratio for each bit of the received symbol as follows:

$$\lambda(v_k^i) = \log\left[\frac{P(S_k^i = 1|R_k, \tilde{I}_k)}{P(S_k^i = 0|R_k, \tilde{I}_k)}\right] \tag{5.16}$$

After being deinterleaved, $\lambda(v_k^i)$ is delivered to the SISO decoder. The SISO decoder treats that information as the *a priori* information for the coded bits and the iteration between the OFDM demodulator and the SISO decoding keeps running. The hard-decisions of the information bits can be made at the final iteration based on the *extrinsic* information $P(u_k^i; O)$. The other output of the SISO decoder is the *extrinsic* probability $P(c_k^i; O)$, which is interleaved before being fed back as the input of the information domain MMSE estimator.

If the SISO decoder does not transfer the *extrinsic* information $P(c_k^i; O)$ to the information domain MMSE estimator, the system is simply referred to as BI-COFM.

5.2.3 Iteration scheduling

As mentioned in Section 5.1, the proposed iterative receiver for BI-COFDM-ID includes two iteration loops, i.e., the outer and the inner loops. It is therefore interesting and important to investigate the strategies to schedule the iteration processes between the outer and the inner loops. There are many different ways that the two iteration loops can interact. This section investigates and compares the error performance of three different scheduling schemes, namely the parallel, the serial, and the mixed iteration schemes.

For the parallel iteration scheduling, the iterations of the outer and the inner loops are processed in parallel. In particular, one iteration of the whole receiver includes two iterations, one in the outer loop and one in the inner loop. In other words, the outer loop and the inner loop exchange information in every iteration by carrying out the iterations of the outer and the inner loops simultaneously.

Opposite to the parallel iteration scheme, in serial iteration scheme, iterations of the outer and the inner loops are operated in serial. The iterations of the outer loop are processed first. After a few iterations of the outer loop, the iteration process of the inner loop is carried out. Hence, the iteration of the inner loop can only help to increase the reliability of the decision at the final iteration of the outer loop and it does not affect the results of the estimations of the intermediate iterations.

Finally, the mixed iteration strategy is a combination of the parallel and serial strategies. For each iteration of the outer loop, a number of iterations are processed in the inner loop before continuing to the next iteration of the outer loop. Due to the more iterations implemented in the inner loop the reliability of the extrinsic information $P(v_k^i; I)$ increases before it is fed back as the input of the information domain estimator in the next iteration. In this way, a higher reliability of the extrinsic information is provided to each iteration of the outer loop.

At this point, it is appropriate to comment on the complexities of three iteration schemes. It can be seen that the serial iteration scheme is the simplest iteration scheme compared to the other two schemes. In the serial iteration scheme, the information $P(S_k^i = b|R_k, \tilde{I}_k)$ needs to be computed once at the last iteration of the outer loop and the estimated information symbol sequence $\tilde{\mathbf{S}}$ needs not to be available after each iteration of the inner loop. Therefore many calculations in the outer loop can be skipped and the serial iteration scheme is preferred in terms of complexity. If the time consumption and complexity of the outer and the inner loops are considered to be equivalent, the parallel and mixed iteration schemes have the same complexity when the total numbers of iterations carried out in the outer and the inner loop of the two iteration schemes are the same. The detailed performance comparisons of different iteration schedules are discussed in the following section.

5.3 Results and discussion

This section investigates the error performance of BI-COFDM-ID systems employing $N = 1024$ subcarriers. Two modulations schemes considered are 8PSK and 4QAM. The convolutional codes of rates 2/3, 1/2 and 1/3 shall be used. In particular, the 4-state rate-2/3 convolutional code has generator polynomials $\mathbf{G} = [1001; 0001; 1100]$, the 4-state rate-1/2 code has $\mathbf{G} = [101; 110]$ and the 2-state rate-1/3 code has $\mathbf{G} = [01; 11; 11]$. Each information block has a length of 4096 bits. Three different mapping schemes, shown in Fig. 4.2, namely Gray, set partitioning (SP) and semi set partitioning (SSP) mappings of 8PSK (phase-shift keying), are

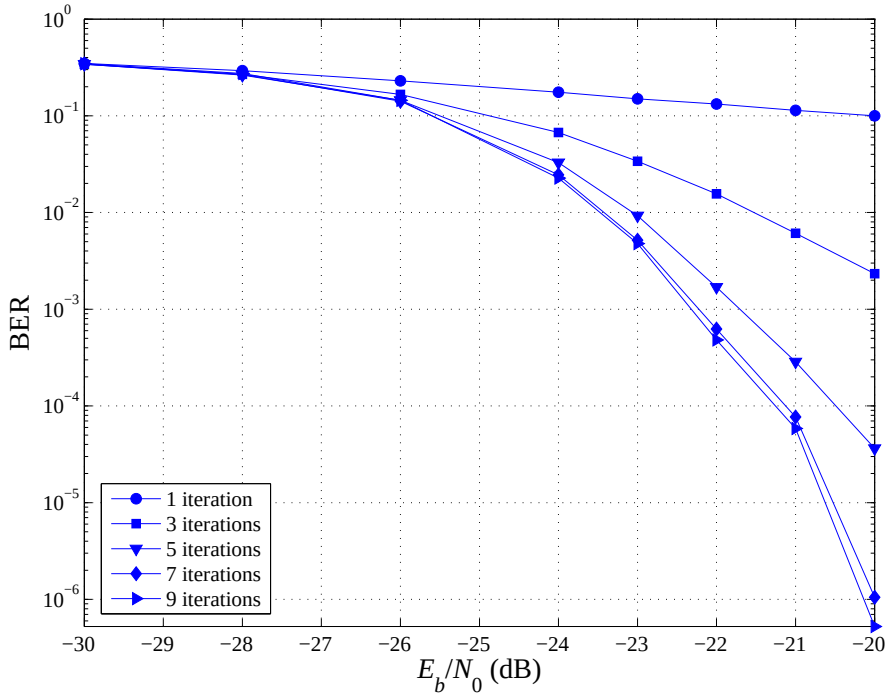

Figure 5.3: BER performance of BI-COFM-ID over an AWAN channel with $A = 0.1$ and $\Gamma = 10^{-3}$: A 4-state, code rate-2/3 convolutional, 8PSK and SSP mapping.

considered.

First, Figs. 5.3, 5.4, 5.5 show the bit error rate (BER) performance of BI-COFDM-ID when parallel iteration scheme is carried out for SSP, SP and Gray mappings, respectively. In all of these figures, the impulsive parameters are $\{A = 0.1,\ \Gamma = 10^{-3}\}$ and the rate-2/3 convolutional code is used. As can be seen, error performance improvement due to iterations is very significant for all cases of mappings.

Also note that, different from BICM-ID with Gray mapping in Chapter 4, here as shown in Fig. 5.5, iterations can significantly improve the error performance even when Gray mapping is used. This is reasonable because the proposed iterative receiver of BI-COFDM-ID is different from that of the conventional BICM-ID. Basically, the OFDM demodulator is itself an iterative decoding and the iteration process in the OFDM demodulator is independent of the mapping. The outer iterations therefore help to improve the overall performance of the proposed BI-COFDM-ID, regardless of the mapping schemes.

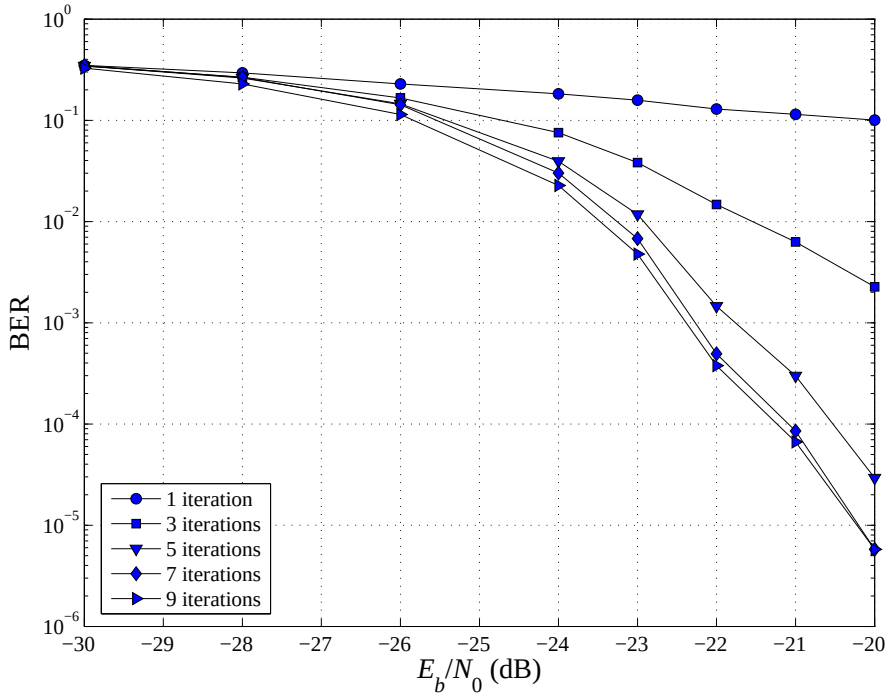

Figure 5.4: BER performance of BI-COFM-ID over an AWAN channel with $A = 0.1$ and $\Gamma = 10^{-3}$: A 4-state, rate-2/3 convolutional code, 8PSK and SP mapping.

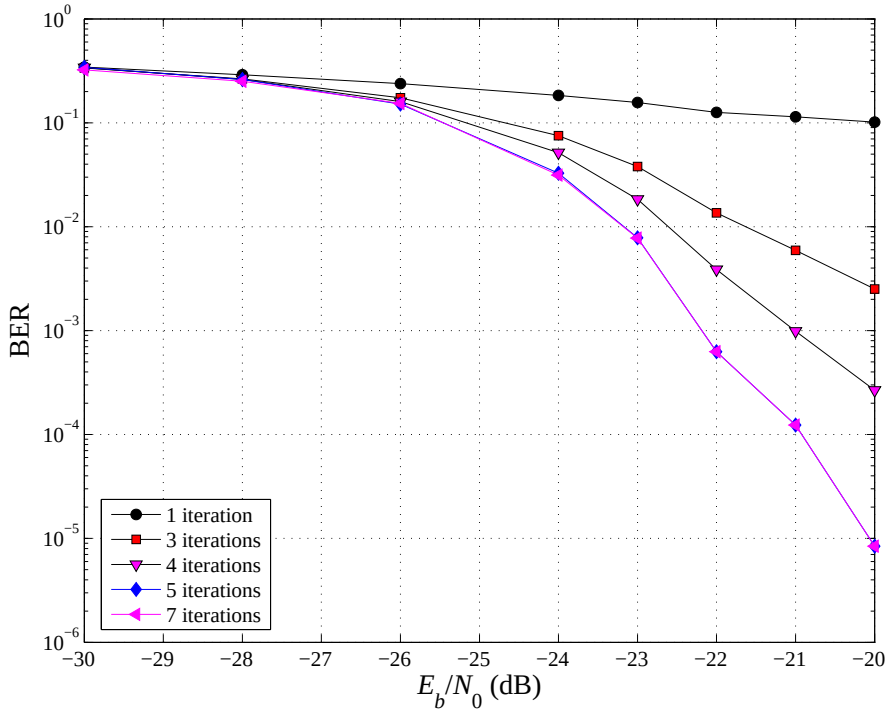

Figure 5.5: BER performance of BI-COFM-ID over an AWAN channel with $A = 0.1$ and $\Gamma = 10^{-3}$: A 4-state, rate-2/3 convolutional code, 8PSK and Gray mapping.

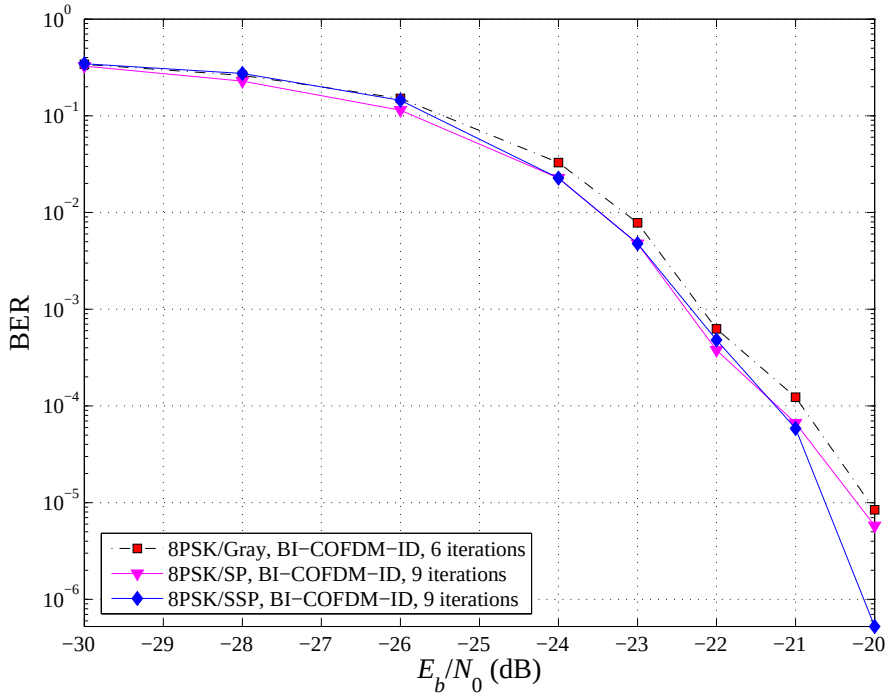

Figure 5.6: Performance comparison of 8PSK BI-COFM-ID over an AWAN channel with $A = 0.1$ and $\Gamma = 10^{-3}$: Different mapping schemes.

Next, Fig. 5.6 explicitly compares the error performance of the proposed BI-COFDM-ID employing different mapping schemes of 8PSK. Similar to BICM-ID, the results in Fig. 5.6 show that the using SSP mapping gives the best BER performance with iterations. However, different from BICM-ID in Chapter 4, here performance improvement by SSP mapping is not very significant compared to the other mapping schemes. For example, at the BER of 10^{-5} and after 9 iterations, the SSP mapping achieves SNR gains of only 0.5dB and 0.7dB over the SP and Gray mappings, respectively. These SNR gains for BI-COFDM-ID are very small compared to the SNR gains observed in BICM-ID systems in Chapter 4. This is because unlike BICM-ID, the error performance of BI-COFDM-ID can be improved significantly by the outer iteration loop, regardless of the mapping scheme used.

5.3.1 Comparison of BI-COFDM-ID and BI-COFDM

To investigate the effect of the inner loop iterations, Figs. 5.7 and 5.8 compare the error performance between the proposed BI-COFDM-ID and the BI-COFDM,

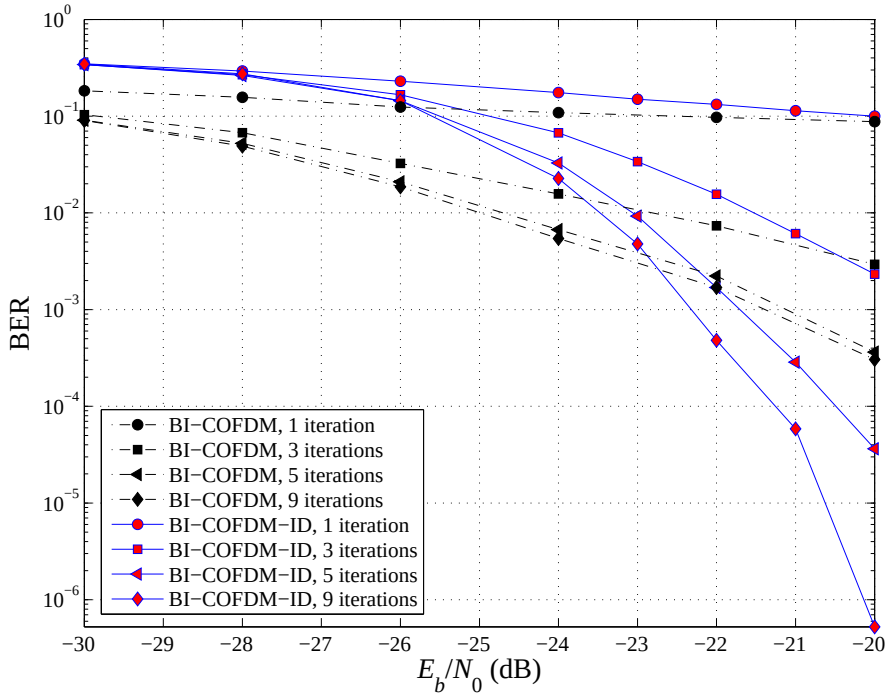

Figure 5.7: Performance comparison of BI-COFDM-ID and BI-COFDM using rate-2/3 convolutional code, 8PSK/SSP mapping over an AWAN channel with $A = 0.1$ and $\Gamma = 10^{-3}$.

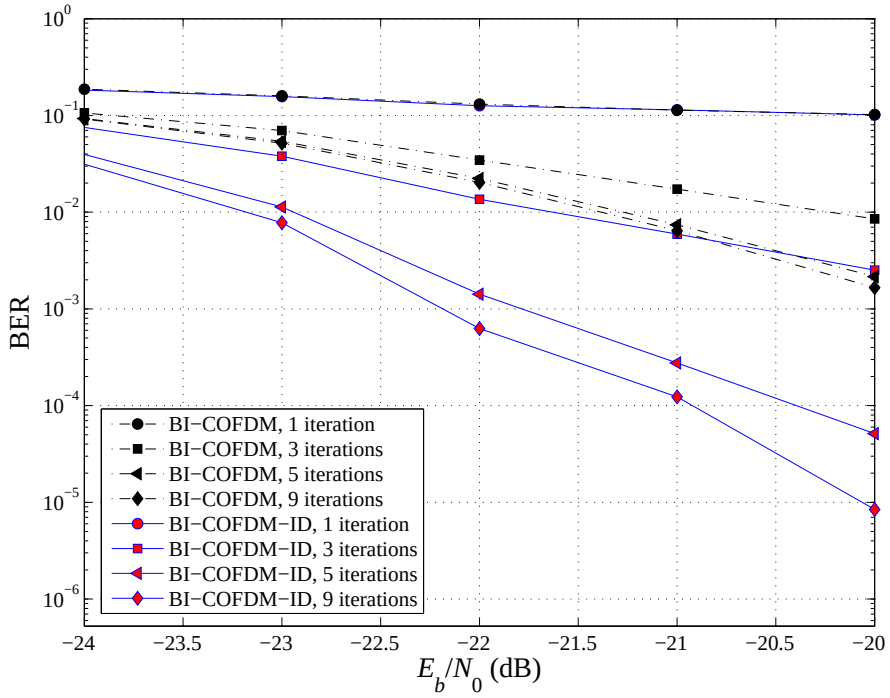

Figure 5.8: Performance comparison of BI-COFDM-ID and BI-COFDM using rate-2/3 convolutional code, 8PSK/Gray mapping over an AWAN channel with $A = 0.1$ and $\Gamma = 10^{-3}$.

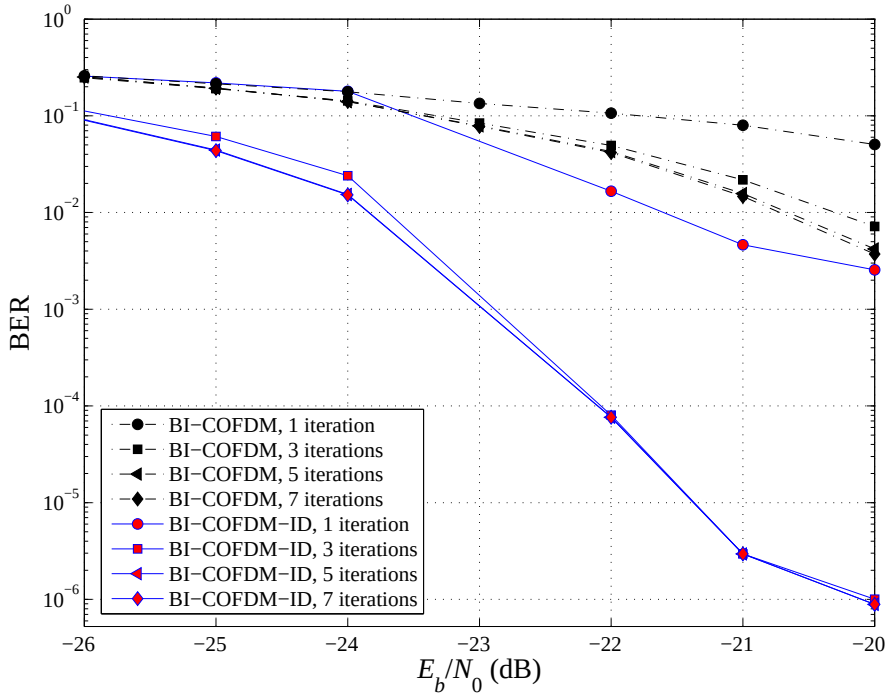

Figure 5.9: Performance comparison of BI-COFDM-ID and BI-COFDM using rate-1/3 convolutional code, 8PSK/SSP mapping over an AWAN channel with $A = 0.1$ and $\Gamma = 10^{-3}$.

where there is no feedback from the SISO decoder to the OFDM demodulator. The comparisons are investigated for channel parameters $\{A = 0.1,\ \Gamma = 10^{-3}\}$, rate-2/3 convolutional code and 8PSK modulation. Two different mapping schemes, namely SSP and Gray mappings, are used in Figs. 5.7 and 5.8, respectively. It is obvious from both Figs. 5.7 and 5.8 that the inner iteration loop can help to improve the error performance of BI-COFDM-ID significantly. In particular, after 9 iterations the SNR gains due to the inner loop are 2.5dB and 3.5dB at the BER level of 10^{-4} as can be seen from Fig. 5.7 and predicted from Fig. 5.8, respectively.

Similarly, Fig. 5.9 presents the error performance comparison of BI-COFDM-ID and BI-COFDM for the impulsive parameters $\{A = 0.1,\ \Gamma = 10^{-3}\}$ and when a convolution code of rate 1/3 is used. Again, BI-COFDM-ID significantly outperforms BI-COFDM. From the comparisons in Figs. 5.7, 5.8, 5.9, it is, therefore, necessary and beneficial to run the inner iteration loop in the proposed receiver of BI-COFDM-ID system.

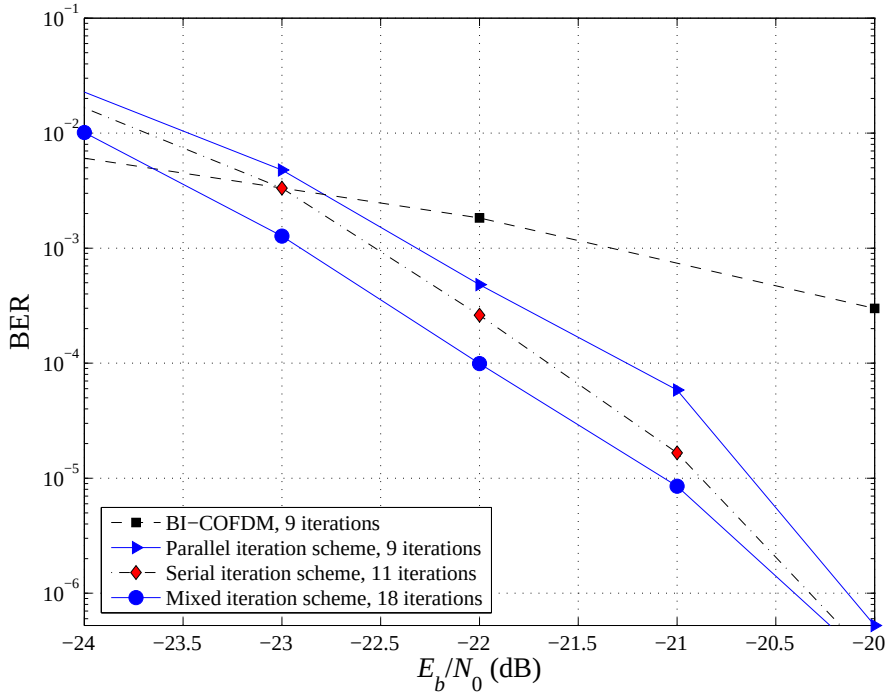

Figure 5.10: Performance comparison of 8PSK/SSP BI-COFM-ID over an AWAN channel with $A = 0.1$ and $\Gamma = 10^{-3}$: different iteration strategies.

5.3.2 Effects of iteration scheduling to the performance of BI-COFDM-ID

In Fig. 5.10, the error performance of BI-COFDM-ID with rate-2/3 convolutional code and 8PSK/SSP mapping is investigated with different iterative schemes for channel parameters $\{A = 0.1,\ \Gamma = 10^{-3}\}$. Here, the mixed scheme is designed with 1 outer iteration followed by 3 iterations of the inner loop. Hence, the error performance of 18 iterations in the mixed scheme corresponds to 6 iterations in the outer loop, each includes 3 iterations in the inner loop. The error performance of 11 iterations in the serial scheme is obtained by processing 6 iterations in the outer loop first, then carrying out 5 iterations in the inner loop. Similarly, the error performance of 9 iterations with parallel scheme is obtained when 9 iteration decoding is simultaneously processed in both the outer and the inner loops.

As can be observed from Fig. 5.10, all three iteration schemes can help to improve the error performance of BI-COFDM-ID compared to BI-COFDM. It is also seen from

this figure, the mixed scheme offers the best error performance. In particular, at the BER level of 10^{-4}, the mixed iteration scheme provides SNR gains of 0.7dB and 0.4dB compared to the parallel and the serial schemes, respectively. Also note that, BI-COFDM-ID with serial iteration scheme also performs well with a smaller number of iterations. As shown in Fig. 5.10, after 11 iterations, the error performance of BI-COFDM-ID with serial iteration scheme comes close to that of the system with the mixed scheme, especially at a low level of BER.

5.3.3 Comparison of BI-COFDM-ID and BICM-ID

As demonstrated in Chapter 4, BICM-ID designed for impulsive noise is a very attractive solution to PLC. However, the excellent performance of this BICM-ID over impulsive noise environment degrades when the channel is less impulsive or close to Gaussian noise. In fact, the main purpose of introducing BI-COFDM-ID in this chapter is to deal with the less impulsive noise environment where BICM-ID

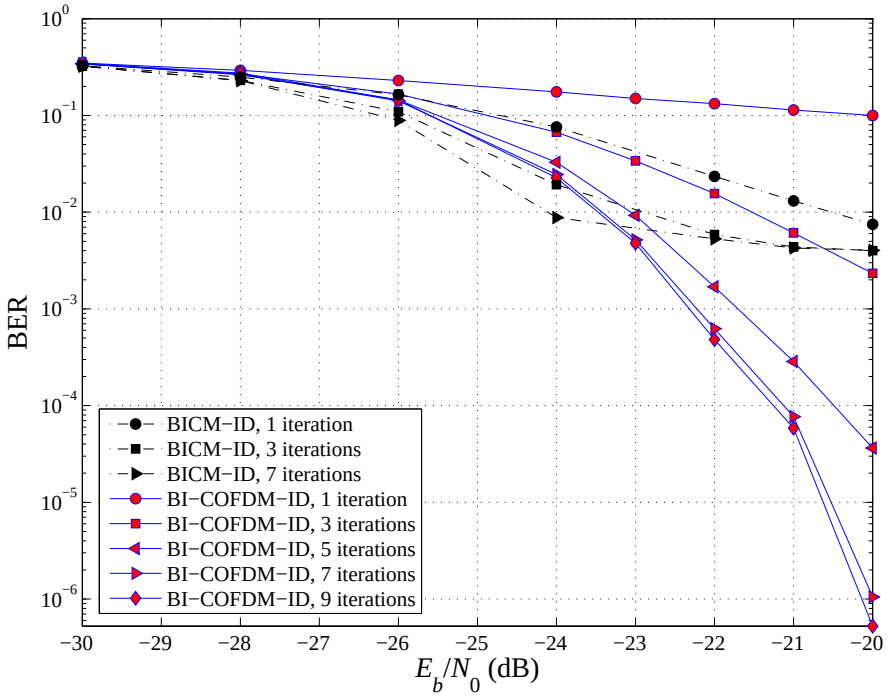

Figure 5.11: Performance comparison of BI-COFM-ID and BICM-ID over an AWAN channel with $A = 0.1$ and $\Gamma = 10^{-3}$: rate-2/3 convolutional code, 8PSK/SSP mapping.

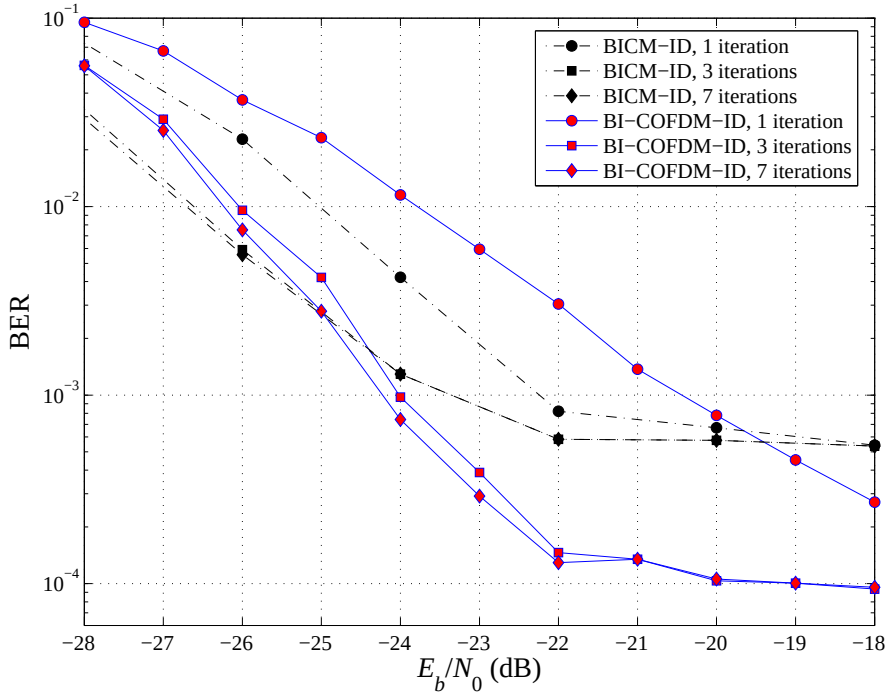

Figure 5.12: Performance comparison of BI-COFM-ID and BICM-ID over an AWAN channel with $A = 0.1$ and $\Gamma = 10^{-3}$: rate-1/2 convolutional code, 4QAM/natural mapping.

shows a poor error performance. Therefore, this chapter concentrates on performance comparison of the proposed BI-COFDM-ID and BICM-ID over a less impulsive noise environment.

Figs. 5.11, 5.12 and 5.13 present the error performance with parallel iteration scheme, convolutional code of different rates and over impulsive noise environment with parameters $\{A = 0.1,\ \Gamma = 10^{-3}\}$. In particular, convolutional codes with rates 2/3, 1/2 and 1/3 are used in Figs. 5.11, 5.12 and 5.13, respectively. The modulation scheme used for code rates 2/3 and 1/3 is 8PSK, whereas 4QAM is employed for the code rate 1/2.

All three figures show that at high to medium BER level, the proposed BI-COFDM-ID outperforms BICM-ID, regardless of the convolutional code used. In particular, after 7 iterations of both BI-COFDM-ID and BICM-ID, the SNR gains at the BER level of 10^{-3} are 3dB and 2dB for rate-2/3 and rate-1/2 convolutional

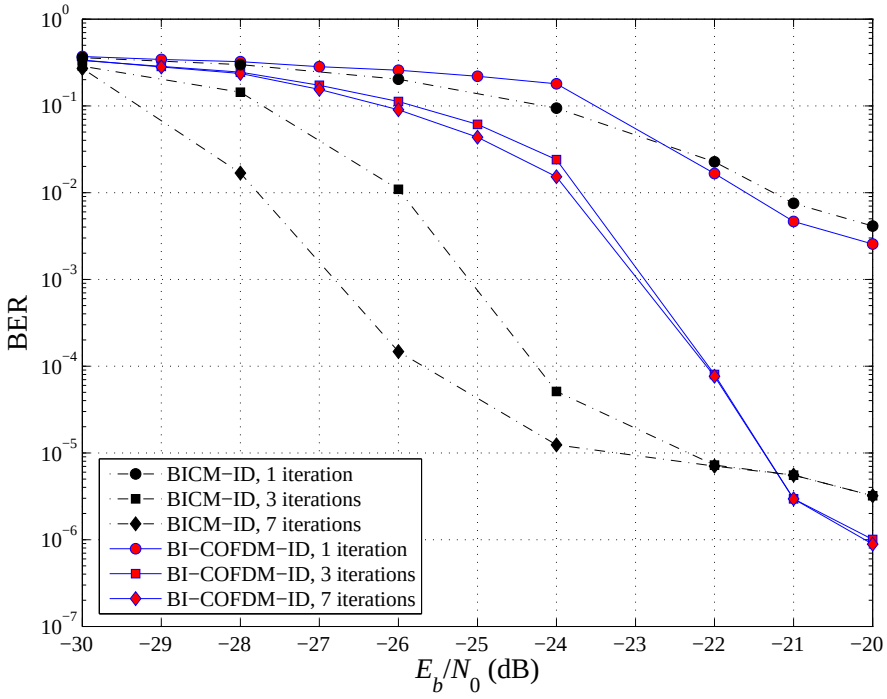

Figure 5.13: Performance comparison of BI-COFM-ID and BICM-ID over an AWAN channel with $A = 0.1$ and $\Gamma = 10^{-3}$: rate-1/3 convolutional code, 8PSK/SSP mapping.

codes, respectively. From these figures, one can also see that the performance advantage of BI-COFDM-ID over to BICM-ID degrades if a more powerful convolutional code is used. This is because a more powerful convolutional code can help to improve the error performance of BICM-ID more significantly than it does for BI-COFDM-ID. However, BI-COFDM-ID still promises to give a better error performance than BICM-ID at high SNR, even when a very powerful convolutional code is used. This can be observed from Fig. 5.13, where both BI-COFDM-ID and BICM-ID use the rate-1/3 convolutional code. In particular, at a very low BER of 10^{-6} the SNR gain of BI-COFDM-ID over BICM-ID is 1dB.

5.3.4 Comparison of BI-COFDM-ID and iteratively-decoded OFDM

As discussed in Chapter 3, OFDM is also a common technique to combat impulsive noise [19, 20, 45]. As shown in [20], viewing OFDM as a code over complex

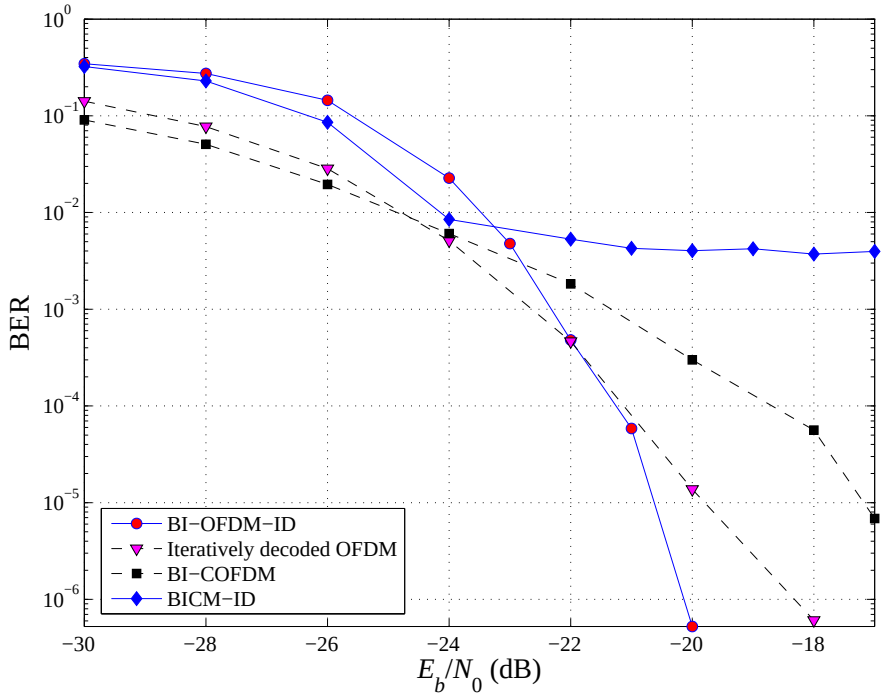

Figure 5.14: Performance comparison of BI-COFM-ID and iteratively-decoded OFDM over an AWAN channel with $A = 0.1$ and $\Gamma = 10^{-3}$.

numbers and using iterative decoding, impulsive noise can almost be completely removed. Specifically, after 4 iterations, the error performance of iteratively-decoded OFDM can converge to the Gaussian bound. It is therefore of interest to compare the error performance of BI-COFDM-ID and iteratively-decoded OFDM. To make a fair comparison in terms of spectral efficiency, here, the BI-COFDM-ID is investigated with 8PSK mapping, a rate-2/3 convolutional code and 1024 subcarriers. Sine no channel coding is used in iteratively-decoded OFDM, 4QAM modulation is employed.

Fig. 5.14 compares BER performance after 9 iterations of BI-COFDM-ID, BICM-ID and iteratively-decoded OFDM, where the impulsive parameters are $\{A = 0.1,\ \Gamma = 10^{-3}\}$. As can be seen from this figure, BICM-ID performs poorer than iteratively-decoded OFDM. Moreover the iteratively-decoded OFDM can give a better error performance compared to BI-COFDM. However, the proposed BI-COFDM-ID outperforms the iteratively-decoded OFDM at high SNR. In particular, at the BER level of 10^{-6}, the SNR gain provided by BI-COFDM-ID over iteratively-decoded OFDM

is 2dB. Note also that performance improvement achieved with BI-COFDM-ID at higher SNR values comes at the expense of degraded performance at the low SNR region.

6. Conclusions and suggestions for further research

6.1 Conclusions

The application of BICM-ID to improve the error performance and spectral efficiency of PLC systems was considered in the first part of this thesis, where Middleton's class-A impulsive noise channel model is adopted. Both optimal and suboptimal soft-output demodulators were developed to facilitate the implementation of the iterative receiver for this channel model. The advantage of using the optimally-designed demodulator for BICM-ID over impulsive noise was demonstrated by computer simulation. It was shown that for any impulsive noise parameter, the use of the proposed demodulator significantly improves the BER performance of BICM-ID over the use of the standard demodulator designed for Gaussian noise.

The effects of different mapping schemes were also investigated for BICM-ID over impulsive noise. It was shown that using SSP mapping of 8PSK helps to significantly improve the BER performance with iterations and gives the best BER performance compared to SP and Gray mappings.

The error-free-feedback bound was also derived to accurately predict the asymptotic error performance of BICM-ID systems. The tightness of the derived bound is confirmed by simulation results. This accurate prediction also matches with the predictions made by applying the EXIT chart technique. Moreover, the EXIT chart technique showed how the performance converges to the asymptotic bound with different mappings.

The superior performance of BICM-ID compared to both BPSK and OFDM techniques was also illustrated. With proper mapping and iterative decoding the proposed

BICM-ID not only achieves a better performance but also can provide a higher spectral efficiency compared to BPSK. It was clearly shown that, BICM-ID also significantly outperforms both the conventional OFDM as well as the iteratively-decoded OFDM, especially when the channel is very impulsive. However, when the channel is less impulsive, the proposed BICM-ID performs poorer than the iteratively-decoded OFDM.

To overcome this problem, the second part of the thesis proposed a novel BI-COFDM-ID to combat impulsive noise. The proposed BI-COFDM-ID is a combination of iteratively-decoded OFDM and BICM-ID. A suboptimal iterative receiver was developed for BI-COFDM over the impulsive noise channel. Computer simulation results showed that the proposed BI-COFDM-ID outperforms both the iteratively-decoded OFDM and BICM-ID.

In the proposed iterative receiver of BI-COFDM-ID, besides the iterative decoding implemented inside the OFDM demodulator, there is another iterative decoding which exchanges the information between the SISO decoder and the suboptimal OFDM demodulator. The implementation of the OFDM demodulator was first discussed. Then the effects of scheduling the information exchange between the SISO decoder and the OFDM demodulator were investigated. Three different iteration strategies were investigated in this thesis. Simulation results suggest that the mixed iteration scheduling is the best choice in terms of the error performance. However, the serial iteration strategy is more attractive in terms of complexity.

Different mapping schemes were also investigated for 8PSK in BI-COFDM-ID. Similar to BICM-ID system, iterative decoding can help to improve the error performance of BI-COFDM-ID remarkably for all three mapping schemes of 8PSK, namely SSP, SP and Gray mappings. The error performance of BI-COFDM-ID with SSP mapping is the best compared to the other two mappings. However, different from BICM-ID, performance improvement by using SSP mapping is smaller compared to the improvement observed in BICM-ID systems in Chapter 4.

Finally, the superior performance of the BI-COFDM-ID over both the iteratively-decoded OFDM and BCM-ID was also illustrated for the case that the channel is less impulsive. In particular, performance comparisons between BI-COFDM-ID and BICM-ID were made for different convolutional codes. It was demonstrated that BI-COFDM-ID can outperform BICM-ID regardless of the convolutional code used. Simulation results also showed that BI-COFDM-ID can achieve a better error performance than the iteratively-decoded OFDM.

6.2 Suggestions for further research

This thesis only investigated BICM-ID and BI-COFDM-ID that employ simple two-dimensional constellations and mapping schemes over class-A impulsive noise. Employing other mapping schemes as well as multi-dimensional constellations/mapping for both systems to achieve even better error performance improvement is an attractive subject of further research. The question on whether there exists an algorithm to construct the optimal mappings for both two-dimensional and multi-dimensional constellations needs to be answered and it is another interesting topic for future studies.

The application of BI-COFDM-ID over impulsive noise was first introduced in this thesis with some different mappings and convolutional codes. The effects of both mapping schemes and different convolutional codes to the error performance of BI-COFDM-ID were only studied and discussed with simulation results. However, error performance analysis for these systems has not been carried out. Hence, other interested topic is to develop an analytical framework for the study of the convergence as well as the asymptotic error performance of BI-COFDM-ID under class-A impulsive noise.

In PLC, both impulsive noise and multipath effects result in performance degradation. This thesis only addressed the effect of impulsive noise in PLC in investigating the performance of BICM-ID and BI-COFDM-ID. Therefore, further studies of BICM-ID and BI-COFDM-ID under both multipath effects and impulsive noise are

very attractive.

Finally, in this thesis, the applications of BICM-ID and BI-COFDM-ID were only investigated with Midlenton's class-A impulsive noise channel. As discussed in Chapters 1 and 2, other models exist for impulsive noise. It is therefore interesting to study the applications BICM-ID and BI-COFDM-ID with other impulsive noise channel models or the real-world power-line channels.

A. The least square estimation of the regression coefficients

To implement the MMSE estimators in both the codeword and information domains, one needs to obtain the scalar coefficients with the least square regression estimation. This appendix derives the least square estimations of coefficients $\alpha_s^{(l)},\ \alpha_i^{(l)},\ \alpha_g^{(l)}$ for codeword domain MMSE estimator. Estimation of the coefficients for the information domain MMSE estimator can be carried out similarly.

In the codeword domain estimator, the impulsive noise can be modeled by:

$$\tilde{\mathbf{i}}^{(l)} = \alpha_s^{(l)}\mathbf{s} + \alpha_i^{(l)}\mathbf{i} + \alpha_g^{(l)}\mathbf{g} + \mathbf{e}^{(l)} \tag{A.1}$$

where the vectors $\mathbf{s},\ \mathbf{i}$ and $\mathbf{g}$ are randomly generated and used as the training data to estimate $\alpha_s^{(l)},\ \alpha_i^{(l)},\ \alpha_g^{(l)}$ at the lth iteration. The vector $\tilde{\mathbf{i}}^{(l)}$ is known as the output of the codeword domain estimator. The error vector $\mathbf{e}^{(l)}$ is unknown and its variance needs to be minimized. For notational simplicity, the superscript (l) is omitted in the following computations.

First, Equation (A.1) can be rewritten as:

$$\tilde{\mathbf{i}} = [\mathbf{s}\ \mathbf{i}\ \mathbf{g}] \begin{bmatrix} \alpha_s \\ \alpha_i \\ \alpha_g \end{bmatrix} + \mathbf{e} \tag{A.2}$$

The average squared error over one OFDM symbol is computed by:

$$\Phi = \frac{1}{N}\sum_{k=0}^{N-1} |\tilde{i}_k - \alpha_s s_k + \alpha_i i_k + \alpha_g g_k|^2 \tag{A.3}$$

Denote $\mathbf{X} = \tilde{\mathbf{i}} - \mathbf{e}$, $\mathbf{H} = [\mathbf{s}\ \mathbf{i}\ \mathbf{g}]$ and $\boldsymbol{\alpha} = \begin{bmatrix} \alpha_s \\ \alpha_i \\ \alpha_g \end{bmatrix}$. The squared error $J(\boldsymbol{\alpha})$ for training

vector with length L is:

$$\begin{aligned} J(\boldsymbol{\alpha}) &= \sum_{k=0}^{NL-1} |\tilde{i}_k - X_k|^2 \\ &= (\tilde{\mathbf{i}} - \mathbf{H}\boldsymbol{\alpha})^H (\tilde{\mathbf{i}} - \mathbf{H}\boldsymbol{\alpha}) \\ &= \tilde{\mathbf{i}}^H\tilde{\mathbf{i}} - \tilde{\mathbf{i}}^H\mathbf{H}\boldsymbol{\alpha} - \boldsymbol{\alpha}^H\mathbf{H}^H\tilde{\mathbf{i}} + \boldsymbol{\alpha}^H\mathbf{H}^H\mathbf{H}\boldsymbol{\alpha} \end{aligned} \tag{A.4}$$

where the superscript H denotes Hermitian transpose of a matrix. Before taking the derivation of the squared error $J(\boldsymbol{\alpha})$, recall the following derivatives of linear functions:

$$d/d\mathbf{x}(\mathbf{x}^T\mathbf{a}) = d/d\mathbf{x}(\mathbf{x}\mathbf{a}^T) = \mathbf{a} \tag{A.5}$$

$$d/d\mathbf{x}(\mathbf{x}^H\mathbf{A}) = 0 \tag{A.6}$$

$$d/d\mathbf{x}(\mathbf{x}^H\mathbf{C}\mathbf{x}) = \mathbf{C}^T\mathbf{x} \tag{A.7}$$

where the vector $\mathbf{a}$ and the matrices $\mathbf{A},\ \mathbf{C}$ do not depend on the vector $\mathbf{x}$.

Now, the derivation of the squared error $J(\boldsymbol{\alpha})$ can be obtained as:

$$\frac{\partial J(\boldsymbol{\alpha})}{\partial(\boldsymbol{\alpha})} = 0 - (\tilde{\mathbf{i}}^H\mathbf{H})^T - 0 + (\mathbf{H}^H\mathbf{H})^T\boldsymbol{\alpha}^* = 0 \tag{A.8}$$

$$(\mathbf{H}^H\mathbf{H})^T\boldsymbol{\alpha}^* = (\tilde{\mathbf{i}}^H\mathbf{H})^T \tag{A.9}$$

$$(\mathbf{H}^T\mathbf{H}^*)\boldsymbol{\alpha}^* = \mathbf{H}^T(\tilde{\mathbf{i}}^H)^T = \mathbf{H}^T\tilde{\mathbf{i}}^* \tag{A.10}$$

Thus, the scalar coefficients are given by:

$$\hat{\boldsymbol{\alpha}} = Real\left\{(\mathbf{H}^T\mathbf{H}^*)^{-1}\mathbf{H}^T\tilde{\mathbf{i}}^*\right\} \tag{A.11}$$

Substituting this value of $\hat{\boldsymbol{\alpha}}$ into Equation (A.4), one can obtain the minimum of the squared error $J(\hat{\boldsymbol{\alpha}})$. Finally, the variance of the error vector $\mathbf{e}$ can be calculated from the parameters $\{\Phi\}_{f=1}^{L}$ as follows:

$$\sigma_{\mathbf{e}}^2 = \frac{1}{2}E\{|e_k|^2\} = \frac{1}{2}\max_{f=1,\ldots,L}\{\Phi_f\} \tag{A.12}$$

where Φ_f is the average squared error for each training OFDM symbol and can be obtained as:

$$\Phi_f = \frac{1}{N}J(\hat{\boldsymbol{\alpha}})$$

References

[1] A. Majumder and J. Caffery, "Power line communications," *Potentials, IEEE*, vol. 23, pp. 4 – 8, Oct., 2004.

[2] H. C. Ferreira, H. M. Grove, O. Hooilen, and A. Han Vinck, "Power line communications: overview," in *IEEE AFRICON 4th*, pp. 558 – 563, Jun., 1996.

[3] N. Pavlidou, A. J. Han Vinck, J. Yazdani, and B. Honary, "Power line communications: state of the art and future trends," *IEEE Commun. Mag.*, pp. 34–40, Apr., 2003.

[4] A. D. Spaulding and D. Middleton, "Optimun reception in an impulsive interference environment - part I: coherent detection," *IEEE Trans. Commun.*, vol. 25, pp. 910–922, Sep., 1977.

[5] Y. Ma, P. So, and E. Gunawan, "Performance analysis of OFDM system for broadband power line communications under impulsive noise and multipath effects," *IEEE Trans. Power Delivery*, vol. 20, pp. 674 – 682, Apr., 2005.

[6] T. Faber, T. Scholand, and P. Jung, "Turbo decoding in impulsive noise environments," *Electronics Letters*, vol. 39, pp. 1069–1071, Jul., 2003.

[7] X. Wang and R. Chen, "Blind turbo equalization in Gaussian and impulsive noise," *IEEE Trans. Veh. Technol.*, vol. 50, pp. 1092 – 1105, Jul., 2001.

[8] H. V. Poor and M. Tanda, "Multiuser detection in flat fading non-Gaussian channels," *IEEE Trans. Commun.*, vol. 50, pp. 1769–1777, Nov., 2002.

[9] D. Middleton, "Statistical - physical models of electromagnetic interference," *Electromagnetic compatibility; Proceedings of the Second Symposium and Technical Exhibition*, vol. EMC-19, pp. 331–340, Jun, 1977.

[10] E. Biglieri and P. de Torino, "Coding and modulation for a horrible channel," *IEEE Commun. Mag.*, vol. 41, pp. 92 – 98, May, 2003.

[11] S. Miyamoto, M. Katayama, and N. Morinaga, "Performance analysis of QAM systems under Class-A impulsive noise environment," *IEEE Trans. Electromagnetic Compatibility*, vol. 37, pp. 260–267, May, 1995.

[12] D. Umehara, H. Yamaguchi, and Y. Morihiro, "Turbo decoding in impulsive noise environment," in *Proc. IEEE Global Telecommun. Conf.*, pp. 194–198, Jul., 2004.

[13] T. Fukami, D. Umehara, and Y. Morihiro, "Noncoherent PSK optimum receiver over impulsive noise channel," in *Proc. of the 2002 ISPLC Conf.*, pp. 235–238, Mar., 2002.

[14] J. Haring and A. Han Vinck, "Performance bounds for optimum and suboptimum reception under Class-A impulsive noise," *IEEE Trans. Commun.*, vol. 50, pp. 1130–1136, Jul., 2002.

[15] H. Dai and H. V. Poor, "Turbo multiuser detection for coded DMT VDSL systems," *IEEE J. Select. Areas in Commun.*, vol. 20, pp. 351 – 362, Feb., 2002.

[16] M. Ardakani, F. R. Kschischang, and W. Yu, "Low-density parity-check coding for impulse noise correction on power line channels," in *Proc. of the 2005 ISPLC Conf.*, pp. 90 – 94, Mar., 2005.

[17] Y. Lin, H. A. Latchman, M. Lee, and S. Katar, "A power line communication network infrastructure for the smart home," *IEEE Wireless Commun.*, vol. 9, pp. 104 – 111, Dec., 2002.

[18] M. Karl and K. Dostert, "Selection of an optimal modulation scheme for digital communications over low voltage power lines," in *IEEE 4th Intl. Symp. Spread Spectrum Tech. and Apps.*, p. 1087 1091, Sept., 1996.

[19] J. Haring and A. Han Vinck, "OFDM transmission corrupted by impulsive noise," in *Int. Symp. Powerline Communication (ISPLC)*, pp. 9 – 14, Apr., 2000.

[20] J. Haring and A. Han Vinck, "Iterative decoding of codes over complex numbers for impulsive noise channels," *IEEE Trans. Inform. Theory*, vol. 49, pp. 1251 – 1260, May, 2003.

[21] J. Haring, *Error tolerant communication over the compound channel*. Shaker Verlag, 2001.

[22] S. Baig and N. D. Gohar, "A discrete multitone transceiver at the heart of the physical layer of an in-home power line communication local-area network," *IEEE Commun. Mag.*, vol. 41, pp. 48 – 53, Apr., 2003.

[23] S. Lin and D. J. Costello, *Error control coding*. Prentice Hall, 2nd ed., 2004.

[24] J. L. Massey, "Coding and modulation in digital communications," in *Proc. of International Zurich Seminar on Digital Communications*, Mar., 1974.

[25] N. H. Tran, *Signal mapping designs for bit-interleaved coded modulation with iterative decoding* $BICM - ID$. M.Sc. thesis, University of Saskatchewan, Dec., 2004.

[26] C. Berrou, A. Glavieux, and P. Thitimajshima, "Near Shannon limit error-correction coding and decoding: Turbo codes," in *Proc. IEEE Int. Conf. Commun.*, pp. 1064–1070, May, 1993.

[27] X. Li and J. A. Ritcey, "Bit-interleaved coded modulation with iterative decoding," *IEEE Commun. Letters*, vol. 1, pp. 169–171, Mar., 1997.

[28] X. Li and J. A. Ritcey, "Trellis-coded modulation with bit interleaving and iterative decoding," *IEEE J. Select. Areas in Commun.*, vol. 17, pp. 715–724, Apr., 1999.

[29] X. Li, A. Chidapol, and J. A. Ritcey, "Bit-interleaved coded modulation with iterative decoding and 8-PSK," *IEEE Trans. Commun.*, pp. 1250–1256, Aug., 2002.

[30] A. Chindapol and J. A. Ritcey, "Design, analysis, and performance evaluation for BICM-ID with square QAM constellations in Rayleigh fading channels," *IEEE J. Select. Areas in Commun.*, vol. 19, pp. 944–957, May, 2001.

[31] S. ten Brink, J. Speidel, and R. H. Yan, "Iterative demapping for QPSK modulation," *Electronics Letters*, vol. 34, pp. 1459–1460, Jul., 1998.

[32] S. ten Brink, "Designing iterative decoding schemes with the extrinsic trinsic information transfer chart," *AEU Inter. of Elec. and Commun.*, vol. 54, pp. 389 – 398, Dec., 2000.

[33] N. H. Tran and H. H. Nguyen, "Signal mappings of 8-ary constellations for BICM-ID systems over a Rayleigh fading channel," in *IEEE Canadian Conference on Electrical and Computer Engineering (CCECE)*, pp. 1809–1813, May, 2004.

[34] N. H. Tran and H. H. Nguyen, "Improving the performance of BICM-ID systems by mapping on the hypercube," in *Proc. IEEE Veh. Technol. Conf.*, pp. 1299–1303, Sep., 2004.

[35] N. H. Tran and H. H. Nguyen, "Multi-dimensional mappings of M-ary constellations for BICM-ID systems," in *IEEE Canadian Conference on Electrical and Computer Engineering (CCECE)*, pp. 124–127, May, 2005.

[36] N. H. Tran and H. H. Nguyen, "Design and performance of BICM-ID systems with hypercube constellations," *IEEE Trans. on Wireless Commun.*, vol. 5, pp. 1169– 1179, May, 2006.

[37] N. H. Tran and H. H. Nguyen, "Signal mappings of 8-ary constellations for bit-interleaved coded modulation with iterative decoding," *IEEE Transactions on Broadcasting.*, vol. 52, pp. 92–99, Jan., 2006.

[38] F. Schreckenbach, N. Gortz, J. Hagenauer, and G. Bauch, "Bit-interleaved coded modulation with iterative decoding," *IEEE Commun. Letters*, vol. 7, pp. 593 – 595, Dec., 2003.

[39] S. V. Vaseghi, *Advanced Digital Signal Processing and Noise Reduction.* John Wiley and Sons, 3rd ed., 2006.

[40] M. Zimmermann and K. Dostert, "Analysis and modeling of impulsive noise in broad-band powerline communications," *IEEE Trans. on Eletromagnetic Compatibility*, vol. 44, pp. 249 – 258, Feb., 2002.

[41] A. Papoulis and S. U. Pillai, *Probability, Random Variables and Stochastic Processes*. McGraw-Hill, 4th ed., 2002.

[42] J. G. Proakis, *Digital communication*. McGraw-Hill, 4th ed., 2000.

[43] J. Seo, S. Cho, and K. Feher, "Impact of non-Gaussian impulsive noise on the performance of high-level QAM," *IEEE Trans. Electromagnetic Compatibility*, vol. 31, pp. 177–180, May, 1989.

[44] G. R. Lang, "Rotational transformation of signals," *IEEE Trans. Inform. Theory*, vol. IT-9, pp. 191 – 198, Jul., 1963.

[45] J. Bingham, "Multicarrier modulation for data transmission: An idea whose time has come," *IEEE Commun. Mag.*, vol. 28, pp. 5 – 14, May, 1990.

[46] P. Robertson, E. Villebrun, and P. Hoeher, "A comparison of optimal and sub-optimal map decoding algorithms operation in the log domain," in *Proc. IEEE Int. Conf. Commun.*, pp. 1009–1013, Jun., 1995.

[47] S. Benedetto, D. Divsalar, G. Montorsi, and F. Pollara, "Soft-input soft-output Maximum a Posteriori (MAP) module to decode parallel and serial concatenated codes," in *Proc. IEEE Int. Conf. Commun.*, pp. 1009–1013, Nov., 1995.

[48] J. Hagenauer, E. Offer, and L. Papke, "Iterative decoding of binary block and convolutional code," *IEEE Trans. Inform. Theory*, vol. 42, pp. 1–20, Mar., 1996.

[49] G. T. G. Caire and E. Biglieri, "Bit-interleaved coded modulation," *IEEE Trans. Inform. Theory*, vol. 44, pp. 927–946, May, 1998.

[50] E. Zehavi, "8-PSK trellis codes for a rayleigh fading channel," *IEEE Trans. Commun.*, vol. 40, pp. 873–883, May, 1992.

[51] S. ten Brink, "Convergence behavior of iteratively decoded parallel concatenated codes," *IEEE Trans. Commun.*, vol. 49, pp. 1727 – 1737, Oct., 2001.

[52] H. H. Nguyen and T. Q. Bui, "Bit-interleaved coded modulation with iterative decoding in impulsive noise," *to appear in IEEE Trans. on Power Delivery*, 2006.

[53] T. Q. Bui and H. H. Nguyen, "Bit-interleaved coded modulation with iterative decoding in impulsive noise," in *IEEE Proc. of the ISPLC Conf.*, pp. 98 – 103, Mar., 2006.

[54] T. Q. Bui and H. H. Nguyen, "Error performance of BICM-ID in impulsive noise," in *IEEE Canadian Conference on Electrical and Computer Engineering (CCECE)*, pp. 201–204, May, 2006.